EFFECT OF REINFORCEMENT CORROSION ON THE BOND STRENGTH OF RC MEMBERS

Thesis

Submitted in partial fulfilment of the requirements for the degree of

DOCTOR OF PHILOSOPHY

by

AKSHATHA SHETTY

DEPARTMENT OF CIVIL ENGINEERING

NATIONAL INSTITUTE OF TECHNOLOGY KARNATAKA

SURATHKAL - 575 025

November, 2014

NATIONAL INSTITUTE OF TECHNOLOGY KARNATAKA, SURATHKAL

D E C L A R A T I O N

by the Ph.d. Research Scholar

I hereby *declare* that the Research Thesis entitled **Effect of Reinforcement Corrosion on the Bond Strength of RC Members** which is being submitted to the National Institute of Technology Karnataka, Surathkal, in partial fulfillment of the requirements for the award of the Degree of **Doctor of Philosophy** in **Civil Engineering**, is a *bonafide report of the work carried out by me*. The material contained in this Report has not been submitted to any University or Institution for the award of any degree.

CV12F08, AKSHATHA SHETTY

(Register Number, Name & Signature of the Research Scholar)

Department of Civil Engineering

Place: NITK-SURATHKAL

Date: .11.2014

NATIONAL INSTITUTE OF TECHNOLOGY KARNATAKA, SURATHKAL

CERTIFICATE

This is to *certify* that this Research Thesis entitled **Effect of Reinforcement Corrosion on the Bond Strength of RC Members** submitted by **Akshatha Shetty** (Register Number: **CV12F08)**, as the record of the research work carried out by her, *is accepted as the Research Thesis submission* in partial fulfillment of the requirements for the award of the degree of **Doctor of Philosophy.**

(KATTA VENKATARAMANA)
Research Guide
(Name and Signature
with Date)

(K. S. BABU NARAYAN)
Research Guide
(Name and Signature
with Date)

(Chairman-DRPC)
(Name and Signature
with Date and Seal)

ACKNOWLEDGEMENTS

I would like to express my deep sense of gratitude to research supervisor, **Dr. Katta Venkataramana,** Professor in Civil Engineering Department and Dean Academic, NITK, Surathkal for his invaluable suggestions, guidance and constant inspiration during the work period. His comments, remarks and commitment played a distinct role in bringing this thesis to good shape.

I owe my heartfelt thanks to research supervisor, **Dr. K.S. Babu Narayan,** Professor, Department of Civil Engineering, NITK, Surathkal for his elucidative and comprehensive encouragement at every stage of this work. His moral support, critical guidance and ever helpful attitude will always be admired, valued and cherished.

I was very much privileged to learn from **Dr. S. M. Kulkarni,** Professor, Department of Mechanical Engineering and **Dr. R. Shivashankar,** Professor, Department of Civil Engineering, NITK Surathkal for their support and useful suggestions as my RPAC panel members. I take this time to specially thank them.

Thanks are also due to **Dr. Indrani Gogoi**, Associate Professor, Department of Civil Engineering, Assam Engineering Institute, Guwahati, for introducing this research topic, for her support and encouragement.

I wish to thank Head of the Department of Applied Mechanics and Hydraulics for permitting me to carry out part of the experiments in the Strength of Materials laboratory.

I am greatly indebted to **Mr. Dinesh**, Draughting section, for providing me the structural details to carry out the field study. I also wish to thank Swimming pool complex authorities for permitting me to carry out part of the field study.

I extend my appreciation to all the laboratory staff of Department of Civil Engineering, Department of Applied Mechanics and Hydraulics for their help in carrying out the experimental investigations. Especially **Mr. Ramanath Acharya, Mr. Sadanand Kadri, Mr. Vishwanath and Mr. Shashikanth, Mr. Yathish** were of great help and support.

I extend my sincere thanks to each and every teaching, non-teaching faculty and my friends, who had helped directly or indirectly, for the successful completion of my work.

My warm thanks to my husband, **Mr. Rajath Samani S.** for his continuous encouragement and support in all my academic activities.

Above all, I wish to express my gratitude, love and affection to my mother and family members who are my strength.

Finally, I would like to thank Board of Research in Nuclear Sciences (BRNS), for their generous financial support to carry out this research work.

NITK, SURATHKAL

Date: .11.2014 AKSHATHA SHETTY

CONTENTS

LIST OF FIGURES

LIST OF TABLES

LIST OF NOTATIONS

Symbol	Description
i_{corr}	Corrosion current density
i_{app}	Applied Current
Wi	Initial weight of steel bars
F	Faradays constant
w	Equivalent weight of iron
t	Time in seconds
ρ	Degree of corrosion (%)
d	Diameter of bar
l	Length of the bar
R_p	Polarisation resistance
τ	Bond stress
L_d	Embedded length of the reinforcing bar
P	Maximum measured load
f_t	Modulus of rupture
f_{ck}	Compressive strength of concrete
f_y	Yield strength of steel
E_s	Modulus of elasticity of steel
E_c	Modulus of elasticity of concrete
τ_{bd}	Average bond stress
ϕ_1	Reduced Diameter
f_s	Bar force (Steel stress values)

W_f	Final weight of rebar
ϕ	Initial diameter
p	Weight loss
s	Slip value
c	Thickness of cover layer
$f_{t,s}$	Concrete's splitting tensile strength
η	Corrosion level
β	Reduction factor
ε	Strain
ε_1	Initial strain
ε_0	Ultimate strain
f	stress
du_1	Deflection at ultimate load
du_2	Deflection at 0.75Pu in the post ultimate region
P_u	Ultimate load
EX	Elasticity of concrete and steel
PRXY	Poisson's ratio
B	Breadth of the beam
D	Depth of the beam
L	Length of the beam
Ast	Area of tension steel
Asc	Area of compression steel
C	Mass of cement
S_c	Specific gravity of cement
S_{fa}	Specific gravity of fine aggregate

S_{ca}	Specific gravity of coarse aggregate
V	Gross volume of fresh concrete
b	Width of flange
I_{xx}	Moment of inertia about X axis
I_{yy}	Moment of inertia about Y axis
t_f	Thickness of flange
t_w	Thickness of web
r_{min}	Minimum radius of gyration
λ_{min}	Minimum slenderness ratio
Mu	Ultimate moment
C	Compressive force
T	Tensile force
Xu	Depth of neutral axis
d	Effective depth
l	Effective length of beam
m	Modular ratio
I_{cr}	Moment of inertia of cracked section
I_{eff}	Effective moment of inertia
M_r	Cracking moment
Z	Lever arm
b_w	Breadth of web

ABSTRACT

Corrosion of reinforcing steel is the most detrimental effect endangering the structural performance. Present investigation has been taken up to study the detrimental effect of corrosion on bond behaviour. Anchorage bond strength and Flexural bond strength characteristics are studied in this research. Two types of cements namely Ordinary Portland Cement (OPC) and Portland Pozzolona Cement (PPC) have been used. Bond strength study has been carried out for controlled beam specimen and for specimens subjected to different levels of corrosion. Loss in mass of reinforcement bar has been taken as the basis to fix corrosion levels. Accelerated corrosion technique has been adopted to control corrosion rate by regulating current over predetermined durations.

For the study of anchorage bond strength, cylindrical specimens have been adopted. Concrete grade of M20 and Fe-415 grade of 16mm diameter bar have been used. From the study it has been observed that for corrosion levels upto 2.5%, bond strength is unaffected. But for corrosion levels beyond 2.5%, there is considerable decrease in bond strength.

For understanding the performance of flexural bond strength, National Bureau of Standard (NBS) beams have been investigated. Concrete grade M30 and steel Fe-415 have been used. From the experimental investigation it has been observed that load carrying capacity drops by about 1.6%, for every percentage increase in corrosion level. Bond strength degradation of 2.6% at slip initiation and 2.1% at end of slip have been observed for every percentage increase in corrosion level for OPC concrete beam specimens. For PPC concrete, bond strength degradation of 2% at slip initiation and 2.1% at end of slip have been observed.

In numerical study, finite element method was used. ANSYS commercial software is used for the study. From the numerical modelling it has been observed that load carrying capacity drops by about 1.8%, for every percentage increase in corrosion

level. The bond strength degradation values are 3% and 2.4% at initiation of slip and end of slip respectively per percentage increase in corrosion level.

Lastly, an attempt has been made to apply the proposed prediction equations to estimate corrosion in real life structures.

Key Words: corrosion, bond strength, OPC, PPC, load, strain, deflection

CHAPTER 1

INTRODUCTION

1.1 GENERAL

Tremendous increase in demand for resources and acute shortage of the same is like a double edged sword. Codes and construction practices are emphasizing durability to cope with the situation. One of the most important concerns with reinforced concrete construction is deterioration due to reinforcement corrosion. Corrosion effects on structures cannot be ignored and replaced.

Corrosion is defined as the destruction or deterioration of a material because of its reaction with environment. In case of corrosion formation, an oxide of iron due to oxidation of the iron atoms in solid solution is a well-known example of electrochemical corrosion, commonly known as rusting. These oxides are usually weaker than steel.

Chloride ingress into the concrete is a major cause of steel corrosion. Presence of chloride ions at the rebar level leads to the breakdown of passive firm thin film layer and consequently initiates the corrosion (Pradhan and Bhattacharjee, 2009). Rust produced as a result of corrosion increases its volume 2 to 6 times than that of original steel; it causes increase in volume of tensile stresses in concrete (Bhaskar et al. 2010).

The process of corrosion is initially slow and later it progresses exponentially. Corrosion initiation process in RC structures depends on the atmospheric conditions, thickness of cover, quality of concrete present at the cover depth, stress levels of corrosion in rebar, cracking effect etc. Macro corrosion cell-both the anodic and cathodic reactions frequently take place in different places with some distance apart (Browne, 1975). Physical model for steel corrosion in concrete sea structures is proposed by Bazant, (1979). Effects of reinforcement corrosion on the performance of RC elements are summarised in Fig.1.1 (Azher, 2005).

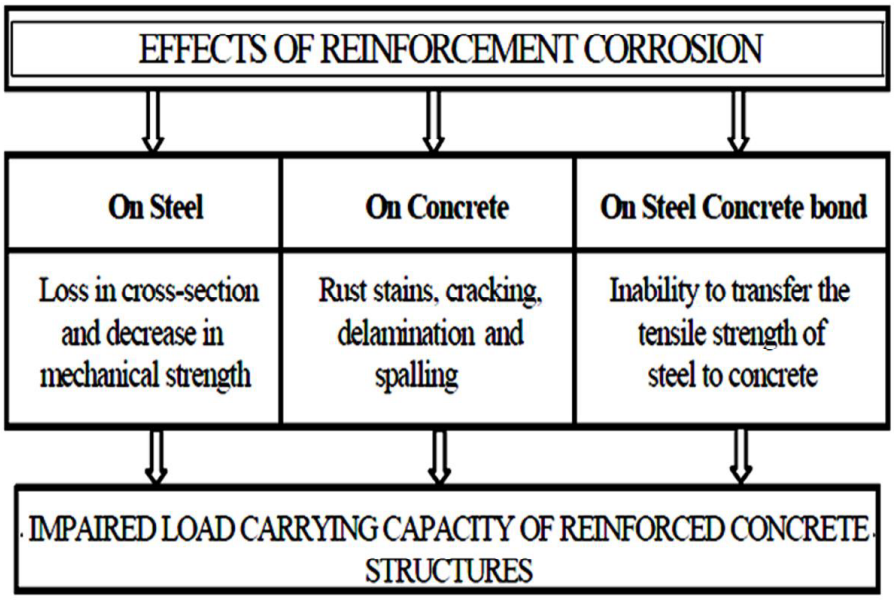

Fig.1.1: Effect of Reinforcement Corrosion on the Performance of RC Elements (Azher, 2005)

The basic cycle of micro cracking, cracking of concrete and influence of various environmental factors, resulting in the corrosion of embedded steel contribute to further cracking and reprocessing, until the steel corrodes extensively and/or concrete gets deteriorated or delaminated is shown in Fig.1.2.

1.2 EFFECTS OF CORROSION ON THE STRUCTURAL BEHAVIOR

Corrosion of reinforcing bars produces effects on the structural behaviour of RC members. This phenomenon is due to the reduction in the bond strength of two composite materials i.e. steel and concrete. The effects of steel corrosion are summarized in Fig.1.3, distinguishing between the "local" effects, i.e. at the RC member level, and the "global" effects, i.e. at the RC structure level. It is worth noting that, the global consequences of corrosion on the structural performance include various phenomena such as decline of load carrying capacity and ductility, and also the shift of the failure mechanism and occurrence of detrimental torsion effects. Structural performance of concrete beams under simultaneous loading and

reinforcement corrosion are studied by Du, et al. (2013). Assessments of corrosion-damaged concrete structures are studied by Webster, (2000).

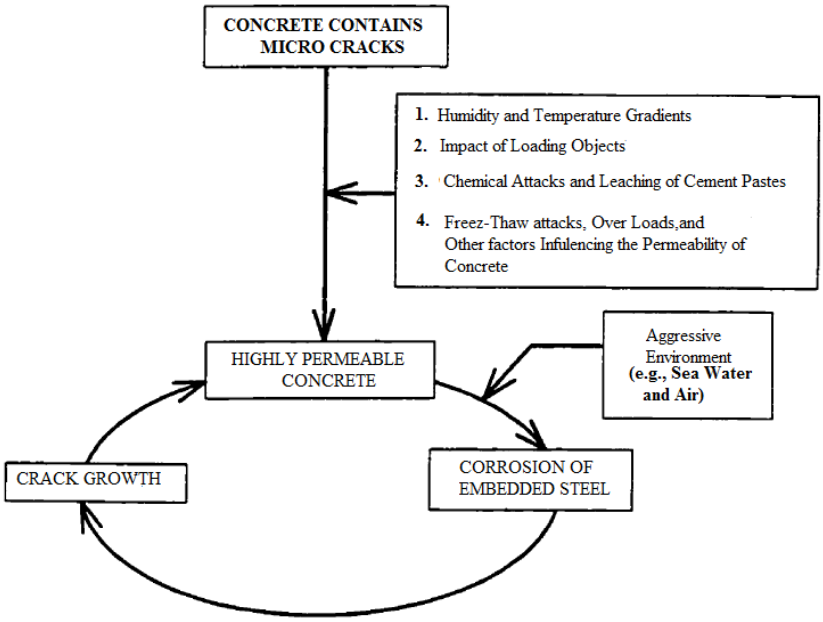

Fig.1.2: Schematic representation of the cracking-corrosion-cracking cycle in reinforced concrete (Mehta 1993).

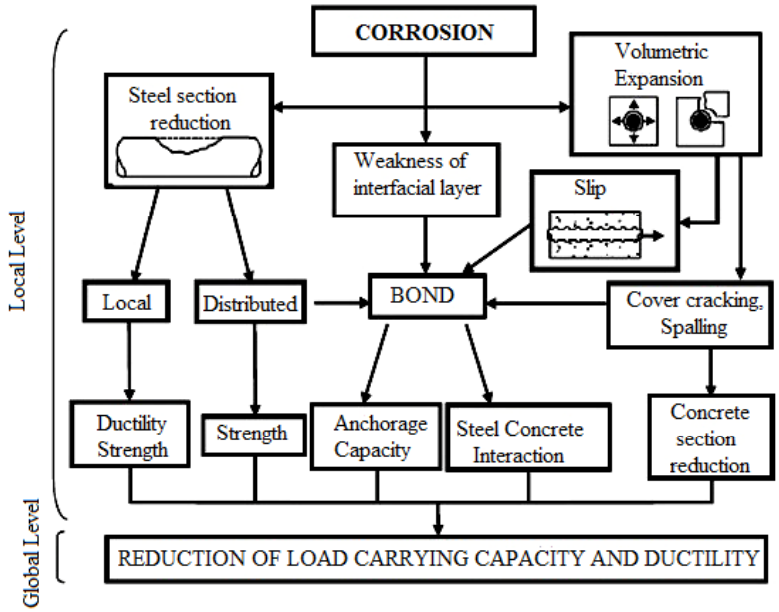

Fig.1.3: Corrosion effects on the structural performance (Simioni, 2009).

1.3 CORROSION MECHANISM

Corrosion of steel embedded in concrete is an electrochemical process. The surface of the corroding steel functions as a mixed electrode that is a composite of anodes and cathodes electrically connected through the body of steel itself, upon which coupled anodic and cathodic reactions take place. Concrete pore water functions as an aqueous medium, i.e., a complex electrolyte. Therefore, a reinforcement corrosion cell is formed, as shown in Fig.1.4 (Ahmad, 2003).

Corrosion reactions at the anodes and cathodes are broadly referred to as half-cell reactions. The anodic reaction is the oxidation process, which results in dissolution or loss of metal whilst the cathodic reaction is the reduction process which results in reduction of dissolved oxygen forming hydroxyl ions.

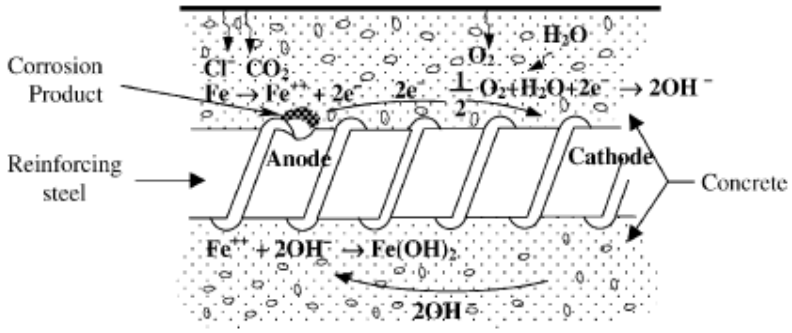

Fig.1.4: Schematic illustration of the Corrosion of Reinforcement in Concrete- as an electrochemical process (Ahmad, 2003)

To understand and appreciate the effects of natural conditions causing corrosion, tremendous amount of time and resource are needed. Hence for the present study, simulation of condition in an accelerated way (using impressed current technique) is considered; whereby time can be saved and existing structures performance can be better understood. Also corrective and preventive measures can be suggested expeditiously.

1.3.1 Pourbaix Diagram

Pourbaix diagram, also known as a potential/pH diagram, E_H-pH diagram or a pE/pH diagram, maps out possible stable (equilibrium) phases of an aqueous electrochemical system. Predominant ion boundaries are represented by lines. This can be read much like a standard phase diagram with a different set of axes.

Stability regions for corrosion products are shown in the Fig.1.5. At potentials more positive than -0.6 and at pH values below about 9, ferrous ion (Fe^{2+} or Fe II) is the stable substance. This indicates that iron will corrode under these conditions. In other regions of the iron E-pH diagram, it can be seen that the corrosion of iron produces ferric ions (Fe^{3+} or Fe III), ferric hydroxide [$Fe(OH)_3$], ferrous hydroxide [$Fe(OH)_2$], and at very alkaline conditions, complex $HFeO_2^-$ ions. The solid corrosion products considered are different than earlier, ferric oxide (Fe_2O_3) and magnetite (Fe_3O_4), both important iron ore constituents (Fonatana, 2005).

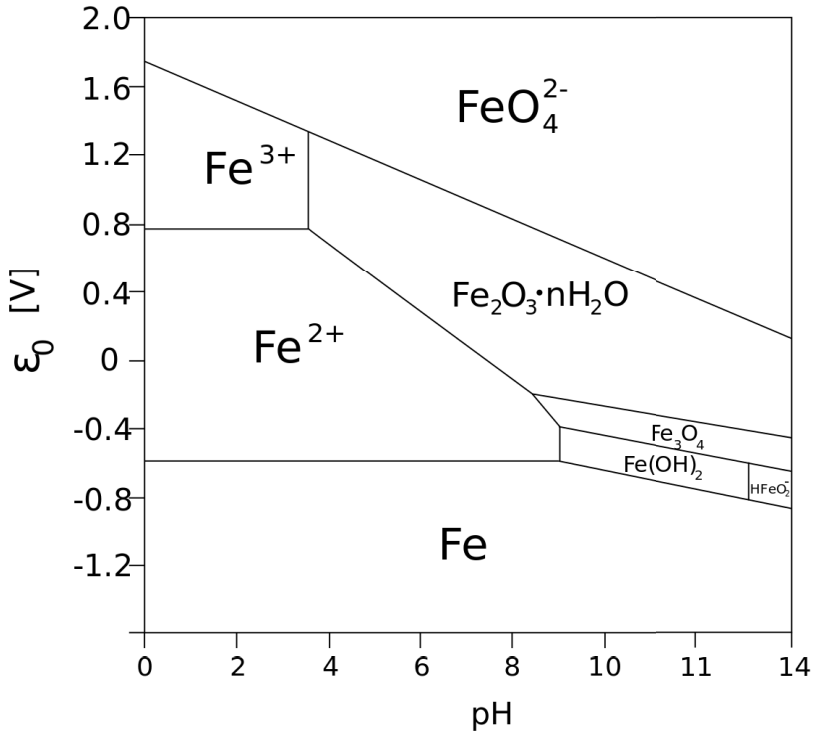

Fig.1.5 Pourbiax diagram (Fontana, 2005)

1.3.2 Impressed Current Technique

Impressed current technique involves applying a constant current from a DC source to the embedded steel to induce desired amount of corrosion. After applying current for a given duration, the degree of corrosion percentage can be determined by obtaining the values of corrosion current density using Applied Corrosion Monitoring Instrument (non destructive method). Actual amount of steel percentage lost in corrosion can be calculated with the help of a gravimetric test (destructive method) conducted on the extracted bars.

1.4 TIME-DEPENDENT STATES OF REINFORCEMENT CORROSION

The state of corrosion in reinforced concrete is expected to change as a function of time. Corrosion process has three distinct stages, namely; depassivation, propagation, and final state, as shown in Fig.1.6. Depassivation is the loss of oxide (passive) layer over the rebar, which is initially formed due to the high alkalinity of concrete. The process of depassivation takes an initiation period, t_p, which is the time from construction to the time of initiation of corrosion (depassivation). It has been noted that the initiation and propagation of corrosion in the specimens depend on many factors; important among them are given below (Ahmad, 2003):

a) Permeability of the concrete matrix;
b) Cover thickness;
c) Electric current applied;
d) Density of the solution used;
e) The environmental temperature.

Propagation phase starts from the time of depassivation (t_p), to the final state, is reached at a critical time (t_{cr}), at which corrosion would produce spalling of concrete cover or cracking through the whole of concrete cover. During the propagation period, i.e. corrosion period (t_{cor}), which begins at the moment of depassivation, the rebar corrosion is usually assumed to be in a steady state, as indicated by a straight line in Fig.1.5. The critical time (t_{cr}), can be expressed as:

$$t_{cr} = t_p + t_{cor} \tag{1.1}$$

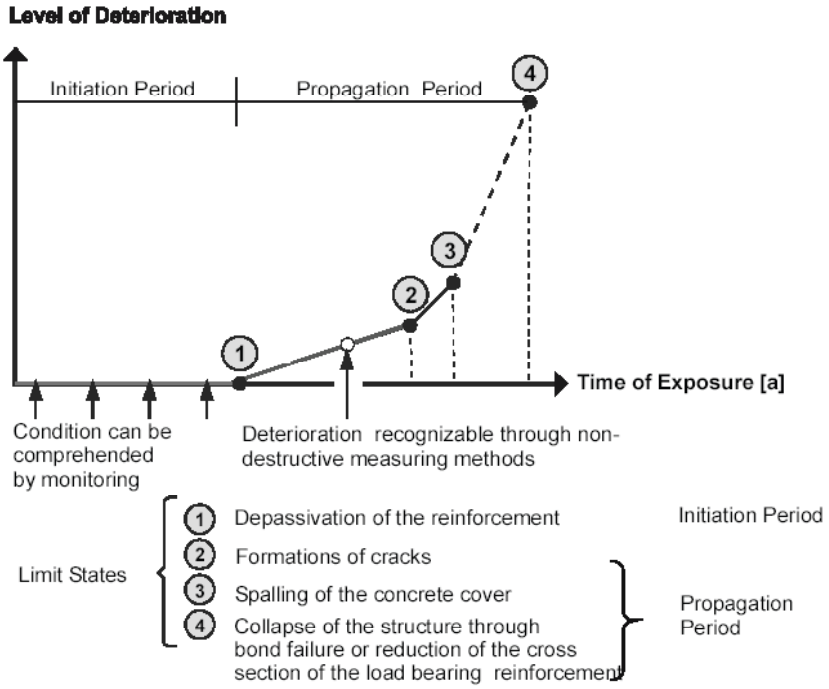

Fig.1.6: Typical Deterioration Levels for a Reinforced Concrete Structure Suffering from Corrosion [fib Bulletin 34, 2006].

The time up to the initiation of the corrosion process is determined by the flow of penetrating substances into the concrete cover and by the threshold concentration for corrosion to start (Tuutti, 1982).

Corrosion of reinforcement is a prime concern as stability, strength, safety, serviceability, and durability and economy of RC structures are severely affected. One of the most important prerequisites of reinforced concrete construction is adequate bond between the reinforcement and the concrete.

1.5 SIGNIFICANCE OF BOND STRENGTH

Reinforced steel bar can receive its external loads only from the surrounding concrete, because external loads are very rarely applied directly on it. Composite action between concrete and reinforcing steel cannot occur without proper bond.

Bond resistance of reinforcing bars embedded in concrete depends primarily on frictional resistance and mechanical interlock. Chemical adhesion provides withholding property between steel and concrete. Frictional bond provides initial resistance against loading and further loading mobilises the mechanical interlock between the concrete and bar ribs. Mechanical interlocks leads to inclined bearing forces which in turn lead to transverse tensile stresses and internal inclined splitting (bond) cracks along reinforcing bars. These cracks are commonly referred as Goto cracks (Goto, 1971).

1.6 TYPES OF BOND STRESS

Bond stress in reinforced concrete members arises due to two distinct situations: (a) from the anchorage of bars in case of tension or compression and (b) from the change in bar force along its length due to change in bending moment along the member (Purushothaman, 1984).

Anchorage bond, if uniform bond stress along the bar is assumed, is expressed as (Purushothaman, 1984):

$$L_d = d_b\left(\frac{f_s}{4\tau_{bd}}\right) \tag{1.2}$$

where: L_d= embedment length, d_b= diameter of bar, f_s =bar force, τ_{bd} = bond stress.

In case of flexural bond, change in tensile force dT in steel (Fig.1.7) is mobilized over the length dx as below (Purushothaman, 1984):

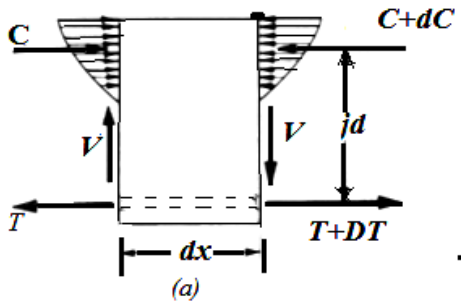

Fig.1.7 (a): Free body sketch of reinforced concrete element

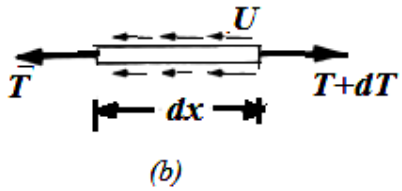

Fig.1.7 (b): Free body sketch of reinforced steel element

Change in bending moment *dM* produces a change in bar force

$$dT = \left(\frac{dM}{jd} \right) \tag{1.3}$$

where, *jd* = internal lever arm between tensile and compressive force resultants.

If *U* is the magnitude of the local average bond stresses per unit of bar surface area, then, by summing horizontal forces,

Bond force = change in bar force

$$U \sum\nolimits_o dx = dT \tag{1.4}$$

where, $\sum_o$ is the sum of all perimeters of the bars. Thus

$$U = \left[\frac{dT}{\sum_0 (dx)} \right] \tag{1.5}$$

Ultimately by substituting Eq. (1.3) in Eq. (1.5), unit bond stress can be written as

$$U = \left[\frac{dM}{\sum_0 jd\,(dx)} \right] \tag{1.6}$$

From which

$$U = \left[\frac{V}{\sum_0 jd} \right] \tag{1.7}$$

Eq. (1.7) is the "elastic cracked selection equation" for flexural bond stress, and it indicates that the unit bond stress is proportional to the shear at a particular section, i.e., to the rate of change of bending moment.

1.7 INFLUENCE OF CORROSION ON BOND

As steel bar corrodes, increased volume of corrosion products results in a "bursting" pressure, which causes longitudinal cracks in specimens. With increase in corrosion level, crack width increases which results in breakdown of adhesion and friction at the steel-concrete interface. At low corrosion levels exclusive of longitudinal cracking, corrosion products have a beneficial effect of improving bond characteristics at the steel-concrete interface. At higher corrosion levels, the steel bars display localized pitting and loss of some of the ribs over the bar length, thereby weakening the rib-concrete mechanical interlocking force transfer mechanism (Al-Sulaimani et al. 1990). An examination of number and spacing of transverse cracks shows that as level of corrosion increases, transverse crack spacing also increases, reflecting the deterioration of bond characteristics at the steel-concrete interface (Amleh and Mirza, 2000).

Corroded reinforced concrete structures lead to huge costs for assessment, maintenance, analysis and surrogating of the infrastructure worldwide. To understand the performance of structures there is a need to study the rate at which different corrosion levels occur.

1.8 NUMERICAL MODELLING

The experimental method that produces real life response is often extremely time consuming and the use of materials can be quite costly [Saifullah et al. 2011]. To minimize these costs, numerical modelling using finite element method (FEM) has

become popular. However to get an idea about the finite element software complete understanding of experimental methodology is necessary.

Finite element analysis is a numerical approach widely applied to the concrete structures based on the use of the nonlinear behaviour of materials. An effective method to analyze the load carrying capacity of corroded reinforced concrete components is Numerical analysis [Yuan and Yongsheng, 2009].

In finite element method of analysis, a complex region defining a continuum is discretised into simple geometric shapes called finite elements. The original body is then considered as an assemblage of these finite elements connected at a finite number of joints called nodes or nodal points (Seshu, 2006).

To overcome the intractability of realistic types of continuous problems (continuum), various methods of discretisation have been proposed from time to time (Zienkiewicz et al. 2007). As long as the discrete element size is suitable and the constitutive relation is correct, the model results will reach the real value and engineering requirements will be satisfied with a small variation (Cook et al. 2001).

1.8.1 Modelling in ANSYS

ANSYS is a finite element analysis (FEA) software package and has many analysis capabilities. FEA calibration study includes, modelling a concrete beam with dimensions and properties. To create the finite element model in ANSYS there are multiple tasks that have to be completed for the model to run properly. For this model, the graphical user interface (GUI) was utilized to create the model. Analysis of a structure with ANSYS is performed in following three stages:

I. Pre-processing-defining the finite element model and environmental factors to be applied to it.
II. Analysis solver- solution of finite element model.
III. Post-processing of results like stress-strain contours, deflections, etc., using visualization tools.

1.9 ORGANIZATION OF THE THESIS

Chapter 1 gives a brief account of corrosion and its mechanism, effect of corrosion on the structural behaviour, significance of bond strength, types of bond and corrosion effect on bond strength, and an introduction to finite element analysis.

A comprehensive review of literature has been presented in Chapter 2 and in the light of literature review the scope and objectives of the present investigation have been highlighted.

Details of National Bureau of Standard (NBS) beam employed in the investigation, materials and methods followed for anchorage bond strength and flexural bond strength have been presented in Chapter 3.

Chapter 4 provides elaborate account of finite element analysis carried out to simulate the actual condition.

Results of corrosion current density, effect of corrosion on anchorage bond, load-deflection behaviour, ultimate load carrying capacity, crack width and flexural bond strength characteristics and prediction equations obtained from analysis of results of the investigation are presented and discussed in Chapter 5.

Potential structural health monitoring applications of present investigation are presented in Chapter 6 by considering case studies.

Conclusions and contributions of present investigation have been summarised in Chapter 7.

CHAPTER 2

REVIEW OF LITERATURE

2.1 GENERAL

Corrosion impacts the bond strength between concrete and steel. According to Park and Paulay (1975), "Bond stress is the name assigned to shear stress at the steel bar-concrete interface which by transferring the load between the surrounding concrete and the bar, modifies the steel stresses". For reinforced concrete beams, load directly acts on concrete whereas the reinforcement is subjected to transmit loads. Tension in steel is transmitted by the concrete due to surface resistance action between both. This surface resistance is known as bond stress. It is force per unit of nominal surface area of reinforcing bar acting on the interface between the surrounding concrete and the bar [McGinley (1990), Pillai (1999) and Karve and Jain (2000)].

A review of literature elaborating factors affecting bond, anchorage and flexural bond strength, state of the art is presented here.

2.2 FACTORS AFFECTING THE BOND STRENGTH

Bond strength is attributed to four factors: (1) Chemical adhesion of the concrete to the steel; (2) Friction at the bar-concrete interface from mill scale, rust, and other surface irregularities; (3) Bearing against the rib faces; and (4) Shear acting along a cylindrical concrete surface between adjacent ribs.

The bond strength and mode of bond failures are influenced by many factors such as given below:

i. Concrete Strength and Composition

Compressive strength is a key parameter in bond behaviour, because the force is transferred by bearing and bond and failure can occur by tensile splitting and shearing of concrete (Orangun et al. 1977). It has been found that the induction of 0.2 percent polypropylene fibers by volume into concrete improves the bond resistance of concrete, especially at post-cracking levels of corrosion (Al-Sulaimani et al. 1990); this is due to reduced level of damage at the concrete-steel interface and to an intrinsic contribution in improving the confining and holding capacity of the surrounding concrete for the reinforcing bar. Bond characteristics are not only influenced by the strength but also by the composition and consistency of the concrete mix. Concrete with fly ash exhibited better resistance to corrosion damage than open concrete basically because of its higher electrical resistivity (Cabrera and Ghoddoussi 1992, Pradhan and Bhattacharjee 2009). The properties of concrete, both in tension and compression, contribute to the development of bond stresses; micro-cracking is controlled by the tensile resistance. Bearing stresses induce high compressive stresses in front of the ribs (Amleh 2000).

ii. Concrete Cover

Tepfers (1973) and Orangun et al. (1977), observed that the concrete cover and the shear or tensile reinforcement spacing significantly influence the type of bond failure. Splitting tensile failure occurs with small concrete covers and the bond capacity in pullout was higher for the larger cover thickness. The resistance to corrosion initiation and further propagation is provided by two barriers: a) the resistance of the concrete cover to chloride penetration which depends on its thickness, and permeability and b) the resistance of the reinforcement bars to corrosion which in turn depends on the type of steel and the alkalinity of the surrounding concrete and the composite action of both concrete and steel, due to the bond deterioration (Rodriguez et al. 1994).

Bond strength increases with increasing cover thickness. Although bond strength of deformed bars and concrete increases with corrosion up to a certain amount, but with progressive increase in corrosion, the bond strength decreases and the cracking of the concrete cover seems to have no effect on the bond strength (Jin and Zhao 2001). To reduce the permeability or ingress of chloride to the rebar level, mineral admixture may be added or the cover thickness may be increased (Bhaskar et al. 2011).

iii. Water Cement Ratio

Amleh (2000) from their study concluded that the water-cement ratio can be eliminated from the parameters as the bond stress is related to the concrete strength. However high water-cement ratios can lead to bleeding under the bars, especially the top bars and results in lower bond strength. The w/c ratio does not itself control the rate of corrosion of reinforcement. The depth of penetration of a particular chloride threshold value and carbonation depth increase with an increase in the w/c ratio. The oxygen diffusion coefficient also increases with an increase in the w/c ratio. Diffusion of oxygen is a vital limiting factor for corrosion reaction only when the concrete is submerged or in a high RH environment with a dense concrete cover and low *w/c* ratio (Hussain et al. 2012).

iv. Confining reinforcement

Confining reinforcement prevents widening of longitudinal crack resulting from corrosion. A reduced level of damage at the concrete-steel interface is observed, due to an intrinsic contribution in improving the confining and holding capacity of the surrounding concrete for the reinforcing bar (Al-Sulaimani et al. 1990).

While it is easy to imagine how detrimental corrosion can be to the durability and strength of a structure, corrosion can at times also be beneficial. For low corrosion levels [0-4%], there is an increase in bond strength (Almusallam, 2001). This can be understood by factoring in the radial pressure developed due to increased volume of the corrosion products which increases the confining effect and also the

increase in frictional resistance brought about by the rust. At higher corrosion levels, the radial pressure leads to development of longitudinal cracks and ultimately spalling of the concrete cover. Spalling of the concrete cover accelerates the corrosion process by exposing the surface of the reinforcement corrosion to external environment.

Fang et al. (2004) concluded from their experimental investigations that for deformed bars without confinement, bond strength is very sensitive to corrosion levels and generally decreases with the corrosion level. For deformed bars with confinement, corrosion has no substantial influence on the bond strength. For smooth bar without confinement, when corrosion level is low, bond strength increases as corrosion level increases. For smooth bar with confinement, bond strength increases as corrosion level increases, up to a relatively high degree of corrosion.

v. Bar Profile

Pullout tests by Rehm (1957), Lutz and Gergly (1966*)* showed that for bars with steep rib face angle α (larger than about 40 degrees with the bar axis) slip occurs only by the compression of the concrete in front of the bar rib, while in bars with flat ribs, i.e., the angle α is small, slip occurs with the ribs sliding relative to the concrete as the rib tends to push the concrete away from the bar. This wedging action can be a major cause of longitudinal splitting along the bar. For $45°<\alpha<70°$, the deformations must reverse in direction on each side of the bar. With reference to the steep face angle (Fig.2.1), (Lutz and Gergely 1967) stated that the bond of deformed bars is developed mainly by the bearing pressure of the bar ribs against the concrete. It was observed that there is an initial increase in bond which is due to the increased toughness of the reinforcing bar surface with the growth of a firm layer of corrosion (Al-Sulaimani et al. 1990).

A study on relative bond effectiveness of the embedded bars at different stages of corrosion based on the details of the transverse and longitudinal splitting cracks was carried out by Amleh and Mirza (2000). Bond strength was observed to

decrease rapidly with an increase in the corrosion level, dropping from a 9 percent decrease in the average bond stress for a steel weight loss of 4 percent, to a bond stress decrease of 92 percent for a weight loss of 17.5 percent. The severe loss in bond strength was attributed to deterioration of the bar ribs.

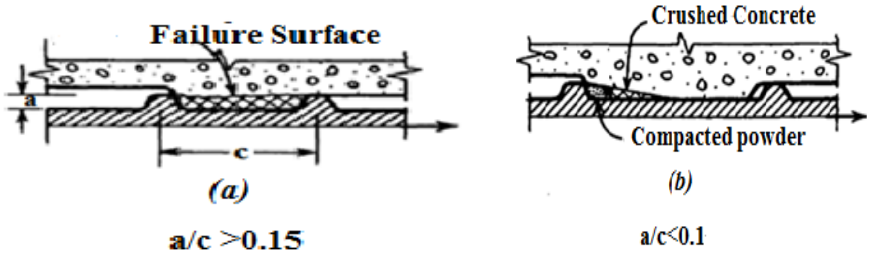

Fig.2.1: Failure mechanism at the ribs of deformed bars (Park and Paulay 1975).

At the initial stages of corrosion, load-slip curve becomes stiffer, which improves the friction at interface (Bhaskar et al. 2010). After that, the stiffness reduces consistently as the corrosion level increases. In the case of severe localized corrosion, the bond behaviour is influenced by the severely deteriorated reinforcing bar ribs, by the lubricating effect of the flaky corroded metal on the reinforcing bar surface and by the reduced confinement of the reinforcing bar due to the widening of the longitudinal crack resulting from corrosion.

vi. Availability of Oxygen

Investigations by Shalon and Raphael (1959) indicate that the rate of steel corrosion is very slow even though chlorides are present if the concrete is continuously water-saturated. The presence of oxygen is an essential factor for the corrosion of iron in concrete. In the case of concrete saturated with water, the diffusion of oxygen is strongly affected by the degree of saturation. This effect is best demonstrated in the work of Griffin and Henry (1963). The level of corrosion increases as the sodium chloride concentration increases until a maximum concentration is reached, beyond which the rate of corrosion decreases despite the

increased chloride concentration (Fig.2.2). This is due to the reduced solubility and hence the availability of oxygen to sustain the corrosion process.

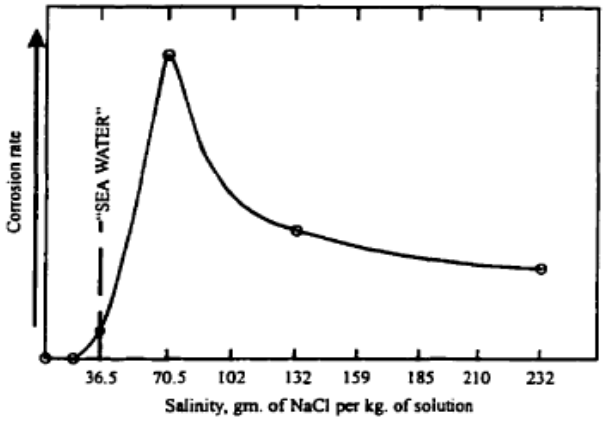

Fig.2.2: Effect of concentration of sodium chloride on corrosion rate (Griffin and Henry 1963)

vii. Relative Humidity and Temperature:

Within 50–100% relative humidity, the increase of environmental relative humidity decreases carbonation of concrete. Within 50–30% relative humidity, a decrease in environmental relative humidity may not cause a decrease in carbonation of concrete especially in normal concentration of CO_2 even after a long period of exposure. If the situation is conducive for corrosion to take place, the corrosion rate is increased by high temperature and high humidity, which will have an increase impact on the bond (Ahmad, 2003).

2.3 TYPES OF BOND STRENGTH

Bond strength can be determined using either Flexure bond (beam) or Anchorage bond (pullout) specimens. Bond values derived from pullout tests cannot be applied in general to design of concrete beams (Lutz, 1978).

Lutz (1978) specified the difference between bond values obtained from pullouts and beams. Although the longitudinal bars develop bond stresses along the

reinforcing bars in both beams and pullout specimens, there is a basic difference in cracking phenomena. In pullout specimen, concrete will be in compression. But in case of beam specimens both steel and concrete will be in tension. As steel stresses increase, transverse cracks develop and each new transverse crack tends to initiate a new longitudinal crack. But in case of pull out specimens, transverse cracks are absent entirely and cracking observed is the longitudinal splitting.

The present research mainly concentrates on the effect of corrosion on bond strength; hence detailed review of literature on anchorage and flexural bond strength behaviour are presented below.

2.4 EFFECT OF CORROSION ON ANCHORAGE BOND STRENGTH

Study on influence of sodium chloride (NaCl) on bond between the reinforcing steel and the concrete was carried out by Sakamoto and Iwasaki (1982). Accelerated corrosion technique was induced on the cube specimen of size (150mmx150mmx150mm) with 16mm diameter reinforcing bar. Molten zinc was maintained at a temperature of 460°C and immersion time was 30 seconds. Curing temperatures of 20°C, 40°C and 50°C were used. From the study they concluded that zinc coating is an effective means to protect the reinforcing steel from the attack of chlorides.

Pullout tests on cubic concrete specimen of size 150mm×150mm×150mm were performed by Al-Sulaimani et al. (1990). Specimens were reinforced with a centrally embedded rebar of 10mm, 14mm and 20mm diameter to give cover-to-bar diameter ratios of 7.50mm, 5.36mm and 3.75mm respectively. Corrosion process was achieved by impressed current technique. Ultimate bond strengths have been reported for pre-cracking, cracking and post-cracking corrosion stages as a function of corrosion percentage.

Laboratory investigation on influence of reinforcement corrosion on bond strength of deformed bars, using beam specimens was undertaken by Cabrera and Ghoddoussi (1992). Specimens were made with Ordinary Portland Cement

(OPC), and pulverized fly ash. Specimens were cured in simulated hot dry environments (35°C and 45 percent relative humidity). To achieve different levels of corrosion, a voltage of 3 volts versus saturated calomel electrode was impressed to accelerate the corrosion process. From the results, relationships between bond strength and corrosion rate were determined. Influence of corrosion on cement types and bond strength were reported.

Rodriguez et al. (1994) studied the corrosion of reinforcing bars and service life of RC structures for corrosion levels of 0% to 0.38%. Average bond strengths and their standard deviation have been reported for different corrosion levels.

Effect of corrosion on bond strength on concrete specimens of size 152mm×254mm×279mm was carried out by Almusallam et al. (1996). Rebar of 12mm diameter having an embedment length of 102mm was used for the study. Corrosion percent was varied from 0% for control specimens to 80% for other specimens. Degree of corrosion was measured as gravimetric loss in weight of reinforcing bars. Ultimate bond strengths have been reported as a percent loss in weight of the reinforcing bar.

Jhy-Chang (1999) has studied the degradation of bond strength between rebar and concrete due to the impressed cathodic current. Results show that bond strength decreases with increase in current density and polarization time.

Corrosion influence on bond between steel and concrete was studied by Amleh and Mirza (2000**)**. Each specimen was reinforced with a centrally embedded rebar of 20mm diameter. During corrosion process specimens were immersed in 5% NaCl electrolyte solution. Corrosion percent was varied from 0% for control specimens to 17.5% for other specimens. Impressed current technique was used to accelerate the process. Results obtained have been reported as a function of corrosion percentage.

Experimental investigation on bond behaviour of corroded reinforcement bars were conducted by Auyeung et al. (2000). Prism size of 175mm×175mm×350mm

was considered for the study. Each specimen was reinforced with two 19mm mild steel bars (one long bar and one short bar). To aid corrosion, 3% chloride based admixture was added to the concrete mixture. During corrosion process, specimens were fully immersed in salt solution and accelerated corrosion was achieved by direct current technique. The corrosion percent was varied from 0% for control specimens to 5.91% for other specimens. Bond strengths have been reported as a function of percent mass loss.

Lee et al. (2002) performed a test to understand the bond properties between concrete and reinforcement as a function of the degree of reinforcement corrosion. An equivalent of 1.45%–2.10% chloride ions by weight of cement was added to the concrete to accelerate the corrosion process. During corrosion process cube specimens were fully immersed in 3% sodium chloride solution. Impressed current technique was used to induce corrosion levels of 0% for control specimens to 30% for other specimens. Amount of rebar corrosion was reported as the percent loss of metal relative to original rebar weight. Maximum bond strengths have been reported as a function of percentage corrosion for different concrete strengths.

Corrosion influence on bond in reinforced concrete was studied by Fang et al. (2004). Concrete cube specimens of size 140mm×140mm×180mm were used for the study. Specimens were reinforced with a centrally placed reinforcing bar of 20mm diameter. Both smooth and deformed bars were used for experimental program. Specimens were tested with and without stirrups. Embedded length to bar diameter ratio was chosen as 4.0. Specimens were immersed in 5% sodium chloride solution for 3 days before subjecting to accelerated corrosion. During impressed current technique process specimens were fully immersed in sodium chloride solution. Corrosion percent was varied from 0% to 9%. Amount of corrosion was measured as loss in weight of reinforcing bar. Bond strengths have been reported as a function of percentage corrosion.

Fang et al. (2006) carried out the study on the effect of corrosion on bond in reinforced concrete under cyclic loading for both confined and un-confined specimens. Corrosion percent was varied from 0% to 6%. Deformed steel bars of 20mm diameter and 420mm in length were used. For specimens with lateral confinement, rectangular closed stirrups were placed at a spacing of 40mm. An electrolyte corrosion technique was used to accelerate the steel corrosion. Specimens were immersed in 5% NaCl solution. In order to measure the slip more accurately, one Crack Opening Displacement (COD) gauge was used during loading, when the slip was less than 0.2mm. Linear variable differential transducer (LVDT) was used all time during loading. Results were compared between the FE analysis and experimental study.

Bond strength prediction for reinforced concrete members with highly corroded reinforcing bars has been studied by Chung et al. (2008). Tests were conducted on 100mm×200mm cylinder specimens, with centrally placed 13mm diameter deformed bar. Chloride admixture was used to aid corrosion and air entraining admixture was used to simulate the concrete used in outside environment. To induce electric current to the specimens, they were completely immersed in 3% NaCl solution. Corrosion levels up to 10% were carried out for both pre-corrosion and post-corrosion methods. Amount of corrosion was expressed as a percentage of mass loss in comparison to the control bar. Bond strength initially increased up to a maximum value, but eventually decreases for greater levels of corrosion. Bond strengths of pre-corroded specimens were less than those of post-corroded specimens.

2.5 EFFECT OF CORROSION ON FLEXURAL BOND STRENGTH

Experimental study on bond of concrete reinforcing bars was conducted by Clark (1949) as a part of work for National Bureau of Standard (NBS). Results were compared for beam and pull out test study. Beam specimen of size (8in ×18in× 78in) with two notches of size 6in long and 3in high were provided near each end to expose the rebar. Specimens were held in the bar cast with 2in from the top of the mould for half of the specimen. Other half of the specimens were bottom cast. Dial gauge attached with a screw to the concrete at the edge of the notch to measure the slip in

the bar directly under the load (loaded end slip). Load points were adjusted corresponded to the three lengths of embedment of the bar. Dial gauges fixed at each end of the beam to measure the free end slip at the end of the bar.

Pull-out specimen of cross section (8in × 9in) and length varied as 8in, 12in and 16in. Two specimens were cast with bars in a horizontal position, in an 18in depth of mould, with one bar held near the bottom and one near the top comparable to the positions in the beams. Slip at the free end was read directly from the gauge. Bond stresses of values 0.01in slip at the loaded end and 0.005in slip at the free end were considered for the study.

Based on the study it was reported that bond strength results of both tests were affected similarly by changes in the geometry of the bars. Bond strength results have been greater for the bottom bars than the top bars of the specimens as cast.

Paul (1978) carried out the top bar effect study on simply supported beams with central point loading. Overall performance of the beam was exemplified in load deflection curves. Experimental results were compared with the theoretical predictions obtained from general flexural theory assuming perfect bond. Comparison of the load deflection responses indicate that specimens with bottom cast bars were stronger, stiffer and fail in a more ductile manner than their companion specimens with top cast bars.

Kayyali and Yeomans (1995) carried out laboratory study on bond-slip behaviour of coated reinforcement in concrete. Beam specimens of size 160mm×320mm×1500mm were cast. Beam specimens were reinforced with black steel bars, ribbed black steel bars and fusion bonded epoxy coated ribbed bars. Deformed bars of diameter 16mm were used as main bars and stirrups of 12mm diameter bars and plain bars of 10mm diameter was used as hanger bar. LVDT was used for the measurement of slip. Slip values of 0.01 and 0.02mm and corresponding loads were noted. For beams reinforced with ribbed bars, black steel and galvanized steel bars, it was reported that there was no significant difference in the value of the load at both 0.01mm and

0.02mm slip. In contrast, for epoxy coated bar, slip increment was significantly lower, of the order of 15-20%, than that for both the black steel and galvanized steel.

Corrosion effects on bond strength in reinforced concrete were studied by Stanish (1997). Slab specimen of size 350mm×150mm×1300mm was used. The centre portions (700mm) were debonded using pipe insulation. Two types of concrete mix were used: normal mix cement with 25% slag replacement by mass, and silica fume mix with 25% slag replacement by mass. Corrosion levels of 2%, 5%, 8% and 10% were induced using impressed current technique. LVDTs were used to monitor the midpoint deflection and to measure the curvature over the constant moment region. At minimal corrosion levels of 2% and 3%, cracking and spalling of the concrete in the end regions were observed for the centre debonded and uncorroded specimens. It was also suggested to use single bar instead of three bars to reduce the problem of differential corrosion.

Experimental study on bond characteristics of corroding reinforcement in concrete beams was undertaken by Mangat and Elgarf (1999). Reinforced concrete beam specimens of size 100mm×150mm×910mm were used. Each specimen comprised of two half lengths of the beam, interconnected at the bottom by two deformed steel bars, each of 10mm diameter and 1100mm length. A steel hinge was provided, near the top portion to allow rotation of the concrete blocks according to RILEM (1973) recommendations. After 15days of curing each specimen was subjected to accelerated galvanic corrosion in 3.5% NaCl solution. Corrosion was induced to obtain different levels of rebar diameter loss of 0, 0.3, 0.5, 1, 2 and 5 percent by impressed current technique. After the corrosion process, the specimens were returned to the water spray chamber to resume curing until the test age of 28days.

Beam specimens were tested under two point loading to determine the load-slip curves. Shear failure was prevented by providing two external steel collars. At each load increment, slip was measured at the start and at the end point by LVDT. Results indicated that bond strength of corroding reinforcement occurs at 0.4% of corrosion. Longitudinal cracks induced by corrosion up to 0.4%, along the reinforcement do not exceed 0.05mm. At low levels of corrosion up to 0.4%, for free end slip of 0.12mm,

maximum load remains constant and then increases linearly with increasing degree of corrosion. Beyond 0.4% degree of corrosion, bond strength decreases sharply.

Jin Wei-liang and Zhao Yu-xi (2001) investigated the effect of reinforcement corrosion on the bond behaviour and bending strength of reinforced concrete beams. Tests were conducted on 100mm×100mm×100mm cubic concrete specimens, with 12mm diameter plain and deformed bars of 80mm length embedded centrally. During corrosion process specimens were fully immersed in 5% sodium chloride solution. Accelerated corrosion was achieved by impressed current technique. From the study it was concluded that the bond strength of plain bars and concrete initially increases with increasing corrosion. Bond strength of deformed bars and concrete increases with corrosion up to a certain amount, but with progressive increase in corrosion, bond strength decreases while the cracking of concrete cover seems to have no effect on bond strength.

Kazim and Yildirim (2003) performed a study on bond strength of reinforcement in splices in beams. Beam specimens of size 180mm×270mm×1900mm were cast, each beams were designed to include two bars in tension, spliced at the centre of the span. The reinforcing bars of 12mm, 16mm and 22mm diameter were used. The splice length of 235mm was selected such that the bar would fail in bond, splitting the concrete cover in the splice region, before reaching the yield point. Beams were tested as simply supported over a length of 1730mm. Deflection readings were noted using a dial gauge and flexural cracks were marked. Based on the study it was concluded that the bond strength increased with reduction in diameter of the rebar. As the bar diameter of tension splice increased, stiffness of the beam increased but ductility of the beam reduced.

Experimental investigation on dynamic interaction (bond slip) of reinforcement with concrete was carried out by Weathersby (2003). Specifically, the effects of concrete confinement, bar deformation and bar diameter on the bond slip, and the influence of loading rates - static to impact effects were investigated. Additionally, the variation of strain along the length of the steel bar and strain transfer to the concrete were investigated. Finite element analyses were performed using the experimental

parameters to determine the value of the chemical adhesion and to compare the experimental results with the analytical values. Results of the study have shown that, for the concrete and steel used in this investigation, the stress due to static friction and chemical adhesion was 960psi for quasi static loading, 2600psi for dynamic loading and 3200psi for impact loading. It was also observed that the steel bar deformations accounted for 70% to 77% of the total resistance to pullout regardless of loading rate. Impact loaded specimens had nearly twice the pullout resistance of the quasi statically loaded specimens. Development length decreased as the loading rate or confinement increased. Bond stresses obtained for both smooth and deformed bars were in good agreement with results obtained in earlier studies involving quasi-static tests.

Ichinose et al. (2004) presented the size effect on bond strength of deformed bars. It was observed that size effect without confining reinforcement was larger than with reinforcement, which was observed both in pull out as well as beam specimen (lap splice test). Larger bond strength was observed in lap splice specimens without confinement than that of pull out test. Large size-effect was roughly equal to that predicted by linear elastic fracture mechanics, and was observed for the pullout specimens without stirrups and with thin cover concrete. Size-effect diminishes as the confinement effects were increased, either due to the increase in cover concrete or with addition of stirrups.

Study by Craig and Soudki (2005) shows post-repair performance of corroded RC beams repaired with Carbon Fiber Reinforced Polymer (CFRP)**.** Beam specimens of size 150mm×250mm×2000mm were used. Bond lengths were varied to examine the effectiveness of CFRP confinement. Beams were designed to fail either by flexure or bond. Bond lengths were controlled at 450mm, 350mm and 250mm. Bond length of 250mm was designed to fail by bond splitting for the uncorroded state. To investigate post-repair behaviour, the specimens were subjected to various corrosion levels of 2%, 5%, 10% and 15% prior to the application of the CFRP laminates. Intermediate bond length of 350 mm, was corroded to the highest degree of post-repair corrosion to investigate the section behaviour at higher levels of mass loss. Specimens were tested to fail in four points bending using the configuration. Specimens were simply

supported over a span of 1800mm; with a constant moment region measuring 300mm. LVDT was used to determine the free end slip value.

Researchers observed that, bond length of 450mm was able to achieve yielding of reinforcing bar prior to loss of load carrying capabilities. Lack of confinement around the reinforcing bar was evident as the concrete cracked and was displaced in the bond region. In terms of overall behaviour, beams repaired at 5% mass loss show a similar trend to those repaired at 2% mass loss. A free end slip of 0.07mm was recorded at the time of failure. Slip initiation occurred at a bond stress of 3.60N/mm^2, which demonstrates a 28% reduction in bond stress at slip initiation relative to the theoretical maximum bond stress.

Vidal et al. (2006) made observations on the reinforced concrete elements which were stored in a chloride environment for 17 years under service loading in order to be representative of real structural conditions. Study concluded the structural performance i.e., stiffness under flexure under service load was mostly affected by the corrosion of tension reinforcement (steel cross-section and the steel–concrete bond reduction). Limit-state service life design based on structural performance reduction in terms of serviceability showed that the propagation period of the corrosion process is an important part of the reinforced concrete service life.

Values of development length obtained using ACI 318: 1999, BS 8110: 1985 and IS 456: 2000 were compared and reported for studies on bond strength in RC flexural members by Shahiq et al. (2007). From the study it was observed that the value of development length obtained in tension using IS Code was 8 percent more as compared to BS Code and 11 percent more as compared to ACI Code, while the development length obtained in compression using IS Code was 3.5 percent more as compared to BS Code and 17 percent more as compared to ACI Code.

Study on the effect of corrosion on reinforcing steel for flexural and shear strength were conducted by Val (2007). Study included subsequently reliability investigation of reinforced concrete beams. Results showed that corrosion of stirrups, especially pitting corrosion, has a significant influence on the reliability of reinforced concrete

beams. Paper considered the effect of general and pitting corrosion on the reliability of RC beams. Two possible modes of failure in flexure and shear were taken into account. Results demonstrated that for the assessment of the performance of RC beams in corrosive environment, we should include consideration of effect of corrosion of stirrups on the shear resistance of a beam; otherwise reliability of the beam may be significantly overestimated.

Laboratory study on bond strength of tension lap slices in full-scale Self Compacting Concrete (SCC) beams were performed by Kazim et al. (2009). From the results it was reported that higher bond strength was obtained for the beams of SCC for both 16mm and 20mm diameters. Finally, although the compressive strength of concretes was almost the same and there were slight differences between the diameters of lap-spliced bars, the normalized bond strengths of the SCC mixes were about 4% higher than those of the Normal Concrete mixes for both bar diameters, indicating that the reinforcing bar was completely covered by SCC due to its filling ability.

Hammoud et al. (2010) conducted an experimental study to addresses the effect of repeated and monotonic loading on the bond of reinforced beams. Three beams were loaded monotonically. Corroded beams were strengthened and subjected to fatigue loads. Strengthening of the beam was done using CFRP sheets. From the study it was concluded that concrete above the bar held by stirrups crushed and resisted slipping, whereas concrete below the bar with no stirrups to hold them split. So concrete above the bar helped in resisting relative slip and the concrete below the bar contributed nothing to resist slip. Other interesting results include the linear relationship between the life of beam and the load applied, and drastic increase in the static capacity on strengthening.

Mehmet et al. (2010) studied the influence of Normal Concrete (NC) and Self Compacting Concrete (SCC) in the bond strength of tension lap sliced bars. Cement was partially replaced by 5%, 10%, 15% and 20% of Silica Fume (SF). Beam specimens of size 200mmx300mmx2000mm were used. Reinforcing bars (20mm) were used with a 300mm splice length as tension reinforcement. Transverse reinforcement of #10 of 80mm c/c was provided and the hanger bar of 12mm was

used for the study. From the study it was found that the bond strength of reinforcement embedded in SCC beams were higher than that of the reinforcement in NC beams, whilst bond strength increased with the increase in replacement of silica fume. Moreover, the beam specimens produced from SCC containing 5% SF had highest normalized of 1.07 followed by SCC beams 10% SF, 15% SF, 20% SF and NC beams.

Experimental study on accelerated life test of concrete in a chloride environment with chloride ion migration equipment was conducted by Zhang and Ba (2011). Chloride concentration in the anode chamber had an approximately linear relationship and increased with the testing time after a different stage. Study concluded that the service life of 10mm concrete cover in chloride environment was between 11.89 and 12.45 years.

2.5.1 Flexural bond strength on epoxy coated and FRP Bars

Bond strength of epoxy-coated reinforcing bars study was performed by Treece and Jirsa (1987). Bond strength was determined by splicing bars in the centre of each beam. Majority of the specimens were cast with bars in the top position to place the splice under the worst bond condition. Two specimens were bottom cast, to determine the effect of casting position on the bond strength of epoxy-coated reinforcing bars. Flexural cracks were usually first noticed in the constant moment region outside of the splice. As loading continued, cracks formed along the length of the constant moment region and within the splice.

From the study it was observed and reported that depth of cracks in the splice region was noticeably less than the depth of cracks outside the splice. Longitudinal cracks formed in the top cover directly over the spliced bars, but did not form in the side cover; the final splitting pattern was a V-notch failure. Results indicated that epoxy-coated bars developed approximately 65% of the bond of uncoated bars, where as failure was governed by splitting of the concrete cover. Average width of cracks in coated bar specimens were 50% greater than in uncoated bar specimens; comparison

of load-deflection diagrams showed no loss of stiffness when using epoxy-coated bars.

To evaluate the flexural bond characteristics of epoxy coated reinforcing steel in concrete bridge deck slabs under static loading, investigation was carried out by Cleary and Ramirez (1989). Specimens were of size 13ft×2ft×8in slab reinforced with epoxy coated bars of 6mm diameter. Reinforcement was spliced at mid span. In order to study the splitting failure, cover depth was maintained to 2in, splice lengths were 16in, 14in, and 12in. End deflection and centre line deflections were measured with linear variable deferential transformers (LVDT's). At the flexural compression zone side 2in gauges were mounted, two per side to measure the concrete surface strain.

Splitting failure of concrete was observed during the study. It was reported that in one of the test, improper alignment of loading ram caused the ram to displace. In other specimen substantial yielding of steel took place before failure and also it appears that a plastic hinge developed at the splice region. Fewer and wider flexural cracks were observed in epoxy coated steel relative to the companion steel. Significant reduction in the bond strength was observed for epoxy coated bars

Investigations on the influence of several parameters on bond behaviour of straight Glass Fiber Reinforced Polymer (GFRP) rebars in concrete were undertaken by Schicheng (1994). Dial gauge was used to measure the slip at the free-end of the rebar at 0.015in and 0.0025in. From the study it was observed that concrete compressive strength, embedment length, clear concrete cover, concrete cast depth, and radius of bend had significant effects on bond of GFRP rebars to concrete. Confinement factors were also derived to reflect the influence of concrete cover and casting position.

Oh et al. (2008) carried out study on flexural bonding test of deformed GFRP rebar. Test was performed under variable amplitude load with four point bending based on the British Standard. Rebar contained approximately 65% of glass fibers and 35% of epoxy resin by volume. The dimension of beam specimen was 180mmx200mmx1300mm. Bonding length of $5d_b$ (47.6mm), $10d_b$ (95.3mm) and $15d_b$ (142.9mm) were considered based on the nominal diameter of the deformed GFRP

rebar. LVDT was installed at the end of the left and right side of the specimen for measuring the load slip relationship. Test result showed that $5d_b$ rebar had pull-out failure, $15d_b$ was subjected to concrete tensile failure, and $10d_b$ showed both Pull-out and tensile failure. It was also observed that from the point of view of failure pattern and number of cycles, static and constant amplitude fatigue loading test of $15d_b$ deformed GFRP showed better bonding performance than that of $5d_b$ deformed GFRP specimen.

Rteil et al. (2008) studied the influence of CFRP repair of corrosion damaged bond region. Beam dimensions of size 152mm×254mm×2000mm were considered. Corrosion levels of 5% and 9% were studied. Repeated loading caused bond fatigue failure in unwrapped uncorroded beams, but some wrapped corroded beams failed by fatigue of the steel at a corrosion pit. The slip versus number of cycle's curves for the wrapped corroded beams differed from that of the uncorroded unwrapped beams. Repairing with CFRP sheets increased the fatigue bond strength of wrapped beams corroded to 5% and 9% mass loss by 11% and 4% respectively above that of the uncorroded unwrapped beams.

2.6 LITERATURE REVIEW ON FINITE ELEMENT MODELLING OF REINFORCED CONCRETE STRUCTURES

Prevalent finite element models adopted for the nonlinear finite element analysis of reinforced concrete structures are discussed below:

Frank et al. (1973) presented the nonlinear finite element analysis, including the elasto-plastic behaviour of steel, bilinear-elasto-plastic behaviour of concrete and the tension stiffening of concrete. Incremental variable elasticity technique was used to obtain the load deflection for any general RC problem. Need for a shear retention factor to provide the torsion and shear stiffness for cracked concrete was demonstrated in the study.

Lin and Scordelis (1975) in their paper reported the nonlinear finite element analysis of reinforced concrete structures in general form. Analysis was carried out to trace the

load deflection response, the crack-propagation through the elastic, in-elastic, and ultimate load ranges. Layered approach with an incremental tangent stiffness solution technique was adopted. From the study it was observed that tension stiffening effect of concrete between cracks has a significant influence in the post cracking load deflection response of under reinforced concrete structures.

A Brief review of the research in development of nonlinear analytical models was given by Scordelis (1989). Application of a series of different concrete models to the analysis of a number of reinforced concrete panels was described by Crisfield and Wills (1993). Simplified approximate analysis procedures were shown by Vecchio and Tata (1999) to reduce the computational effort. Foster et al. (1996) formulated a rotating crack finite element model for the analysis of reinforced concrete structures. To model concrete and steel discrete element was used. Formulation of bar element was made with incorporation of bond slip values.

Load-deflection responses of reinforced and prestressed concrete beams using finite element analysis were studied by Wolanski (2004). Reinforced concrete beam modeled using ANSYS was compared to experimental data. Analysis for the reinforced concrete beam included: non-linear concrete properties, bilinear steel properties, and the influence of progressive cracking of the concrete. Characteristic points on the load-deformation response curve predicted using finite element analysis were compared to theoretical (hand-calculated) results.

Structural behaviour of corroded and non corroded reinforced concrete beam, with a three dimensional finite element model was considered by Parande et al. (2008). Non linear finite element analysis was performed using ANSYS program. Beam specimens had been cast with M20 concrete and were tested for flexural strength. Comparison between ANSYS prediction and field data were made in terms of deflection, stress-strain and crack pattern of concrete beam.

Saether and Sand (2009) carried out a study on the application of finite element analysis to simulate the mechanical behaviour of reinforced concrete members with corroding steel bars using finite element program (DIANA). Since only effects of

corrosion were taken into consideration, loss of steel bar section, and reduced bond between deteriorated concrete and corroded rebar were accounted. Validation of the simulations were limited to the study of medium scale beams and based only on the results of previously published laboratory investigations. Failure loads of beams from the finite element simulations were found to be in good agreement with the experimental values.

Phuvoravan (2010) made observations on the effect of steel corrosion level on flexural behaviour of RC beams by performing nonlinear finite element analysis. Concrete was modelled as three dimensional solid elements while all steel reinforcement was represented by truss elements having nonlinear property for both materials.

Finite element analysis could be used to realistically predict the flexural behaviour of reinforced concrete beams having various reinforcement corrosion levels. From the study it was concluded that, for corrosion of reinforcement in the middle portion of RC beam, percentage reduction in moment capacity was approximately same as that of percentage of corrosion level. But for the whole length of RC beam, the percentage reduction in moment capacity was significantly greater than percentage of corrosion level.

Sen et al. (2010) developed layered shell elements for the modelling of reinforced concrete structures. Element consists of a number of bonded layers of orthotropic materials. In the nonlinear analysis, strain value differs for different sandwich layers when it was subjected to bending. Layered approach was used to manage the constant strain across its thickness. Sen et al. (2010) proposed a degenerated nine node, two dimensional, curved iso-parametric elements with five degrees of freedom at each node, for the modelling of reinforced concrete structures.

To evaluate the effective shear reinforcement pattern and to compare the variation in behaviour of reinforced concrete beam with and without shear reinforcement simulation was carried out by Saifullah et al. (2011). Numerical results were

compared with the theoretical results. From the study it was concluded that web reinforcements were effective for static loading condition.

Finite element investigation on the load carrying capacity of corroded RC beam of size 500mm×100mm×150mm was carried out based on the bond slip between the steel bars and concrete by Xiaoming and Hongqiang (2012). In these models, element of Solid 65 was used to simulate concrete, element of link 8 was used for bars and element of combin39 was adopted to simulate the bond-slip between bars and concrete. Researchers reported that as the corrosion rate increases the stiffness of the corroded beam would decrease, slip between bars and concrete was larger and ductile failure of RC beam was turned to brittle failure. Load carrying capacity of corroded RC beam deteriorates and descending speed was fastest when the corrosion rate falls in the range of 4% to 7%.

2.7. NATIONAL BUREAU OF STANDARD (NBS) BEAM

National bureau of standard procedure provides flexibility in the design of the recommended test specimen and permits the use of different sizes of bars, different concrete strengths and longer embedment lengths needed to develop stresses equal to the high yield strengths of deformed bars. Later with few modification NBS beam was adopted by the ACI committee 408 (1964), as a recommended specimen usually termed the hammer head beam.

Beams have a variable length and shear span and were designed to permit the measurement of the average value of bond stress and the slip at the loaded portion of the bar between supports and load points. The beams were provided with T-shaped ends in order to shift the reactions to point where they would not contribute to the restraint of longitudinal splitting (Paul, 1978). Fig.2.3 shows the plan and elevation of NBS beam.

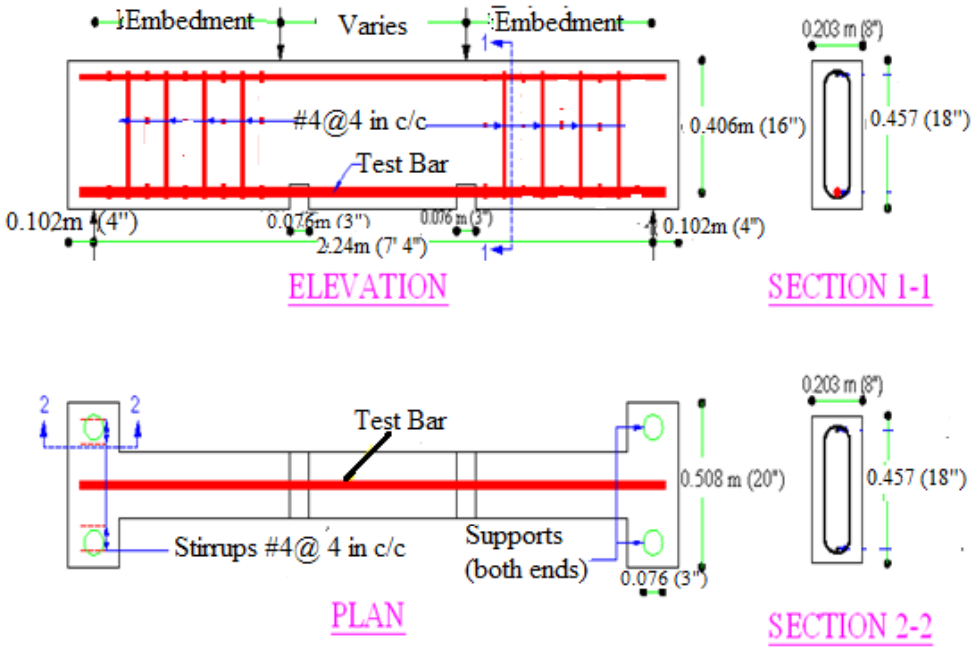

Fig.2.3: National bureau of standards bond beam (Paul, 1978)

2.8 SUMMARY OF LITERATURE REVIEW AND PROBLEM IDENTIFICATION

Critical literature review reveals that exhaustive work has been done on bond between steel and concrete. The works mainly concentrate on splice lengths, variation of bond strength with different types of steel reinforcement and concrete.

Free end slip, invariably has been considered as bond failure ('slip' is the differential displacement between steel and concrete). Vast majority of work is on anchorage bond rather than on flexural bond. Though studies on bars coated with corrosion protection measures have been carried out for bond characteristics, little work has been carried out and reported on the performance of corroded reinforcement.

It has now been understood and accepted that of embedded steel (intersection exposed to air and moisture) corrodes faster than exposed. This fact has made all codes revisit durability provisions. To understand the performance of structures there is a need to study the rate at which different corrosion levels occur.

2.9 SCOPE AND OBJECTIVES OF THE PRESENT WORK

Study emphasize on the effect of corrosion on bond strength. Corrosion rate is an important parameter for quantitatively predicting the service life of reinforced concrete structures. The review of past literature has prompted this research plan, where it has been envisaged to study the performance of TMT (Thermo Mechanically Treated) bar in bond with concrete for anchorage bond and flexural bond study. It has been proposed to make test specimens with OPC (Ordinary Portland Cement) and PPC (Portland Pozzolona Cement) to appraise the claim that PPC is superior to OPC in terms of durability. Accelerated corrosion (not natural corrosion) technique is adopted for the study to induce the corrosion process.

A two phased experimental program is adopted for the research. In the first phase, to understand the process of corrosion, study on anchorage bond is reported. Second phase deals with the studies on the effect of different corrosion levels on flexural bond strength of NBS RC Beams.

Following are the highlights of the study:

1. Impressed current technique is adopted to achieve accelerated corrosion.
2. Cylindrical specimens are used to determine anchorage bond strength test
3. National Bureau of Standard (NBS) test beam specimens are employed to determine flexural bond strength.
4. Different corrosion rates and two types of cements namely OPC and PPC are being considered for the study.
5. Experimental results are compared with those based on numerical modeling.
6. Empirical prediction models are suggested for estimation of bond strength characteristics of RC elements under different stages of corrosion damage.

CHAPTER 3

EXPERIMENTAL INVESTIGATION

3.1 GENERAL

The present investigation is undertaken to study the effect of corrosion on anchorage and flexural bond strength subjected to different corrosion levels. This chapter describes the details regarding qualification of the constituent materials, concrete mix design, preparation of test specimens and accelerated corrosion technique and corrosion measurement using non destructive applied corrosion monitoring instrument. Test set up and procedure followed to determine the bond strength values are also presented in this chapter.

3.2 EXPERIMENTAL METHODOLOGY FOLLOWED FOR ANCHORAGE BOND STRENGTH (PHASE-I)

To appreciate the process and effects of corrosion on RC members, preliminary study was carried out on cylindrical specimens.

3.2 .1 Materials

The properties of materials used in the present investigation are explained below:

(A) Cement: In this investigation commercially available 43 grade Ordinary Portland Cement (OPC) conforming to IS: 8112-1989 and Portland Pozzolana Cement (PPC) was used. Cement was tested as per IS: 4031-1988 and IS 1489 (Part-I):1991 for OPC and PPC concrete respectively. Test results confirm the requirement as per IS code. Test results are presented in Tables 3.1 and 3.2.

(B) Fine and Coarse Aggregate : Fine aggregate (sand) was sourced from local river. Physical tests on fine aggregates were conducted as per IS 2386 (Part III):1968. Test results are tabulated in Table 3.3.

The siliceous coarse aggregates of 20mm and 12.5mm size were obtained from local quarries. These fractions were taken in 1:1 proportion. The grading of 20mm and 12.5mm size aggregate was as per IS 383-1970. Test results are tabulated in Table 3.4.

Table 3.1: Physical Properties of OPC

Sl No	Test Parameters	Results	As per IS 4031:1988 (Specifications of 43 Grade OPC)
1	Initial setting and final setting time	68min and 250min	Not less than 30 min. and not more than 600 min
2	Specific gravity	3.14	
3	Compressive strength:		
	3 Days	26.6 N/mm^2	Not less than 23 N/mm^2
	7 Days	36.4 N/mm^2	Not less than 33 N/mm^2
	28 Days	45.8 N/mm^2	Not less than 43 N/mm^2

Table 3.2: Physical Properties of PPC

Sl No	Test Parameters	Results	As per IS 1489 (Part-I): 1991 (Specifications of PPC)
1	Initial setting and final setting time	70min and 250min	Not less than 30 min. and not more than 600 min
2	Specific gravity	2.92	
3	Compressive strength:		
	3 Days	16.5N/mm^2	Not less than 16 N/mm^2
	7 Days	25.5 N/mm^2	Not less than 22 N/mm^2
	28 Days	37.8 N/mm^2	Not less than 33 N/mm^2

Table 3.3: Test result of fine aggregate used for concrete mix

Cement Types	OPC	PPC
Specific gravity	2.56	2.6
Water absorption	2.61%	2.00%
Moisture content	2.00%	2.00%
Grading	Zone-II	Zone-II

Table 3.4: Test result of coarse aggregate used for concrete mix

Specific gravity	2.69
Shape	Angular
Water absorption	0.50%
Moisture content	Nil

(C) Reinforcing Steel: In the present investigation, to study the effect of reinforcement corrosion, Fe-415 grade of Thermo Mechanically Treated (TMT) rebar of 16mm diameter was used. From the tensile strength test, yield strength and ultimate strength values are 470N/mm^2 and 550N/mm^2 respectively.

(D) Water: Water is an important ingredient of concrete as it actively participates in chemical hydration reaction of cement and pozzolanic reaction. In this investigation, potable water has been used for producing concrete and for curing.

3.2.2 Concrete Mix Design

For the present study M20 grade concrete and water cement ratio of 0.5 was used. Slump ranges of 90-100mm were selected for the study. Mix design calculations were followed as per as per IS 10262:2009. To get the desired slump 0.6% of commercially available chemical admixture was added. Mix proportion of OPC and PPC concrete are given in Table 3.5 and Table 3.6 respectively.

Table 3.5: Mix proportion of OPC concrete

Ingredients	Quantity
Cement	320kg/m^3
Fine aggregate	726 kg/m^3
Coarse aggregate	1168 kg/m^3
Water	160 kg/m^3
Mix Proportion Ratio C : F.A : C.A : W	1: 2.27: 3.65: 0.5

Table 3.6: Mix proportion of PPC concrete

Ingredients	Quantity
Cement	330kg/m^3
Fine aggregate	817 kg/m^3
Coarse aggregate	976kg/m^3
Water	170 kg/m^3
Mix Proportion Ratio C : F.A : C.A : W	1 : 2.45 : 2.95 : 0.5

3.2.3 Preparation of Test Specimens

Cylindrical specimen of size 150mm×300mm was used for the present study. Test matrix used for the present study is given in Table 3.7. A view of cylindrical specimen casting is shown in Fig.3.1.

Reinforcement of 16mm diameter with 850mm in length was centrally embedded in concrete. Rebar length of 20mm was left projecting outside at the bottom surface to measure the slip. Specimens were cured in water for 28 days. Exposed part of the rebar was covered with M-seal to prevent corrosion at this exposed part. Required gadgetry was connected to the rebar to accelerate and to measure the corrosion process.

Table 3.7: Test Matrix used for anchorage bond study

Type of Test	Bar diameter (mm)	Corrosion Level (%)	Induced corrosion		Total number of specimens
			Type of cement		
			OPC	PPC	
Anchorage Bond	16	0	3	3	6
		2.5	3	3	6
		5.0	3	3	6
		7.5	3	3	6
		10	3	3	6
Compressive strength	7 days	(Controlled cube specimens)	3	3	6
	28 days		3	3	6
Total			21	21	42

Fig.3.1: Casting of cylindrical specimens **Fig.3.2: Accelerated corrosion process**

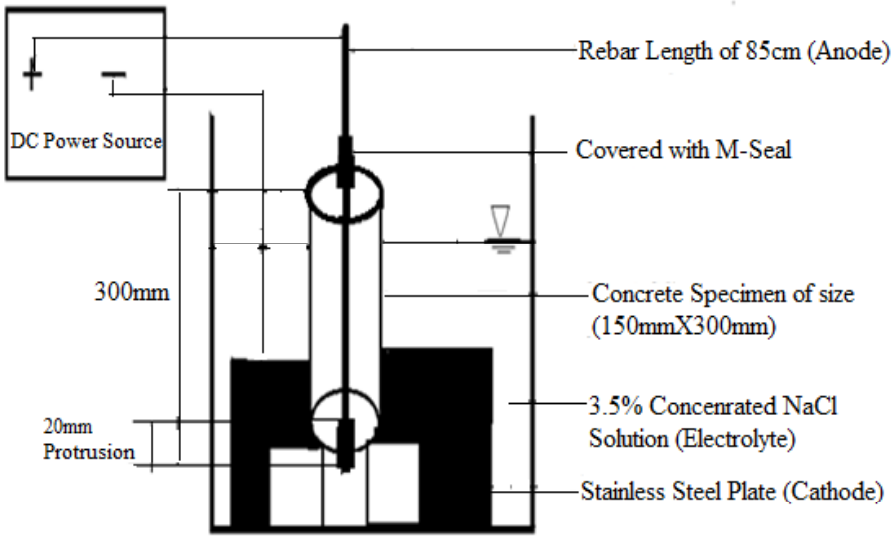

Fig.3.3: Schematic representation of the accelerated corrosion test set up

3.2.4 Accelerated Corrosion Technique

Electrochemical corrosion technique was used to accelerate the corrosion of rebars embedded inside the concrete. To accelerate the corrosion process cylindrical specimen were partially immersed in 3.5% NaC1 solution for 5 days by leaving a clear height 30mm from the top. For the corrosion process to occur both moisture and oxygen are very much essential. For each trial, three specimens were considered. Accelerated corrosion process and detailed schematic representation of the test set-up are shown in Fig.3.2 and Fig.3.3 respectively.

3.2.4.1 Calculation of amount of current required to obtain different corrosion levels:

Current required to achieve different corrosion levels i.e., 2.5%, 5%, 7.5% and 10% can be obtained using Faraday's law. Amount of current to be applied to obtain the required degree of corrosion can be calculated from Eq.3.1 [Ahmad (2009)] as follows:

From Faraday's law,

$$i_{corr} = i_{app} = \frac{\rho \times W_i \times F}{100 \times \pi \times d \times l \times w \times t} \quad (3.1)$$

where,

For cylinder specimen consisting of 16mm diameter reinforcing bar

$$W_i = Initial\ \ weight\ of\ \ steel\ bar [= (0.016)^2 \times (\pi/4) \times 0.85 \times 7850 = 1.3416kg = 1341.6g]$$

$i_{app} = Applied\ \ Current$
$F = 96487\ Amp - \sec$
$l = Length\ of\ the\ bar\ (= 85cm)$
$w = Equivalent\ weight\ of\ iron\ (= 27.925g)$
$\pi dl = \pi \times 1.6 \times 85 = 427.6cm^2$
$t = Time\ in\ \sec onds$
$\rho = Degree\ of\ \ corrosion\ \ percentage$

$$i_{app} = \frac{\rho \times 1341.6 \times 96487}{100 \times 427.26 \times 27.925 \times 5 \times 24 \times 3600} \quad (3.2)$$

$$i_{app} = \rho \times 2.511 \times 10^{-4} \quad (\text{Amps/cm}^2)$$

To calculate the applied current value in ampere (A)

$$i_{app} = \rho \times 2.511 \times 10^{-4} \times \pi dl$$

$$i_{app} = 0.1073 \times \rho\ \ Amps \quad (3.3)$$

Amount of current required to achieve different degrees of corrosion levels for three number of specimens are given in Table 3.8.

Table: 3.8: Amount of Current required to achieve corrosion levels

Degree of corrosion (%)	Current (Amps)	Time required (Days)
2.5	0.81	5
5.0	1.61	5
7.5	2.42	5
10	3.22	5

3.2.5 Corrosion Rate Measurements

After completion of accelerated corrosion process, the corrosion rate for individual cylindrical specimen was measured with applied corrosion monitoring instrument (test set up is shown in Fig.3.4 and Fig.3.5), based on Linear Polarization Resistance (LPR) method.

For the measurement of corrosion level, normal mode of applied corrosion monitoring instrument was switched on. It consists of working electrode which was connected to the rebar, reference electrode and counter electrode which were placed in the salt solution around the concrete specimen is shown in Fig.3.5. Reinforcing steel bar was polarized by applying a small potential shift to it (ΔE) and resultant current (ΔI), between working electrode and counter electrode (Ha-Won song and Saraswathy 2007).

Linear Polarization Resistance (R_p) was determined from the slope of the plot of applied potential versus the measured current. Corrosion current density was then calculated using the Stern-Geary formula.

$$i_{corr} = \frac{B}{R_P} \qquad (3.4)$$

where,

i_{corr} = Corrosion current density (μA/cm^2),

Rp = Polarization resistance (kΩ cm^2),

B = 26 mV for steel in active condition (Fontana, 2005).

Fig.3.4: Corrosion monitoring instrument

Fig.3.5: Corrosion monitoring test set up

Depending on the corrosion rate measured values may be either passive or active. Passive state rate of corrosion of rebar is found to be relatively low in the order of 10^{-9} to 10^{-7}A/cm^2, whereas the active state corrosion rate is found to be relatively high, and in the order of 10^{-6} to 10^{-5}A/cm^2.

3.2.6 Determination of Anchorage Bond Strength

Test procedure was followed according to IS: 2770 (Part I)-(1967).Test specimen was mounted in a universal testing machine (UTM of 400kN capacity) in such a manner that the bar could be pulled axially from the specimen. Test set up used for the study is shown Fig.3.6. Exposed part of the bar at bottom of specimen was attached with dial gauge so as to measure the slip (movement) between the bar and surrounding concrete. It was observed that specimen failed by splitting failure (Fig.3.7). A view of specimen after removal from test set up is shown in Fig.3.8.

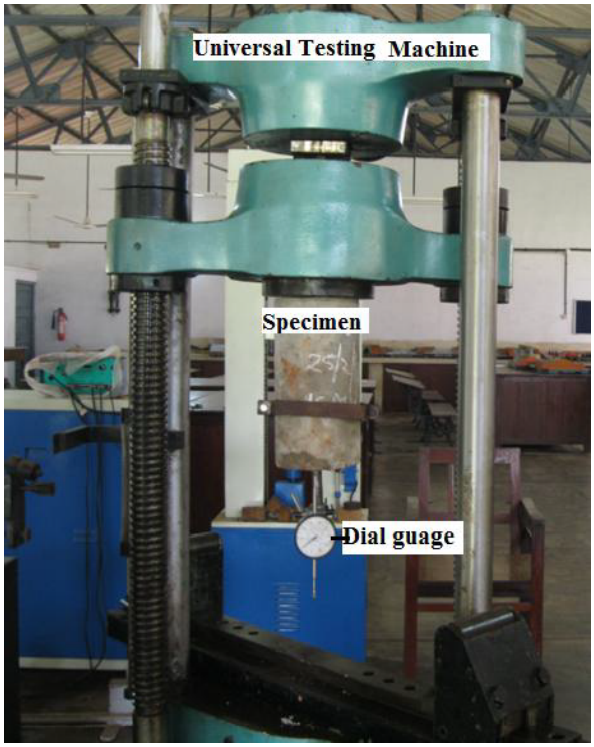

Fig.3.6: Test set up for bond-strength

Applied load and dial gauge readings were noted. Bond stress τ, for each load level was calculated as the average stress between reinforcing steel bar and the surrounding concrete along with the embedded portion of bar, using following relationship:

$$\tau = \frac{P}{\pi \times d \times L_d} \tag{3.5}$$

where,

P = Maximum measured load at 0.25mm slip,

L_d =Embedded length of the reinforcing steel bar (=280mm) and

d = Diameter of reinforcing bar (reduces in its diameter for different corrosion levels).

Reduced diameter values for 0%, 2.5%, 5%, 7.5% and 10% were 15.8mm, 15.6mm, 15.4mm and 15.2mm respectively. Test results are summarized and discussed in Chapter 5.

Fig.3.7: Occurrence of splitting failure

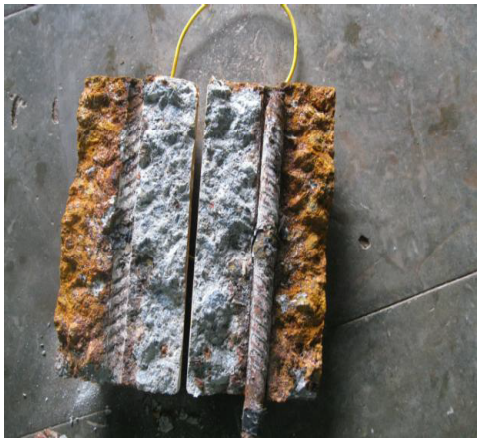

Fig.3.8: View of the specimen after the test

3.3 EXPERIMENTAL METHODOLOGY FOLLOWED FOR FLEXURAL BOND STRENGTH (PHASE-II)

Here RC beam specimens were employed. Effects of different degree of corrosion levels on load deflection curve, crack width and bond stress behavior were studied. For this purpose, a set of three concrete beam specimens were cast for each level of corrosion including controlled specimens. Totally thirty beam specimens were prepared.

3.3.1 Materials

All materials used for the experimental work were tested as per the codal provisions same as that explained in section 3.2.1.

(A) Cement: Test results confirm the requirement as per IS code. Physical properties of cements are presented in Tables 3.9 and 3.10 for OPC and PPC respectively.

(B) Aggregates: Physical properties of fine aggregate were tested as per IS 2386 (Part III):1968 and coarse aggregate were tested as per IS 383-1970 and are tabulated in Table 3.11 and Table 3.12 respectively.

Table 3.9: Test results on physical properties of OPC

Sl No	Test Parameters	Results	As per IS 4031:1988 (Specifications of 43 Grade OPC)
1	Initial setting and final setting time	75 min and 260 min	Not less than 30 min. and not more than 600 min
2	Specific gravity	3.1	
3	Compressive strength:		
	3 Days	24.1N/mm^2	Not less than 23N/mm^2
	7 Days	34.5N/mm^2	Not less than 33N/mm^2
	28 Days	46.9N/mm^2	Not less than 43N/mm^2

Table 3.10 Test results on physical properties of PPC

Sl No	Test Parameters	Results	As per IS 1489 (Part-I): 1991 (Specifications of PPC)
1	Initial setting and final setting time	76 min and 270 min	Not less than 30 min. and not more than 600 min
2	Specific gravity	2.91	
3	Compressive strength:		
	3 Days	16.6N/mm^2	Not less than 16N/mm^2
	7 Days	26.5N/mm^2	Not less than 22N/mm^2
	28 Days	39.8 N/mm^2	Not less than 33N/mm^2

Table 3.11: Test result of fine aggregate used for concrete mix

Specific gravity	2.6
Water absorption	2.00%
Moisture content	5.00%
Grading	Zone-I

Table 3.12: Test result of coarse aggregate used for Concrete mix

Specific gravity	2.8
Shape	Angular
Water absorption	0.50%
Moisture content	Nil

(C) Reinforcing Steel

Tensile strength of reinforcing steel bar was tested using Universal Testing Machine. Stress-strain curves for 25mm Thermo Mechanically Treated (TMT) Fe-415 grade of reinforcing steel bar was obtained by plotting the tension test data. Gauge length of 6.2cm was considered. Typical stress-strain curve for 25mm bar is shown in Fig.3.9. Values of new bar diameters used for the calculation of required length, yield strength, ultimate strength and rupture strength are presented in Table 3.13.

Table 3.13: Yield and ultimate strength of TMT Fe-415 bars

Diameter of Bar (mm)	Yield Strength (N/mm^2)	Ultimate Strength (N/mm^2)	Rupture Strength (N/mm^2)
24.56	485	589	559

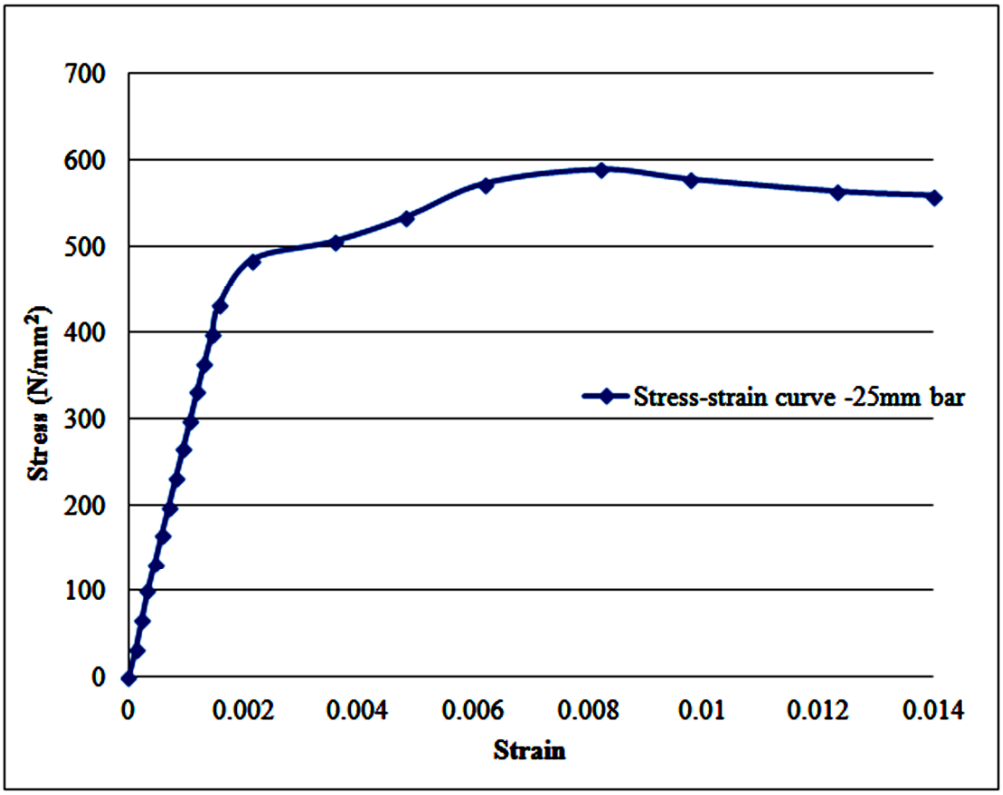

Fig.3.9: Stress-strain curve for 25 mm diameter TMT Fe-415 rebar

3.3.2 Concrete Mix Design

According to the design code IS 456-2000, minimum concrete grade to be adopted in coastal environment is M30 and maximum water cement ratio of 0.45. Hence specified strength of 30N/mm^2 and slump ranges of 50-60mm were selected for the present study. Obtained material test results were used in the calculation of concrete mix design as shown in Appendix A.Trial mixes of OPC and PPC concrete are given in Tables 3.14(a) and 3.14(b) respectively.

Table 3.14(a): Trial mixes of OPC concrete

Name	Cement Brand	Cement Content (Kg/m^3)	Mix Proportions	W/C ratio	Admixture (ml/kg)	Slump (mm)	Average 28 days strength (N/mm^2)
M_1	Ultratech	426	1: 1.6: 2.69	0.45	-	75	35.7
M_2	Ultratech	380	1: 1.93:3.12	0.45	2	55	33.56
*M_3	Ultratech	400	1: 1.77: 2.87	0.45	2	68	38.52

***** Mix recommended for OPC concrete beam specimen preparation

Table 3.14(b): Trial mixes of PPC concrete

Name	Cement Brand	Cement Content (Kg/m^3)	Mix Proportions	W/C ratio	Admixture (ml/kg)	Slump (mm)	Average 28 days strength (N/mm^2)
*M_1	Ultratech	400	1: 1.77: 2.87	0.45	2	58	37.78
M_2	Ultratech	380	1: 1.91:3.09	0.45	2	68	34.52

***** Mix recommended for PPC concrete beam specimen preparation

After several trials, the mix proportion of 1:1.77:2.87 was achieved for both OPC and PPC concrete. An addition of 2ml/kg of commercially available super plasticizer chemical admixture was used to get the desired level of slump.

3.3.3 Preparation of Test Specimens

National Bureau of Standard (NBS) beam specimens of size 2.44mx0.457mx0.203m were used. Design calculation to fix the reinforcement details are given in Appendix B. Specimen size and reinforcement details are detailed in Fig.3.10. A view of NBS beam specimen in AutoCAD is shown in Fig.3.11. Gadgetry required to induce corrosion process and to measure corrosion levels were embedded to the reinforcement before the concrete was poured inside the mould. Total thirty numbers of beam specimens were cast. Test matrix used for the present study is given in Table 3.15.

Table 3.15: Test Matrix used for Flexural Bond Test

Description	**Type of bar**	**Induced corrosion rate (%)**	**Number of specimens**		**Total number of specimens**
			Cement types		
			OPC	**PPC**	
Beam Specimens		**0**	3	3	**6**
	TMT rebar (Thermo Mechanically Treated bars)	**2.5**	3	3	**6**
		5	3	3	**6**
		7.5	3	3	**6**
		10	3	3	**6**
Companion cube specimens	To measure Compressive strength of cubes		6	6	**12**
Cylindrical Specimens	To determine Modulus of elasticity		3	3	**6**
Prism Specimens	To determine Modulus of rupture		3	3	**6**
Total			**27**	**27**	**54**

Formwork with reinforcement cage used for the present work is shown in Fig.3.12 and Fig.3.13. A view of mixing of concrete in concrete mixer is given in Fig.3.14. Measurement level of slump is represented in Fig.3.15. After placement of each layer, concrete was vibrated with needle vibrator (Fig.3.16). A view of concrete finishing work in NBS beam is shown in Fig.3.17. De-moulding of specimen was done after 24 hours of casting and specimens were cured in water for 28 days.

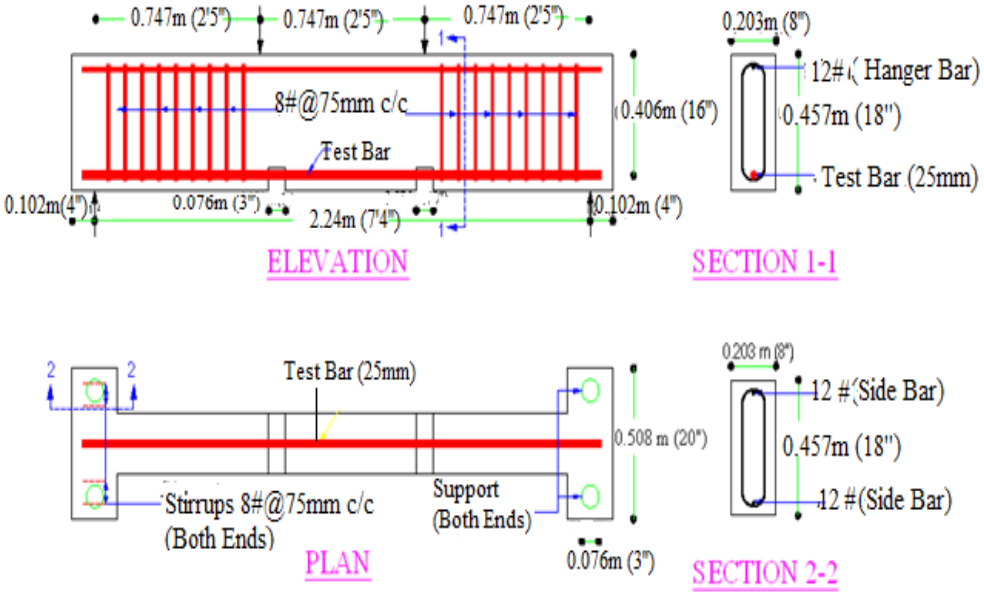

Fig.3.10: Reinforcement details of NBS beam specimen

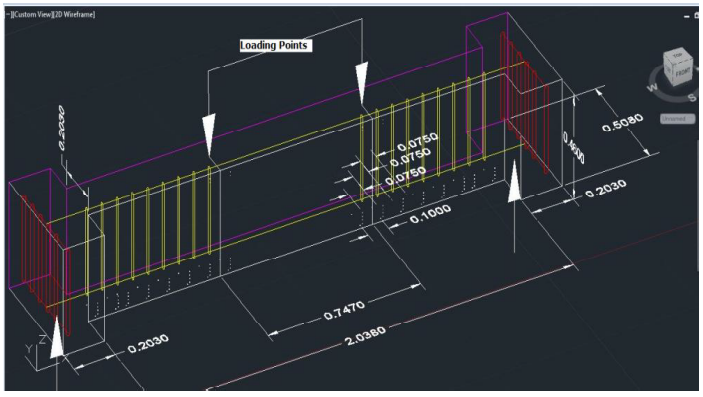

Fig.3.11: A view of NBS beam specimen in AutoCAD

Fig.3.12: NBS beam specimen with Form work

Fig. 3.13: Form work with reinforcement cage

Fig.3.14: Mixing of concrete

Fig.3.15: A view of Slump level

Fig.3.16: Compaction with needle vibrator

Fig.3.17: Concrete finishing work in NBS beam specimen moulds

3.3.4 Preparation of Compressive Strength of Concrete Specimens

To determine the compressive strength of concrete auxiliary specimens were used. Cube specimens (12 numbers) of size 150mmx150mm×150mm were cast and tested [OPC (6 cubes) and PPC (6 cubes)]. Out of six cubes, three cubes were tested on 7^{th} day from the day of casting and three cubes were tested on 28^{th} day. Steel moulds for auxiliary specimens of size 150mm×150mm×150mm as shown in Fig.3.18 (a) were filled in 50mm layers of concrete side by side and were compacted using table vibrator. Top of the control specimens were floated off smoothly in level with the top of moulds as shown in Fig.3.18(b). Cube specimens were demoulded after 24 hours and kept for water curing.

(a) Steel mould for auxiliary specimens (b) After Compaction

Fig.3.18: Cube preparation for determining compressive strength of concrete

Similarly three number of cylindrical specimens (150mmx300mm) and Prism specimen (100mmx100mm×500mm) were cast. After 28 days of curing, specimens were tested as per IS 516-1959, to determine modulus elastcity and modulus of ruptute of concrete respectively, for both OPC and PPC concrete.

Theoretical value of modulus of rupture (N/mm^2) can be calculated from following Equation:

$$f_t = 0.7 \times \sqrt{f_{ck}} \tag{3.6}$$

Theoretical value of modulus of elasticity (N/mm^2) can be obtained from following Equation:

$$E_C = 5000 \times \sqrt{f_{ck}} \tag{3.6a}$$

3.3.5 Accelerated Corrosion Technique

Accelerated corrosion can be accomplished by applying a constant potential or an electric current of constant magnitude to the embedded steel. After curing, specimens were subjected to desired corrosion levels. i.e. 2.5%, 5%, 7.5% and 10%. Electrochemical corrosion technique was used to accelerate the corrosion of rebars embedded in the beam specimens. To simulate the corrosion process, direct current was impressed on rebar embedded inside the concrete specimen using an integrated system, incorporating a direct power supply with an output of 64V and 10 Amps to monitor the current. Test set up consists of 5% NaCl solution in which beam specimens were partially immersed for a duration of 8 days, by leaving a clear height of 20mm from top. For the corrosion process to occur both moisture and oxygen are very much essential. Direction of current was arranged such that, rebars embedded inside the concrete specimen served as anode. Stainless steel plate which was placed along the length of beam functions as cathode. A schematic representation of the test set-up is shown in Fig.3.19. Amount of current to be applied to obtain the required degree of corrosion can be calculated using Faradays law (Eq. 3.1). For each trial, three specimens were considered. Corrosion test set-up used for accelerated corrosion process is shown in Fig.3.20.

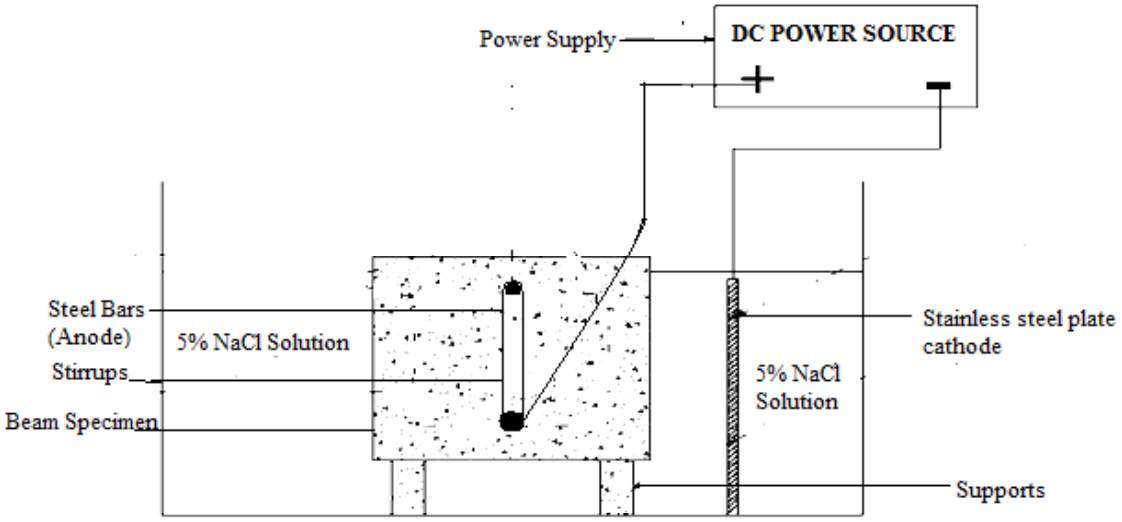

Fig.3.19: Schematic representation of accelerated corrosion of beam specimen

Fig.3.20: Accelerated corrosion of beam specimens

3.3.5.1 Calculation of amount of current required to obtain different corrosion levels:

From Faraday's law from Eq. (3.1) Ahmad (2009)

$$i_{corr} = i_{app} = \frac{\rho \times W_i \times F}{100 \times \pi \times d \times l \times w \times t}$$

For single beam specimen consisting of main bar of 25mm diameter and hanger bar and side bars of 12mm diameter and stirrups of 8mm diameter. Basis can be refered to this from Fonatana, (2005).

W_i= Initial weight of steel (=20,000g)

F=96487 Amp-sec

w= Equivalent weight of iron (=27.925 g)

D_{25}=*Diameter of main bar (25mm) and*

D_{12}=*Diameter of Hanger bar 12mm*

t=time in seconds

$$Area = \pi dl$$

$$Area = \pi(D_{25} + D_{12}) \times L + \pi DL(Stirrups) + \pi DL(Side\,bars)$$

$$Area = \pi(2.5 + 1.2) \times 234 + (\pi \times 0.8 \times 240 \times 26) + (\pi \times 1.2 \times 41 \times 4)$$

$$\pi DL(total) = 19{,}021 cm^2$$

Substituting above values in Eq. (3.1) we get,

$$i_{corr} = \frac{\rho \times W_i \times F}{t \times 100 \times (\pi dl) \times w}$$

$$i_{corr} = \frac{\rho \times 20{,}000 \times 96487}{100 \times 19{,}021 \times 27.925 \times t \times 24 \times 3600}$$

$$i_{corr} = \frac{\rho}{t} \times 4.205 \times 10^{(-4)} \quad Amps/cm^2$$

$$i_{corr} = \frac{\rho}{t} \times 4.205 \times 10^{(-4)} \times 19021$$

$$\Rightarrow i_{corr} = \frac{\rho}{t} \times 7.998 \quad Amps$$

2.5% Corrosion for 8days:

$$i_{app} = \frac{2.5}{8} \times 7.998 = 2.5A \qquad (3.7)$$

Similarly Amount of current required for different degrees of corrosion can be obtained from Eq. (3.8) and are presented in Table 3.16

Table 3.16: Amount of current required to induce corrosion levels in both OPC and PPC beam specimens

Degree of corrosion (%)	Current (Amps)	Time required (Days)
2.5	2.5	8
5	5	8
7.5	7.5	8
10	10	8

3.3.6 Corrosion Rate Measurements

After completion of accelerated corrosion in beam specimens, corrosion rate was measured with Applied Corrosion Monitoring (ACM) instrument. Measurements of corrosion levels based on Linear Polarization Resistance (LPR) method using ACM instrument is shown in Fig.3.21.

3.3.6.1 Measurement of corrosion using guard ring

In LPR method, reinforcing steel bar was polarised potentiostatically by an inner auxiliary electrode and the real time plot of current response was displayed on a laptop screen which controls the guard ring device. Area of steel polarised was confined by a current applied from an outer guard ring electrode. Area of steel was controlled by two sensor electrodes positioned between the inner auxiliary and outer guard ring electrode (Law et al. 2000).

3.3.6.2 Linear polarization resistance technique

LPR procedure is based on Stern-Geary characterization of typical polarization curve for the corroding metal. In this method, a linear relationship is described mathematically for a region on the polarization curve in which slight change in current applied to corroding metal causes corresponding change in potential of the metal. In other words, if a large current was required to change potentials by a given amount, the corrosion rate will be high and on the other hand, if only a small current was required, then corrosion rate will be low.

Corrosion cell consists of a guard ring with reference electrode and reinforcing steel embedded inside concrete specimen functions as working electrode. Reinforcing steel bar was polarized by applying a small potential shift to it (ΔE) and resultant current (ΔI), between working electrode and counter electrode (Ha-Won song and Saraswathy 2007). The corrosion current density was then calculated by using the Stern-Geary formula from Eq. (3.4).

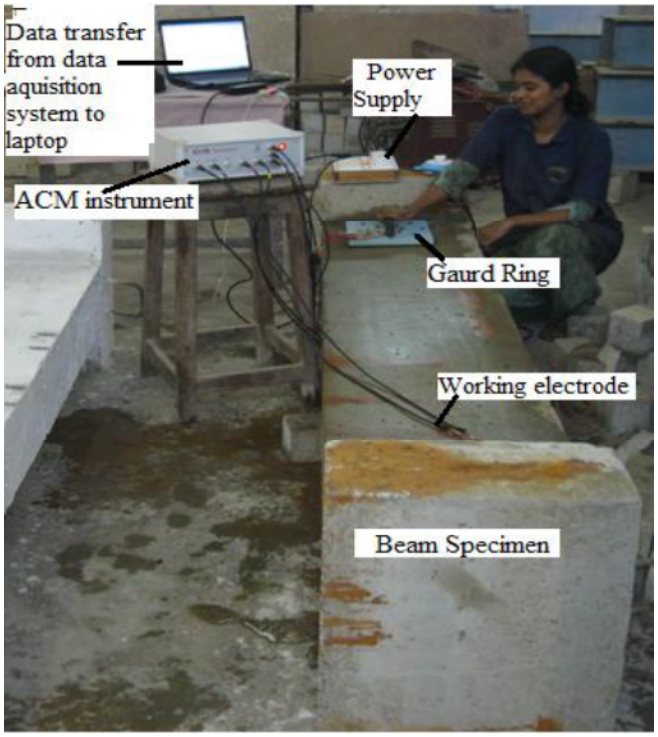

Fig.3.21: Corrosion monitoring set up

3.3.7 Test Setup

After the measurement of corrosion levels in beam specimens, specimens were placed on the test bed. Beam specimens were tested under two point loading condition (Fig.3.22). The load was applied at 15kN increments. Proving ring of 500kN capacity was used to note the applied load. Pump of hydraulic jack (500kN capacity) was operated by a hand lever.

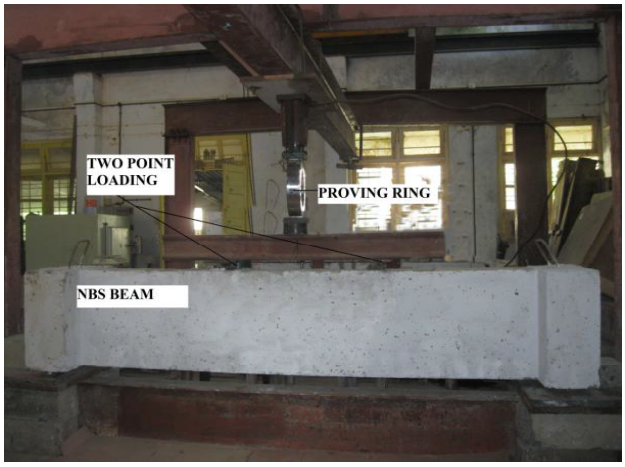

(a)

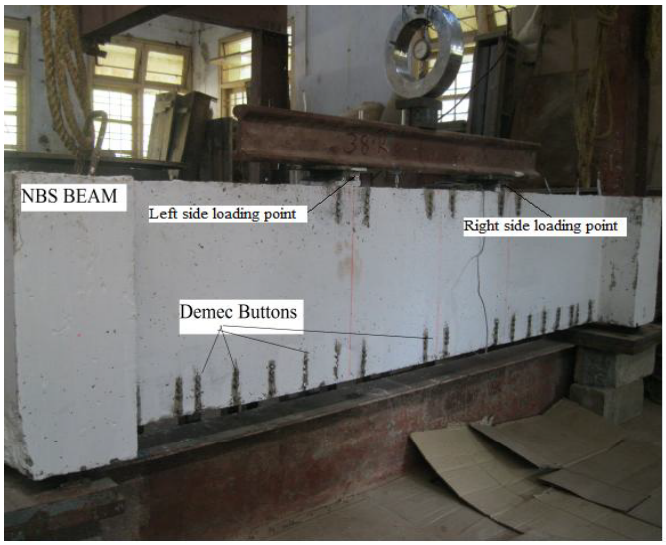

(b)

Fig.3.22: Test set up of NBS beam Specimen

Fig.3.23: Measurement of strain values using demec gauge

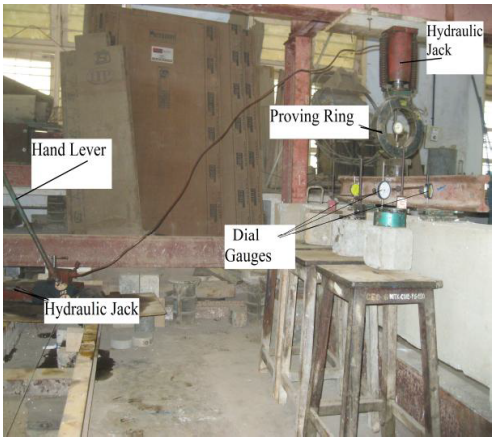

Fig.3.24: Position of dial gauges

Strain recordings were done using demec gauges. Positions of demec gauges are shown in Fig.3.22(b). Initial strain values were noted before application of load. Measurement of strain values using demec gauge are done as in Fig.3.23. Positions of dial gauges are indicated in Fig.3.24.

3.3.8 Strain Measurement

Strain is defined as the amount of deformation per unit length of an object when load is applied. Strain may be compressive or tensile and is normally measured by strain gauges.

In the present study, longitudinal strains were measured using a 100mm demountable mechanical (demec) strain gauge with a range of ±10 to ±5000 micro strains. Photo of mechanical strain gauge is shown in Fig.3.25.

3.3.9 Crack Measurement

In the present investigation crack widths were recorded for all concrete beam specimens from first crack to various numbers of cracks for all OPC and PPC concrete beam specimens. Initially at the base level a mark was made in pencil and measurements were taken at the same point as the increment of load levels. Finer (hair) cracks were identified using magnifying glass (Fig.3.26) and final markings

along the length of the cracks were marked using marker pen. Crack widths were measured with the help of concrete crack microscope, shown in Fig.3.27. Least count of concrete crack microscope is 0.02mm. Results are discussed in Chapter 5.

Fig.3.25 Mechanical (Demec) strain gauge

Fig.3.26: Observation of crack under magnifying glass

Fig.3.27: Concrete crack microscope

3.3.10 Determination of Flexural Bond Stress

Average bond stress values are obtained from Eq. (3.8).

$$\tau_{bd} = \frac{\phi_1 \times f_s}{4 \times L_d} \qquad (3.8)$$

where,

τ_{bd} = Average bond stress (N/mm^2)

ϕ_1 = Reduced Diameter (mm) values (presented in Table 3.17)

L_d = Embedment length of the bar (747mm) from the test setup

f_s = Steel stress values. The stress values were obtained for initiation and end strain values at slip region for different corrosion levels from stress corresponding to strains at that load level.

Reduced diameter after induced corrosion level procedure as follows:

$$Weight\ loss\ (\%) = \frac{W_i - W_f}{W_i} \qquad (3.9)$$

where

$W_i = Initial\ \ weight,\ W_f = Final\ \ weight,\ \phi = Initial\ \ diameter\ \ and\ \ \phi_1 = \text{Re}\, duced\ \ diameter$

Let us take *weight loss =p*

$$p = \frac{\frac{\pi}{4} \times \phi^2 - \frac{\pi}{4} \times \phi_1^2}{\frac{\pi}{4} \times \phi^2}$$

$$p = 1 - \frac{\phi_1^2}{\phi^2}$$

$$\phi_1^2 = (1-p)\phi^2$$

$$\underline{\phi_1 = \phi\sqrt{(1-\frac{p}{100})}} \qquad (3.10)$$

Or

From binominal theorem, and $$\underline{\phi_1 = \phi\left[1 - \tfrac{1}{2}\left(\frac{p}{100}\right)\right]} \qquad (3.11)$$

From Eq. (3.10) or Eq. (3.11) reduced bar diameter for different levels of corrosion were obtained as shown in Table 3.17. Poisson's effect was not taken in to consideration.

Table 3.17: Reduced bar diameter for different levels of corrosion

Corrosion level (%)	Reduced bar diameter (mm)
0.0	25.00
2.5	24.69
5.0	24.37
7.5	24.04
10	23.72

3.3. 11 Calculation of Chloride Concentration in a Tank

To understand the amount of chloride content consumed by the beam during the process of accelerated corrosion technique, calculation of chloride concentration in a tank was carried out and are explained below

(A) Test program

Following apparatus were used to calculate the concentration of chloride in tank: 50-ml burette, 1-ml graduate pipette, silver Nitrate ($AgNO_3$) (0.141N) solution, potassium chromate (pale yellow) indicator, burette stand, two 250-ml conical flasks,

wash bottle filled with distilled water and funnel. Samples were collected from different tanks as shown in Fig.3.28.

(B) Test Procedure

Blank test was carried out with distilled water volume of silver nitrate consumed was 0.1ml. One ml of sample collected from the tank, was diluted to distilled water in a conical flask and 5 drops of potassium chromate (indicator) were added. This solution was titrated against silver nitrate solution till colour changed from pale yellow to brick red. Three trials were carried out for one sample. Obtained results were reduced with blank test values.

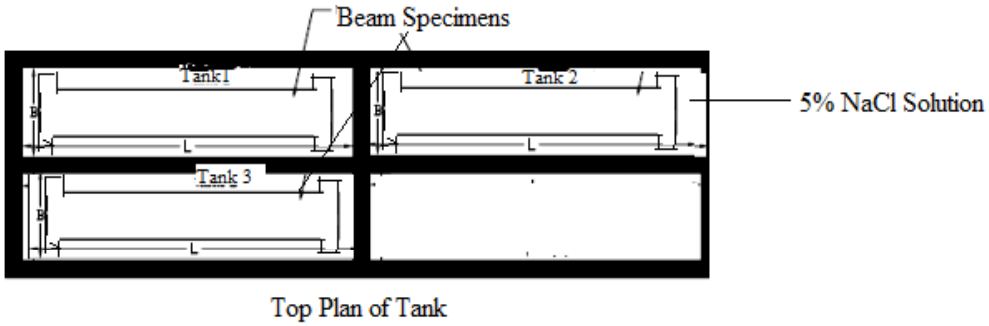

Fig.3.28: Top plan of tank

(C) Calculation of chloride concentration

5% concentration = 50g of NaCl dissolved in 1 litre of water

Molecular weight of sodium chloride is the summation of molecular weight of sodium and molecular weight of chloride.

Therefore molecular weight of NaCl = 23 + 35.46 =58.46 g

Total amount of NaCl required/tank $= 50 \times volume\ of\ \ water\ in\ \tan k \times 10^3 \big/ 1000$

Where, factors 10^3 is conversion to litre and 1000 is conversion to kg

Volume of Tank=0.259m^3

Volume of water=0.2059m^3

$$Salt\ Concentration\ (\%) = \frac{Volume\ in\ (ml) \times 0.141 \times M_w \times D_f}{S_w \times 10} \qquad (3.12)$$

Total amount of NaCl required/tank $= 50 \times 0.2059 \times 10^3 / 1000$

$$= 10.295\text{kg}$$

where M_w=Molecular weight of NaCl, D_f =dissolution factor, S_w= weight of sample in 'gram'. Residual salt concentration after Corrosion in 5% of salt solution can be calculated from Eq. 3.12.

For 2.5% corrosion for OPC concrete

$$Salt\ Concentration\ (\%) = \frac{3.2 \times 0.141 \times 58.46 \times 1}{1 \times 10} = 2.64$$

Salt concentration (%) after inducing different degree of corrosion levels for OPC and PPC concrete beam in 5% of NaCl solution are given in Table 3.18.

Table 3.18: Salt concentration (%) after inducing different degree of corrosion levels for OPC and PPC concrete in 5% of NaCl solution

OPC Concrete			
Corrosion levels (%)	Volume of $AgNO_3$ (ml) (After deducting from value of blank test)	Residual NaCl concentration (%)	Consumed NaCl concentration (%)
2.5	3.2	2.64	2.36
5.0	2.8	2.31	2.69
7.5	2.5	2.10	2.90
10.0	2.2	1.81	3.19
PPC Concrete			
2.5	4.1	3.38	1.62
5.0	3.8	3.13	1.87
7.5	3.4	2.88	2.12
10.0	3.0	2.47	2.53

Note: PPC beams were subjected to corrosion after 92 days of casting (after the completion of OPC beams test).

3.4 SUMMARY

The basic materials used for the study satisfies the physical test of codal requirements. Accelerated impressed current technique followed for the study are elaborated. Assessment of corrosion levels were done using non destructive applied corrosion monitoring instrument. Test procedure followed for the specimens to determine the bond strength values are explained. Discussion on the test results of experimental investigation are presented in the forthcoming chapters.

CHAPTER 4

NUMERICAL MODELLING

4.1 GENERAL

Experimental study on flexural bond behaviour using NBS beam specimen was explained in Chapter 3. In this chapter, to simulate the actual condition, existing features in ANSYS have been exploited to model the beam specimen for different degree of corrosion.

4.2 MODELLING IN ANSYS

Finite element (FE) analysis is one of the widely used analytical tools in structural mechanics. 'ANSYS' provides different element types, which suits the problem on hand. Hence this software is preferred for the present study.

4.2.1 Element Types

Element types used for this model are shown in Table 4.1.

An eight node Solid65 element was used to model the concrete. This element has three degrees of freedom at each node – translations in the nodal X, Y and Z directions. This element is capable of plastic deformation, cracking in three orthogonal directions, and crushing (ANSYS Manual, 2012). A schematic diagram of the Solid65 element is shown in Fig.4.1.

Steel reinforcement was modelled using Link8 element. It has two nodes with three degrees of freedom – translations in the nodal X, Y and Z directions (ANSYS Manual, 2012). This element is capable of plasticity, creep, swelling, stress stiffening, and large deflection. This element is shown in Fig.4.2.

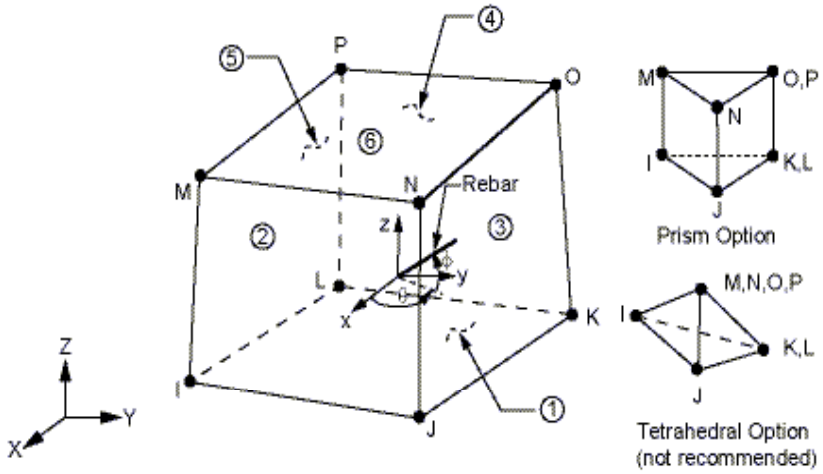

Fig.4.1: Solid65 Element

Table 4.1: Element types for the working model

Material Type	ANSYS Element
Concrete	Solid65
Steel Reinforcement	Link8
Nonlinear Spring	Combin39

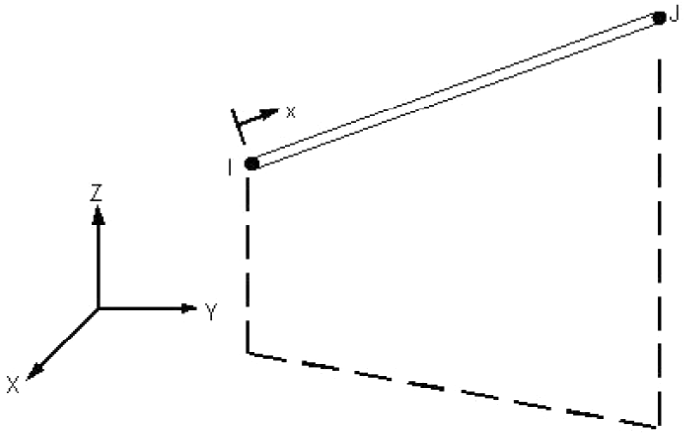

Fig.4.2: Link8 Element

Combin39: In order to simulate the bonding behaviour non-linear spring element was adopted at the bar concrete interface for simulating its bond–slip relationship. Combin39 elements nonlinearity can be defined by giving load displacement relationship as input.

The relationship between local bond stress and slip at the bar concrete interface along the longitudinal direction is given below (Xiaoming and Hongqiang, 2012):

$$\tau(s) = (61.5s - 693s^2 + 3.14\times10^3 \times s^3 - 0.478\times10^4 \times s^4).\, f_{t,s}.\sqrt{c/d} \qquad (4.1)$$

In which,

's' =Slip value (mm);

Based on the IS: 2770 (Part I) - (1967), slip values are assumed between 0 to 0.025mm

'*c*' = Thickness of cover layer (=50mm);

'*d*' = Diameter of reinforcement (=25mm);

$f_{t,s}$ = Concrete's splitting tensile strength (N/mm^2);

where,

$$f_{t,s} = 0.19\times f_{ck}^{\ 0.75} \qquad (4.2)$$

In the FE model of the RC beam, the relationship between the bond Force F and slip value '*s*' can be calculated as follows:

$$F(s) = \tau(s)\,\pi dl \qquad (4.3)$$

where *'d'* = diameter of a bar(mm) and

'*l*' = distance between two adjacent spring elements (1mm).

From Eq. (4.1) and Eq. (4.2), the load displacement relationship (F-D) of the spring element in longitudinal direction can be obtained.

When the corrosion level is η, the reduction factor β of the bond strength at the corroded bar-concrete interface can be calculated as follows (Xu, 2003)

$$\begin{aligned} \beta &= \{1 + 0.5625\eta - 0.3357\eta^2 + 0.055625\eta^3 - 0.003\eta^4 \qquad \eta \le 7\%\} \\ \beta &= \{2.0786\eta^{-1.0369} \qquad \eta > 7\%\} \end{aligned} \tag{4.4}$$

Substituting Eq. (4.4) in to Eq. (4.3), the relationship between the bond force 'F' and slip value 's' after corrosion can be obtained as:

$$F(s) = \beta.\tau(s).\pi dl \tag{4.5}$$

Thus, the force-displacement (F-D) curves of the spring element along the longitudinal direction under different corrosion rates are presented in Fig.4.3.

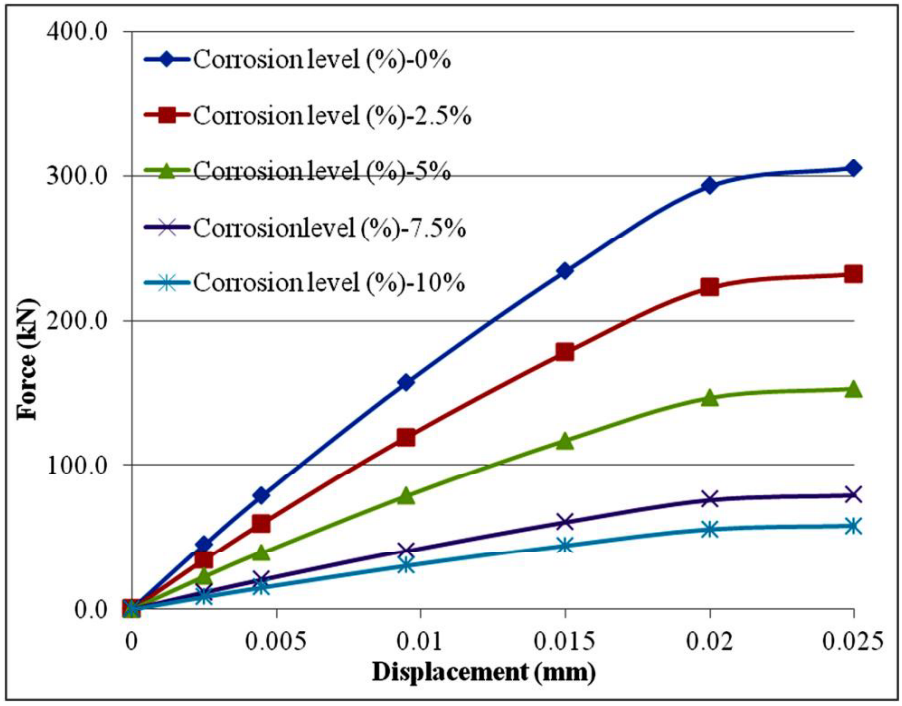

Fig.4.3: Load-displacement relationship of the spring element along the longitudinal direction

4.2.2 Real Constants

Real constants for this model are shown in Table 4.2. Real Constant differs for individual elements. Solid65 element Real Constant Set 1 was used. If the assumed model is smeared, then real constants values can be entered for Material Number, Volume Ratio, and Orientation Angles. Here material number refers to the type of material for the reinforcement. Volume ratio refers to the ratio of steel to concrete in the element. ANSYS allows the user to enter three rebar materials in the concrete. Each material corresponds to X, Y and Z directions in the element.

Table 4.2: Real Constants

Real Constant Set	Element Type	Constants			
			Real Constant for Rebar 1	Real Constant for Rebar 2	Real Constant for Rebar 3
1	SOLID65	Material No.	0	0	0
		Volume Ratio	0	0	0
		Orientation Angle	0	0	0
2	LINK 8	Cross Sectional Area (mm^2)	490.87		
		Initial Strain	0		
3	LINK 8	Cross Sectional Area (mm^2)	113.10		
		Initial Strain	0		
4	LINK 8	Cross Sectional Area (mm^2)	50.27		
		Initial Strain	0		

Reinforcement has uniaxial stiffness and the directional orientation is defined by the user. In the present study the beam was modelled using embedded reinforcement for main bar to determine the bond slip behaviour. For other bars it was modelled as discrete reinforcement. Therefore, a value of zero was entered for all real constants which turned the smeared reinforcement capability of the Solid65 element off.

Real Constant Sets 2, 3 and 4 were defined for the Link8 element. Values for cross-sectional area and initial strain values were entered (Table 4.2). A value of zero was entered for the initial strain because it is assumed that there is no initial stress in the reinforcement. Real Constant Set 5 was defined for the combin39 element Load slip values were given as input from Fig.4.3.

4.2.3 Material Properties

Material properties used for the present study are given in Table 4.3. Solid65 element was referred as material model number 1. To model the concrete (Solid65) element, linear isotropic and multi-linear isotropic material properties are required (Wolanski, 2004). Multi-linear isotropic material uses the von mises failure criterion model to define the failure of the concrete. Modulus of elasticity of concrete (E_c *or* E_x) was based on the equation,

$$E_c = 5000\sqrt{f_{ck}} \qquad (4.6)$$

Where f_{ck} is the Mean cube compressive strength of concrete at the age of 28days; Poisson's ratio $(\gamma \; or \; \text{PRXY})$ was assumed as 0.3 for steel and 0.2 for concrete.

The compressive uniaxial stress-strain relationship for the concrete model was obtained using the following equations to compute the multilinear isotropic stress-strain curve for the concrete (MacGregor, 1992).

$$E_c = 5000\sqrt{f_{ck}} \qquad (4.7)$$

$$E_c = 5000\sqrt{34.4}$$

$$E_c = 29342.8\ N/mm^2$$

Initial Stress

$$f = 0.3 \times f_{ck} \tag{4.8}$$

$$f = 10.33 N/mm^2$$

Initial Strain Value

$$E_c = \frac{f}{\varepsilon_1} \tag{4.9}$$

$$\varepsilon_1 = 3.52 \times 10^{-4}$$

Ultimate Strain

$$\varepsilon_0 = \frac{2 f_{ck}}{E_c} \tag{4.10}$$

$$\varepsilon_0 = 2.35 \times 10^{-3}$$

Assume the strain values between initial and ultimate strain values; get the corresponding stress values from the following Eq. (4.11)

$$f = \frac{E_c \varepsilon}{1 + \left(\frac{\varepsilon_1}{\varepsilon_0} \right)^2} \tag{4.11}$$

where; ε_0=ultimate strain; ε_1 = initial strain, f = stress at any strain ε; E_c=Modulus of Elasticity of concrete; ε=Assumed strain values in between initial and final strain values.

Uniaxial stress strain curve is shown in Fig.4.4. Obtained Multilinear isotropic stress-strain values are presented in Table 4.3.

Other material properties used for the present study are: Shear transfer coefficients range from 0.0 to 1.0, Co-efficient of 0.0 representing a smooth crack (complete loss of shear transfer) and rough crack can represented as 1.0 (no loss of shear transfer). Convergence problems occurred when the shear transfer coefficient for the open crack dropped below 0.2 and more than 1 (Kachlakev, et al. 2001). Hence coefficient for the open crack and closed crack was assumed as to 0.3 and 0.95 (Table 4.3). The uniaxial cracking stress was based upon the modulus of rupture. This value is determined using the relation (Eq. 4.12):

$$f_t = 0.7\sqrt{f_{ck}} \qquad (4.12)$$

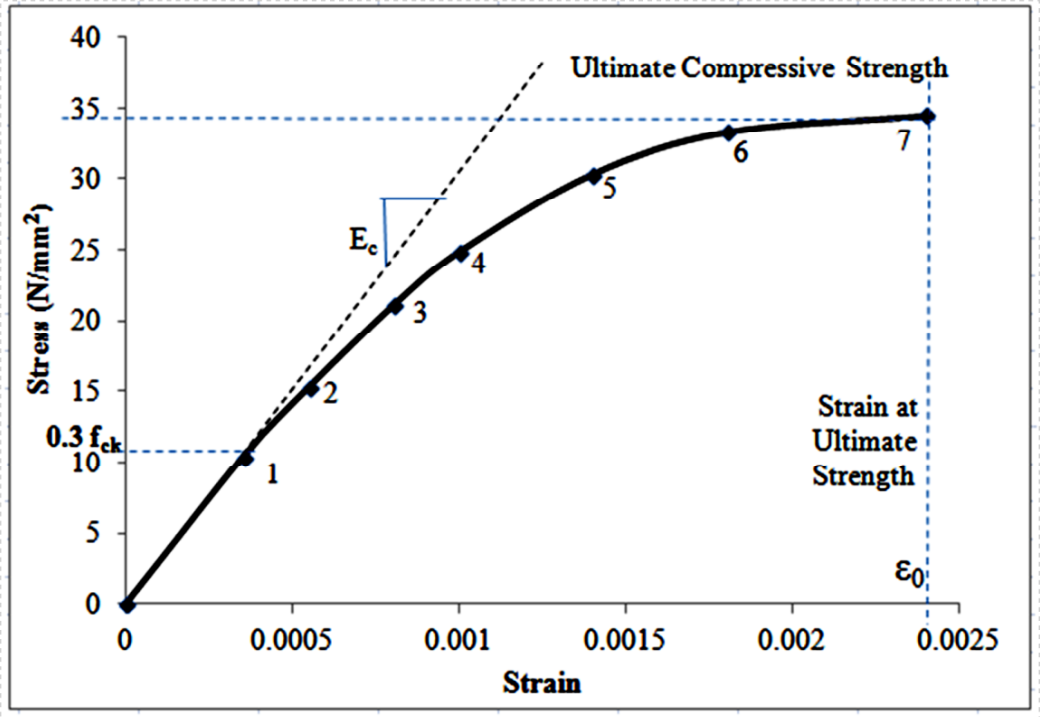

Fig.4.4: Uniaxial Stress-Strain Curve

Table 4.3:Material Models

Material Model Number	Element Type	Material Properties	
1	SOLID65	Linear Isotropic	
		EX	29342.80N/mm^2
		PRXY	0.2
		Multilinear Isotropic	
		Stress	Strain (N/mm^2)
		0	0.00000
		10.33	0.00035
		12.74	0.00045
		15.30	0.0055
		17.72	0.00065
		21.03	0.0008
		24.84	0.001
		27.92	0.0012
		30.31	0.0014
		32.06	0.0016
		33.27	0.0018
		34.00	0.0019
		34.38	0.0022
		34.44	0.0024
		Concrete	
		ShrCf-Op	0.3
		ShrCf-Cl	0.95
		UnTensSt	4.1 N/mm^2
		UnCompSt	-1
		BiCompSt	0
		HydroPrs	0
		BiCompSt	0
		UnTensSt	0
		TenCrFac	0
2	LINK 8	Linear Isotropic	
		EX	2×10^5 N/mm^2
		PRXY	0.3
		Bilinear Isotropic	
		Yield Stress	485 N/mm^2
		Tang Mod	0

The uniaxial crushing stress in this model was based on the uniaxial unconfined compressive strength (f_{ck}). Uniaxial compressive strength value was entered as -1 to turn off the crushing capability of the concrete element as suggested by past researchers (Kachlakev et al. 2001). Link8 element refers to material model number 2. Link8 element was assumed as bilinear isotropic material based on the Von Mises failure criteria.

4.2.4 Modelling and Meshing of the Element

The beam dimension of length 2.44m and cross section of 0.203m×0.457m was used for the modelling. The dimensions for the concrete nodes are shown in Table 4.4.

Table 4.4: Dimensions for concrete nodes

ANSYS	Concrete (mm)	
X1,X2 X-coordinates	0	2440
Y1,Y2 Y-coordinates	0	457
Z1,Z2 Z-coordinates	0	203

Necessary mesh attributes were set, before each section of the element was created. Individual rectangular elements of solid65 were created in the modelling through the nodes formed. Other than main reinforcement which was having separate entities at same location (Link 8 elements and solid 65 elements) were merged; since these reinforcements were modelled through the nodes created by the mesh of the concrete volume. Reinforcement details are shown in Fig.4.5. All precautions were taken to ensure that all different entities were merged in the proper order. In case of main reinforcement modelling (25mm diameter), separate nodes were created at the same

location of concrete nodes. These separate nodes (Link 8 elements and solid 65 elements) were connected with combin39 element to simulate the bond slip behaviour. A view of reinforcements inside concrete volume is shown in Fig.4.6.

4.2.5 Loads and Boundary Conditions

To get the solution as close to reality as possible, existing features in ANSYS have been exploited to model the boundary condition.

Supports were modelled such a way that a roller was created. A single line of nodes on the beam were given constraint in the U_Y and U_Z (translation in Y and Z) directions, applied as constant values of 0. By doing this, the beam will be allowed to rotate at the support. NBS beam model is shown in Fig.4.7. Support and loading conditions are shown in Fig.4.8 (a) and Fig.4.8 (b).

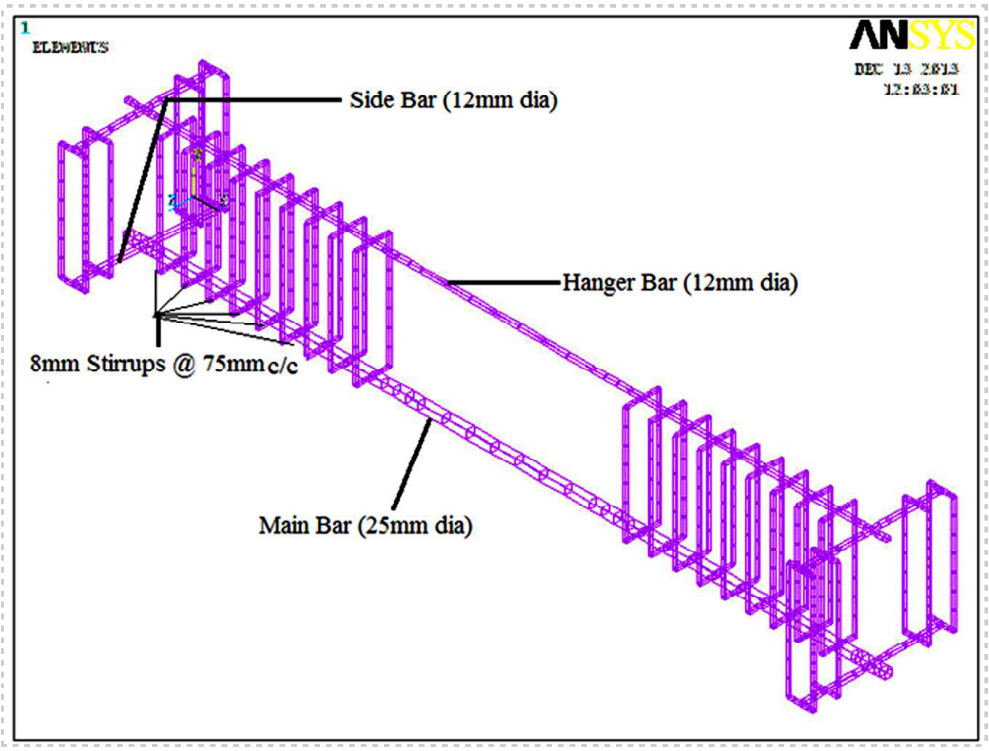

Fig.4.5: Reinforcement details of NBS beam

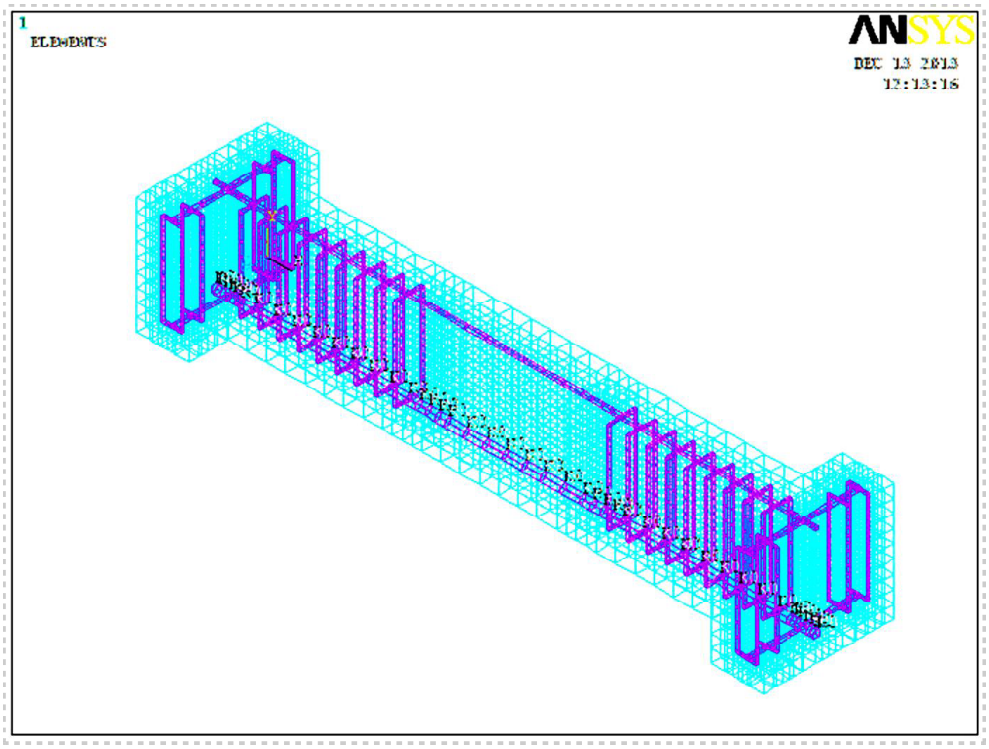

Fig.4.6: View of Reinforcements inside concrete

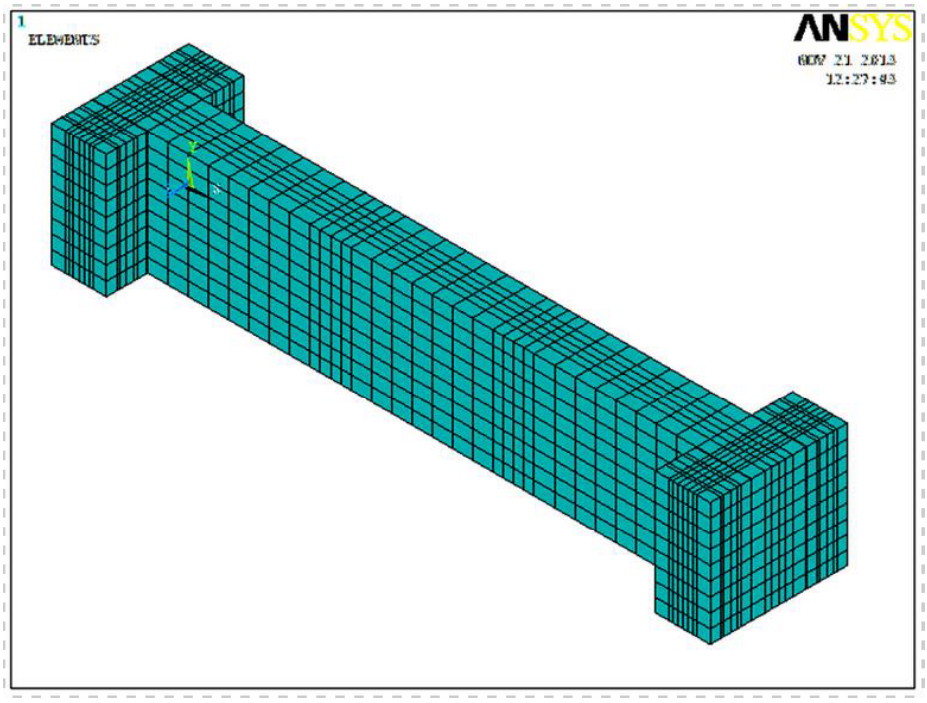

Fig.4.7: NBS beam model in ANSYS

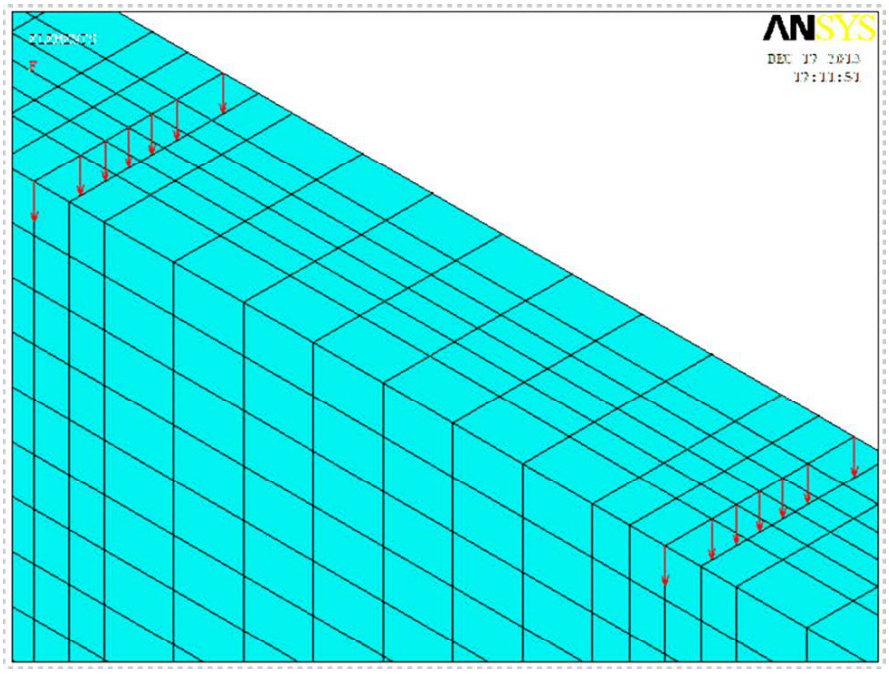

Fig.4.8 (a): Loading condition for NBS beam Specimen

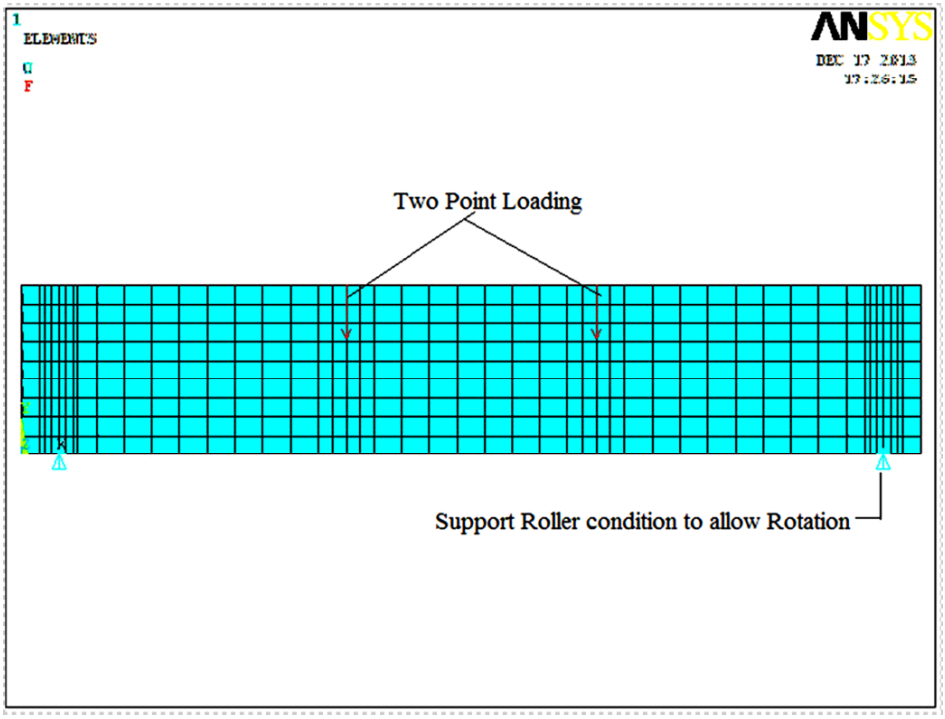

Fig.4.8 (b): Support and Loading conditions of NBS beam specimen

4.2.6 Analysis Type

Static Analysis type was utilized in the present investigation. To restart an analysis after the completion of initial run or load step 'Restart' command was utilized. Linear or non-linear solution for the finite element model can be understood by the Sol'n Controls command. Typical commands utilized in a nonlinear static analysis are given in Table 4.5.

In the present investigation small displacement and static analysis was used. Time at the end of the load step refers to the ending load per load step (Table 4.5). Sub steps were set to indicate load increments used for this analysis. Commands used to control the solver and outputs are given in Table 4.6.

Table 4.5: Commands used to control nonlinear analysis

Analysis Options	Small Displacement
Calculate Prestress Effect	No
Time at End of Load Step	15400
Automatic Time Stepping	On
Number of Substeps	20
Max. Number of Substeps	20
Min. Number of Substeps	20
Write Items to Result File	All Solution Items
Frequency	Write Every Substep

Table 4.6: Commands used to control output

Equation Solvers	Sparse Direct
Number of Restart Files	1
Frequency	Write Every Substep

All these values were set to ANSYS defaults. The commands used for the nonlinear algorithm and convergence criteria are given in Table 4.7. All values for the nonlinear algorithm were set to defaults.

Table 4.7: Nonlinear algorithm and convergence criteria parameters

Line Search		off
DOF Solution Predictor		Program Chosen
Maximum No. of iterations		10000
Set Convergence Criteria		
Label	F	U
Tolerance	0.5	0.5
Norm	L2	L2
Min. Ref.	-1	-1

4.2.7 Analysis Process for the Finite Element Model

Computation of nonlinear response, works on the basis of Newton-Raphson method (Wolanski, 2004). Application of the loads up to failure was done incrementally as required by the Newton-Raphson procedure. After each load increment, restart option was used to go to the next step after convergence. Table 4.8 represents the load steps, sub steps and loads applied per restart file as analysed for the present study.

For different corrosion levels the same steps were followed by changing the real constant (area of cross-section from chapter 3, Table 3.17 and force-displacement values from (Fig.4.3). Obtained results were analyzed from ANSYS main menu ⟶ General Post Processor of plot results by considering the deflection and strain values.

Central deflection values were noted. Strain values were noted from numerical results at the load points and bond strength values were then obtained as explained in Chapter 3 (section 3.3.10).

Table 4.8: Load step for analysis of finite element model

Beginning Time	Time at End of Load Step	Load Step	Sub Step
770	15400	1	20
15400	30400	2	20
30400	45400	3	20
45400	60400	4	20
60400	75400	5	20
75400	90400	6	20
90400	105400	7	20
105400	120400	8	30
120400	135400	9	30
135400	150400	10	30
150400	165400	11	30
165400	180400	12	30
180400	195400	13	30
195400	210400	14	30
210400	225400	15	30
225400	234200	16	30
234200	240400	17	30
240400	245400	18	30
245400	250400	19	30
250400	255400	20	30
255400	260400	21	30
260400	263400	22	30

4.3 SUMMARY

Details of analytical investigations carried out to study the performance of NBS beam under different corrosion levels have been elaborated. Element types and real constants and material properties and modelling procedures used for the study are explained. Boundary condition and analysis type followed in the present study is to determine the bond strength values are presented. Discussion of the test results on comparison of experimental investigation and numerical modelling are presented in the next chapter.

CHAPTER 5

RESULTS AND DISCUSSION

5.1 GENERAL

Results of experimental investigation and analytical investigation are presented and discussed in this chapter. Bond strength prediction equations have been proposed based on data analysis.

5.2 DETERMINATION OF ANCHORAGE BOND STRENGTH (PHASE-I)

In this section results and discussion on compressive strength, and corrosion current density values are presented. Effects of corrosion on pull out load and anchorage bond strength of reinforced concrete specimens are discussed.

5.2.1 Compressive Strength Test

Compressive strength of OPC and PPC concrete is shown in Table 5.1. It is observed that PPC concrete strength is less than OPC concrete strength. Presence of C_2S (dicalcium silicate) compound in PPC results in later strength gaining process compared to OPC.

Table 5.1: Compressive strength of M20 grade OPC and PPC concrete

SI No	Curing duration (days)	Compressive strength (N/mm^2)
OPC (Ordinary Portland Cement) Concrete		
1	7	21.9
2.	28	26.6
PPC (Portland Pozzolona Cement) Concrete		
1	7	15.0
2.	28	23.3

5.2.2 Measurement of Corrosion Current Density

Corrosion rate is measured in terms of corrosion current density, i_{corr}, and is a quantitative index, which represents an overall estimate of the corrosion attack on reinforcement.

To study the induced corrosion levels of beam specimens, corrosion current density was measured using the corrosion measuring system "Gill AC" (Applied Corrosion Monitoring System). Corrosion rate was measured after one day of required amount of current was passed. The corrosion current densities for each specimen of 16mm are shown in Tables 5.2.

Corrosion current density of OPC concrete beam specimen shows variation of 2.37%, 3.93%, 3.97% and 4.02% compared to PPC concrete respectively for corrosion levels of 2.5% to 10% at 2.5% increment.

Table 5.2: Corrosion current density $(\mu A/cm^2)$ of 16mm TMT rebars embedded in OPC and PPC concrete

Concrete Type	OPC				PPC			
Corrosion level (%)	S-1	S-2	S-3	Average	S-1	S-2	S-3	Average
2.5	34.2	33.93	33.76	33.96	32.83	33.45	33.2	33.16
5	64.83	64.55	64.14	64.51	62.07	62.61	61.23	61.97
7.5	102.07	101.79	102.05	101.97	97.93	97.31	98.79	97.92
10	134.48	133.93	134.64	134.35	127.21	130.3	129.31	128.95

5.2.3 Effect of Corrosion on Pull out load and Bond strength

Effect of corrosion on pull out load of cylindrical specimen is shown in Fig.5.1. From the figure it is clear that for less than 2.5% corrosion level, load carrying capacity is unaffected. As the corrosion level increases beyond 2.5% load carrying capacity

decreases by 4.9% and 3.5% respectively for OPC and PPC concrete cylinder specimens.

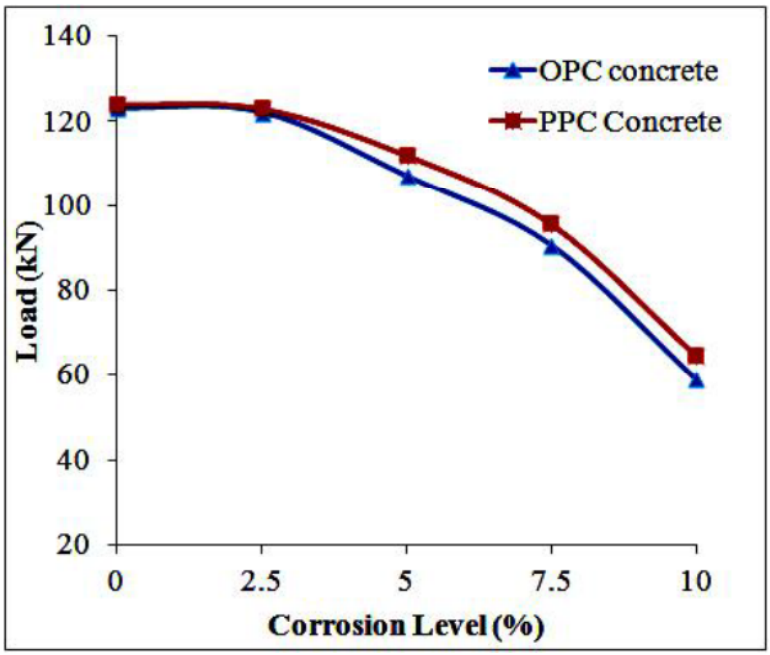

Fig.5.1: Effect of corrosion on maximum Pull out Load

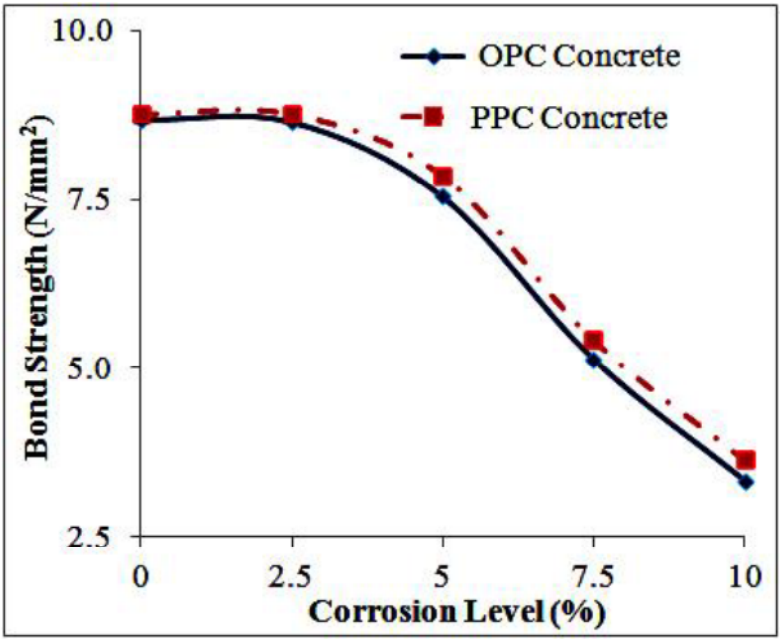

Fig.5.2: Effect of corrosion on bond strength

Effect of degree of corrosion on bond strength behaviour is shown in Fig.5.2**.** Test results clearly indicate that with slight corrosion ($\leq 2.5\%$), bond strength is unaffected due to increased roughness at the bar surface in the initial stages. As the corrosion level increases beyond 2.5% bond strength decreases rapidly.

5.2.4 Comparison of Models Proposed by Past Researchers with the Present Study

Existing empirical models for calculation of Bond Strength

A few empirical models are considered from the literature to calculate loss of bond strength, for different levels of corrosion, and are listed below:

$\tau_{bu} = 23.478 - 1.313X_p$ -M25 concrete (Cabrera, 1996) (5.1)

$\tau_{bu} = 2.21e^{(-0.0561Xp)}$ -M40 concrete (Lee et. al., 2002) (5.2)

where τ_{bu}=bond strength; X_p=Corrosion Level (%)

$R = 2.09X_p^{(-1.06)}$ For $X_p \succ 2\%$ -M20 concrete (Chung et al., 2004) (5.3)

where R is the ratio of bond strength at any specified corrosion level (%) of bond strength at the specific corrosion percentage X_p to the original bond strength (uncorroded specimen).

$R = 1$ For $X_p \leq 1.5\%$ -M40 concrete (Bhargava et al. 2007) (5.4)

$R = 1.192e^{(-0.117X_p)}$ For $X_p > 1.5\%$ (5.5)

The ratios of bond strength R are evaluated for different corrosion levels varying from 0% to 10% at 2.5% increment using the empirical relations from Eq. (5.1) to (5.5) and are presented in Fig.5.3. The value of original bond strength values are considered from the 0% corrosion (uncorroded specimen).

Empirical Models for Loss of Bond Strength based on Present Investigation

Based on the present work following regression analysis equations are obtained from Fig.5.3.

For $X_p \leq 2.5\%$ $R = 1$ - for both OPC and PPC concrete (5.6)

For $X_p \succ 2.5\%$

$R = 0.001X_P^{\ 3} - 0.0209X_P^{\ 2} + 0.055X_P + 0.996$ -for PPC concrete (5.7)

$R = 0.001X_P^{\ 3} + 0.0219X_P^{\ 2} + 0.054X_P + 0.997$ -for OPC concrete (5.8)

Present study shows higher bond strength ratio in initial stages as compared to the existing empirical models as shown in Fig.5.3. This might be due to embedment length taken for present investigation was more than the values used by other researchers. Also it is because of the lower water cement ratio used in the present study. Further it may be noted that, after 5% corrosion, a reduction in the bond strength ratio is observed.

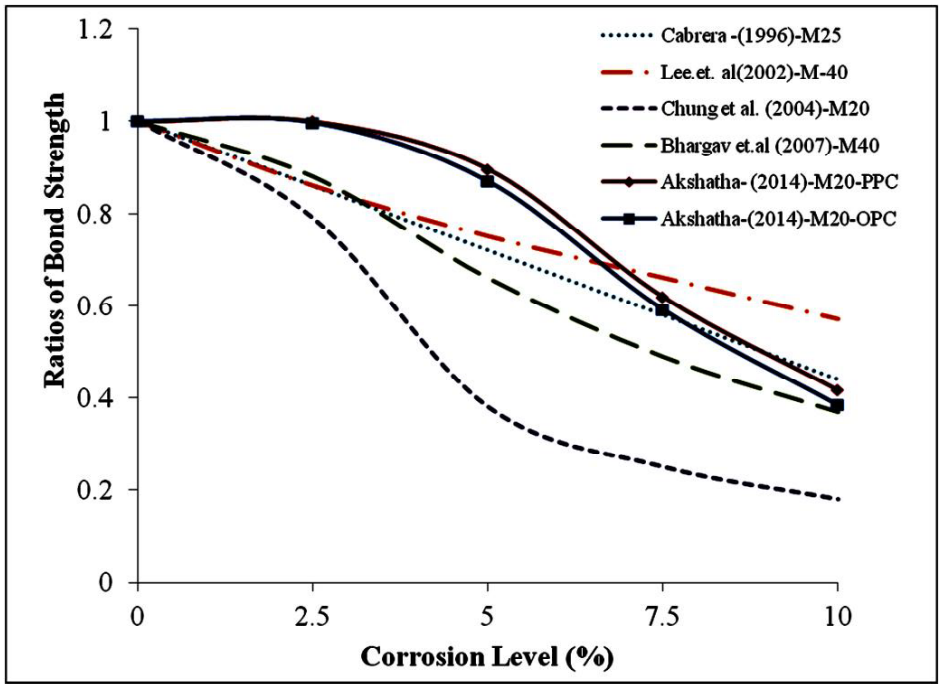

Fig.5.3: Effect of Corrosion on Bond Strength Ratio

5.3 DETERMINATION OF FLEXURAL BOND STRENGTH (PHASE-II)

In this section, results and discussion on compressive strength, modulus of elasticity and modulus of rupture and corrosion current density values are presented. Effect of corrosion on ultimate load carrying capacity, load deflection behaviour, crack width and bond stress of reinforced concrete members are discussed.

5.3.1 Compressive Strength Test

To determine the compressive strength, cubes were tested on 7^{th} and the remaining cubes were tested on 28^{th} day for both OPC and PPC concrete. Compressive strengths of cube specimens are shown in Table 5.3. PPC concrete strength is lesser as compared to the OPC concrete strength for the same (reason as explained in section 5.2.1 i.e. presence of C_2S (dicalcium silicate) compound in PPC results in later strength gaining process compared to OPC)

Table 5.3: Compressive strength of cube specimen for OPC and PPC concrete

Curing duration (days)	Compressive strength (N/mm^2)
Ordinary Portland Cement (OPC) Concrete	
7	25.1
28	34.5
Portland Pozzolona Cement (PPC) Concrete	
7	16.2
28	32.6

5.3.2 Modulus of Elasticity

Theoretical value of modulus of elasticity for OPC concrete is E_c=29677.4N/mm^2, and for PPC concrete is E_c=28535.1N/mm^2 from IS 516-1959. Experimental results of modulus of elasticity of OPC and PPC concrete are given in Table 5.4.

Table 5.4: Modulus of elasticity of OPC and PPC concrete

Types of Concrete	Modulus of Elasticity (N/mm^2)
OPC	31153.0
PPC	29415.4

5.3.3 Modulus of Rupture

Theoretical value of modulus of rupture for OPC concrete is f_t= 4.16 N/mm^2, and for PPC concrete, f_t= 4.0 N/mm^2 from IS 516-1959. Experimental results of Modulus of rupture of OPC and PPC concrete are given in Table 5.5.

Table 5.5: Modulus of rupture of OPC and PPC concrete

SI.No	Width of specimen (mm)	Span length (mm)	Maximum load (kN)	Fracture position (mm)	Depth at point of fracture (mm)	Modulus of rupture (N/mm^2) $= \frac{Pl}{bd^2}$	Average modulus of rupture (N/mm^2)
OPC concrete prism specimen							
1	100	400	15	225.0	100	6.0	6.0
2	100	400	16	248.6	100	6.4	
3	100	400	14	246.9	100	5.6	
PPC Concrete prism specimen							
1	100	400	13	220.7	100	5.2	5.6
2	100	400	15	230.6	100	6	
3	100	400	14	222.4	100	5.6	

5.3.4 Measurement of Corrosion Current Density

Corrosion current density was measured by LPR technique. Corrosion current densities were calculated for each specimen for different grids and average was considered to calculate the weight loss (%).

From Fig.5.4, it is observed that the degree of corrosion varies with the increase in the quantity of applied current. It is seen that corrosion levels increase linearly with increase in the applied current. Average values of corrosion current densities are given in Table 5.6 and Table 5.7 for OPC and PPC concrete beam specimens respectively.

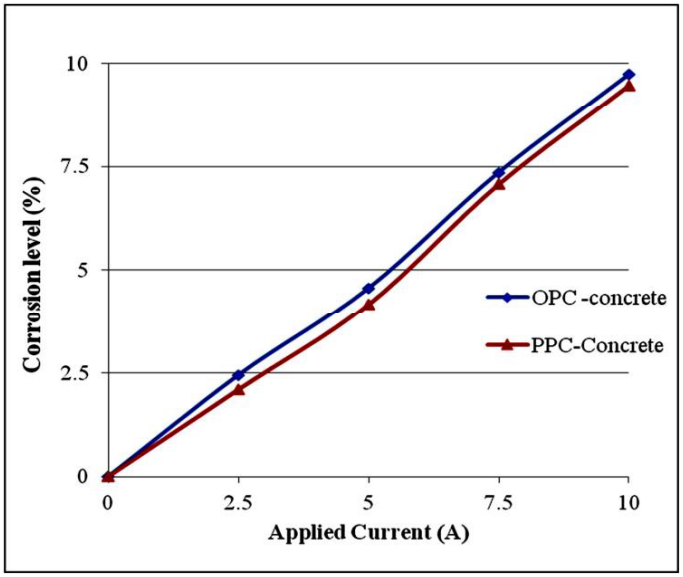

Fig.5.4: Variation of corrosion level with increase in applied current

Table 5.6: Corrosion current density $(\mu A/cm^2)$ of NBS beam in OPC concrete

	Corrosion current density $(\mu A/cm^2)$					
Degree of corrosion (%)	**grid-1**	**grid-2**	**grid-3**	**grid-4**	**grid-5**	**Average**
2.5	130.674	128.567	129.093	128.040	128.039	128.883
5	248.703	244.487	240.799	236.057	232.895	240.588
7.5	389.915	386.227	383.592	390.969	387.808	387.702
10	517.428	514.794	507.417	515.847	510.05	513.107

Table 5.7: Corrosion current density $(\mu A/cm^2)$ of NBS beam in PPC concrete

	Corrosion current density $(\mu A/cm^2)$					
Degree of corrosion (%)	**grid-1**	**grid-2**	**grid-3**	**grid-4**	**grid-5**	**Average**
2.5	111.178	107.490	118.028	112.232	103.275	110.441
5	222.884	216.561	219.196	217.088	223.410	219.828
7.5	379.377	365.677	375.689	366.731	375.162	372.527
10	503.728	496.352	494.244	501.621	499.513	499.092

5.3.5 Experimental Investigation of NBS Beam Specimen

In the present study, 3 controlled specimens and 12 corroded specimens (3 sets for each of 2.5%, 5%, 7.5% and 10% of corrosion) were cast with OPC and PPC concrete mix. These specimens were tested using two-point loading to determine the flexural bond capacity. By this test set up, beams deflection, strain, crack width were measured using dial gauge, mechanical strain (demec) gauge and crack microscope respectively.

5.3.6 Effect of Corrosion on Ultimate Load Carrying Capacity and Crack Width

From Fig.5.5 it is observed that load carrying capacity decreases as the corrosion level increases for both OPC and PPC concrete beam specimens. There is about 1.6% drop in load carrying capacity for every percentage increase in corrosion level. Table 5.8 represents the ultimate load carrying capacity of OPC and PPC concrete beam specimens. Experimentally obtained load and deflection values are more than the theoretical values. Theoretical calculations of load deflections are presented in Appendix C for both OPC and PPC concrete beam specimens.

As the load increases crack width also increases as expected. For comparison purpose crack width at 195kN load level is considered, as shown in Fig.5.6. It is observed that for corrosion levels less than 5%, variation in crack width is less. After 5% corrosion level, crack width increases. PPC concrete beam specimen performs better than OPC concrete beam specimen in case of ultimate load carrying capacity and crack width. A view of propagation of cracks in beam specimens is shown in Appendix D for different levels of corrosion for both OPC and PPC specimens.

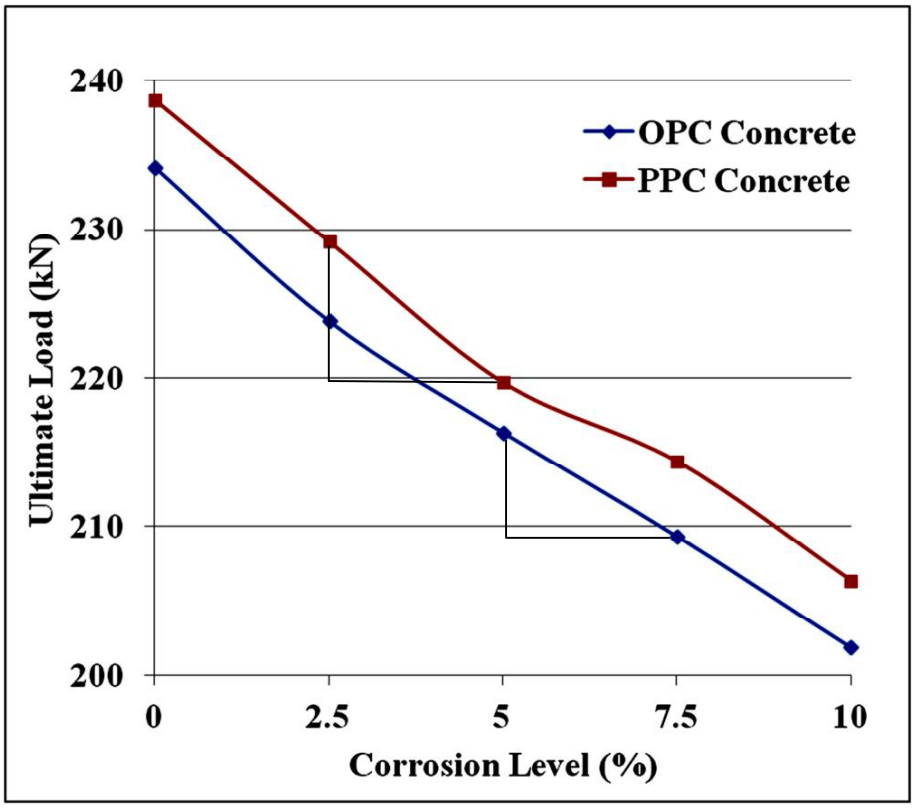

Fig. 5.5: Effect of corrosion on ultimate load carrying capacity

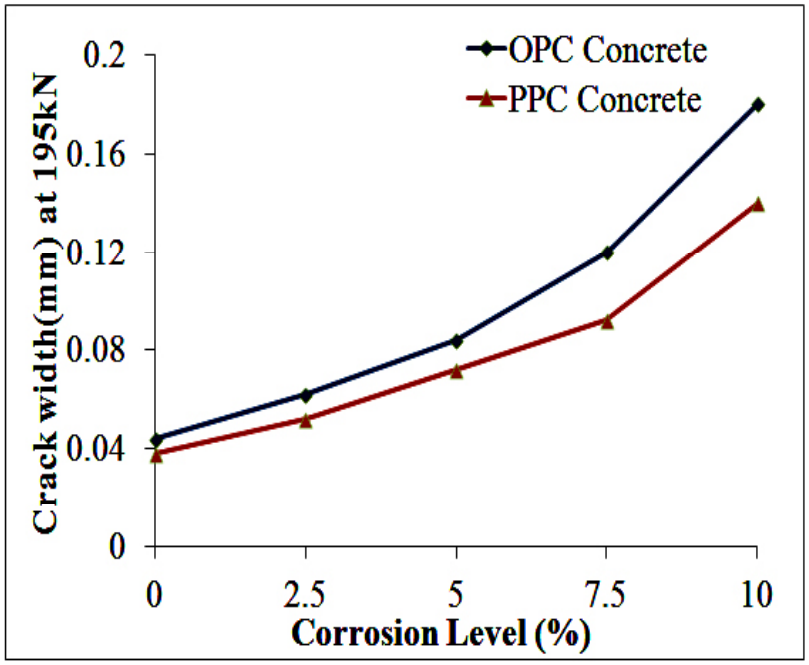

Fig.5.6: Effect of corrosion on crack width at 195kN load level

5.3.7 Effect of Corrosion on Load Deflection Behaviour

As the load increases deflection also increases as expected. Further, as the corrosion level increases, deflection increases at higher rate compared to lower level of corrosion. This is due to the fact that an increase in corrosion level leads to reduction in cross sectional area of steel reinforcement and hence leads to failure of bond between steel reinforcement and surrounding concrete. Effect of corrosion on central deflection of OPC concrete beam specimens is shown in Fig.5.7 and for PPC concrete beam specimens in Fig.5.8 respectively. From the load deflection curves it is observed that deflection increases by 29% to 45% for OPC concrete beam specimens whereas by 25% to 48% for PPC concrete beam specimens, compared to control beam specimens.

Table 5.8: Ultimate Load Carrying Capacity

Beam Designation	Ultimate Load (kN)	
	OPC	PPC
Control Beam		
CB I	240.4	239.4
CB II	236.4	236.4
CBIII	225.4	240.4
2.5%Corrosion		
Beam I	225.4	228. 4
Beam II	223.4	229.9
Beam III	222.9	229. 4
5% Corrosion		
Beam I	218.4	221. 4
Beam II	215. 4	219. 4
Beam III	215.4	218. 4
7.5%Corrosion		
Beam I	210. 4	213. 4
Beam II	207. 4	215. 4
Beam III	210. 4	214. 4
10%Corrosion		
Beam I	201.9	208. 4
Beam II	201.9	204.4

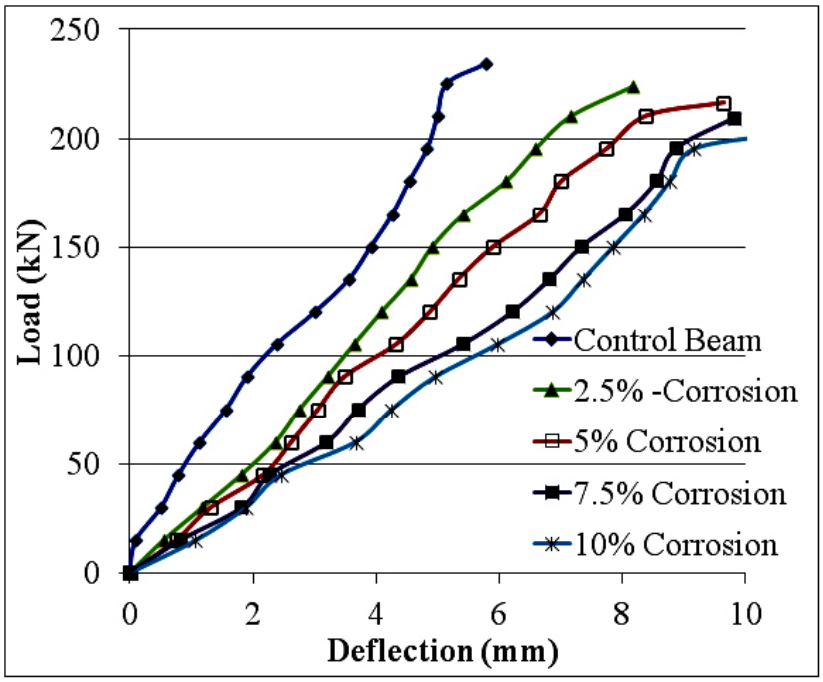

Fig.5.7: Effect of corrosion on central deflection behaviour of OPC concrete beam Specimens

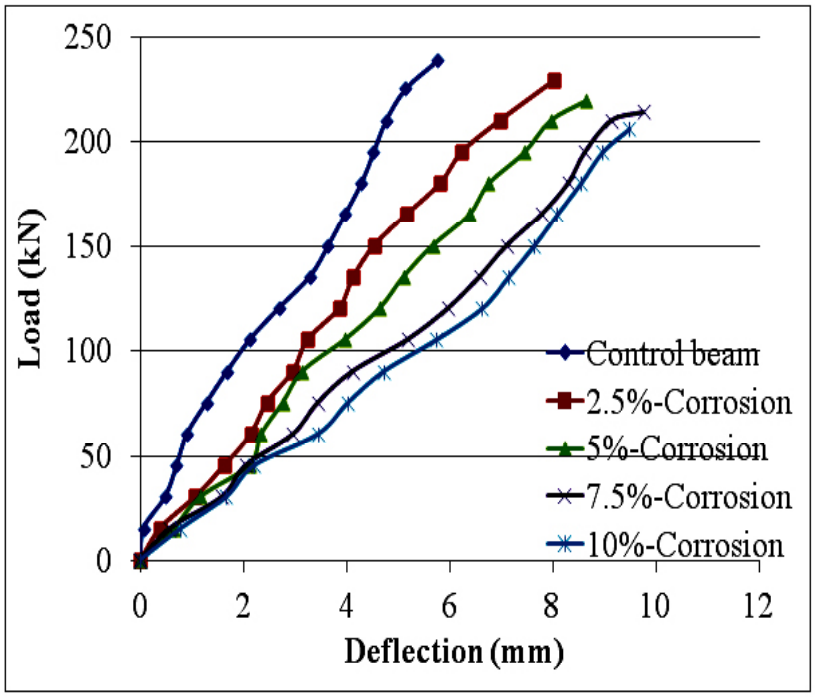

Fig.5.8: Effect of corrosion on central deflection behaviour of PPC concrete beam specimens

Comparison of load deflection behaviour for OPC and PPC concrete beam specimens are shown in Fig.5.9. Values for PPC concrete beams are compared with those for OPC concrete beams. It is seen that the values decrease by 64% to 20% for different levels of corrosion at 195kN load level, (This load is taken constant for comparison purpose).

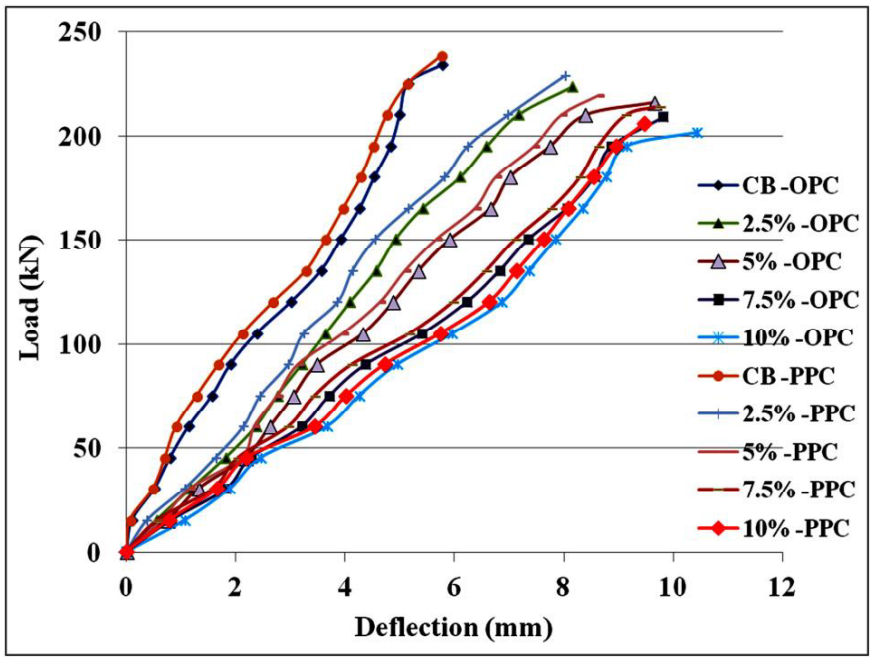

Fig. 5.9: Comparison of effect of corrosion on central deflection behaviour of OPC and PPC concrete beam specimens

5.3.8 Load Strain Behavior

Strain values for the corresponding loads were noted exactly below the load point at the tension side reinforcement level to get the critical average bond stress values. Load strain behaviors of concrete beam specimens are plotted in Fig.5.10 to Fig.5.13. It is seen that as the load level increases, strain value increases linearly in the initial stage. Then at higher corrosion levels, rate of increase of strain value is higher for the same increment of load level, compared to lower levels of corrosion. Control beam specimen performs better compared to increased levels of corrosion. From the load-strain curves, it is clear that the sudden increase in strain levels without increase in load is indicative of slip characteristics owing to drop in bond. It should also be noted that sudden increase in strain values for the beam specimens are much lesser than the

yield strength of main bar used in the study. This behavior is also observed for different levels of corrosion. Higher the accelerated corrosion at surface, lower is the stress level at which such slip occurs. Loss of bond is identified as initial slip point and final slip point at the sudden increase in strain points.

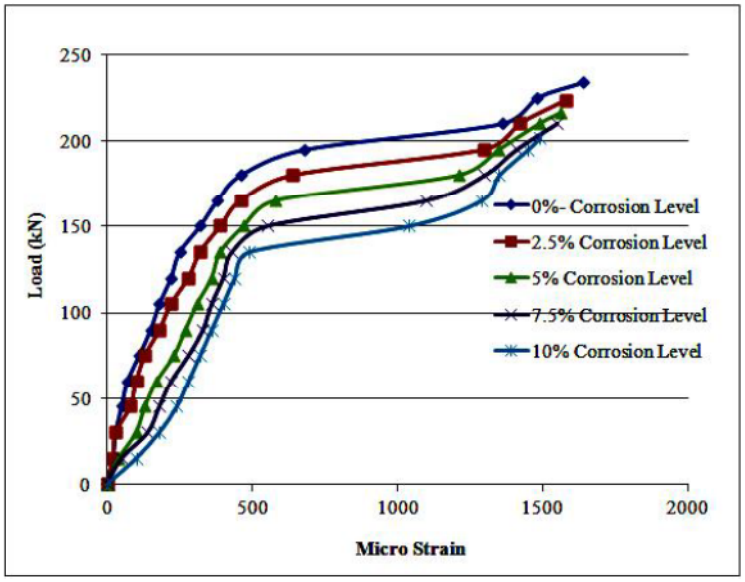

Fig. 5.10: Effect of corrosion on load strain behaviour of OPC concrete beam specimens at left side loading point

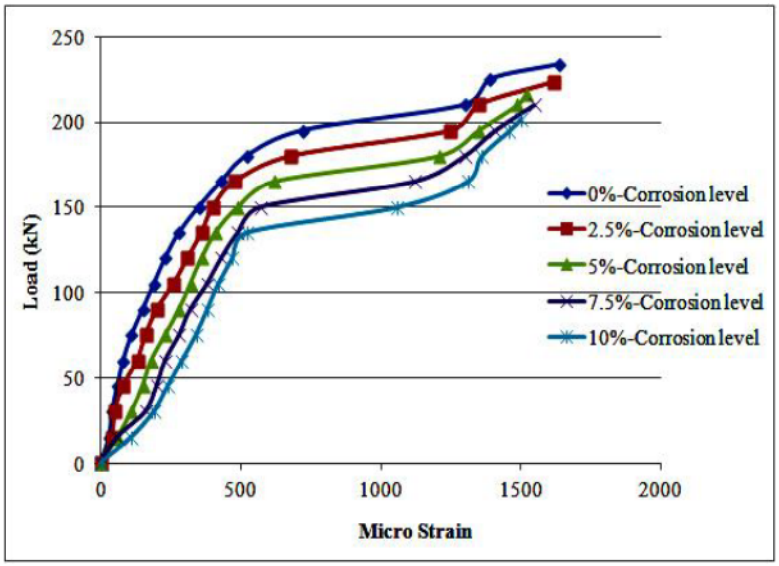

Fig. 5.11: Effect of corrosion on load strain behaviour of OPC concrete beam specimens at right side loading point

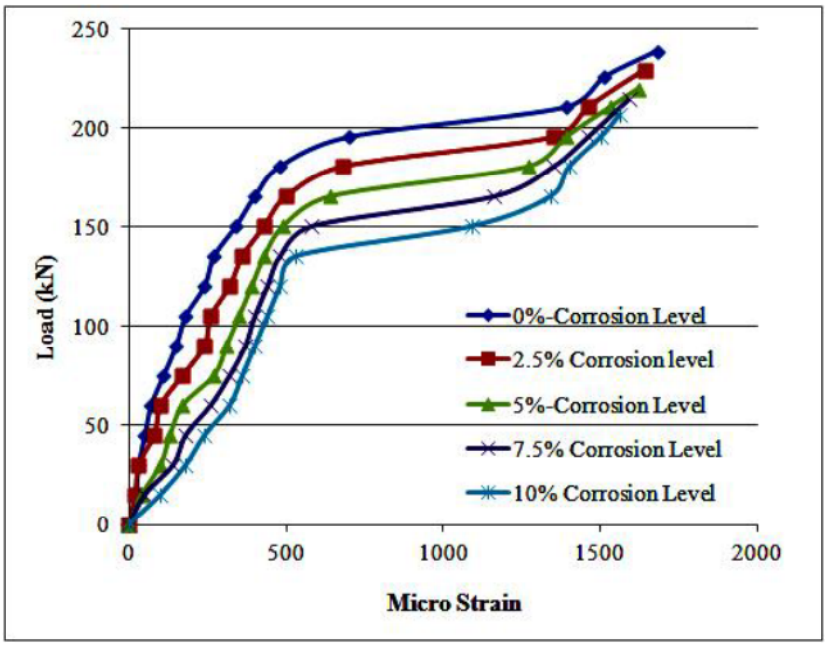

Fig. 5.12: Effect of corrosion on load strain behaviour of PPC concrete beam specimens at left side loading point

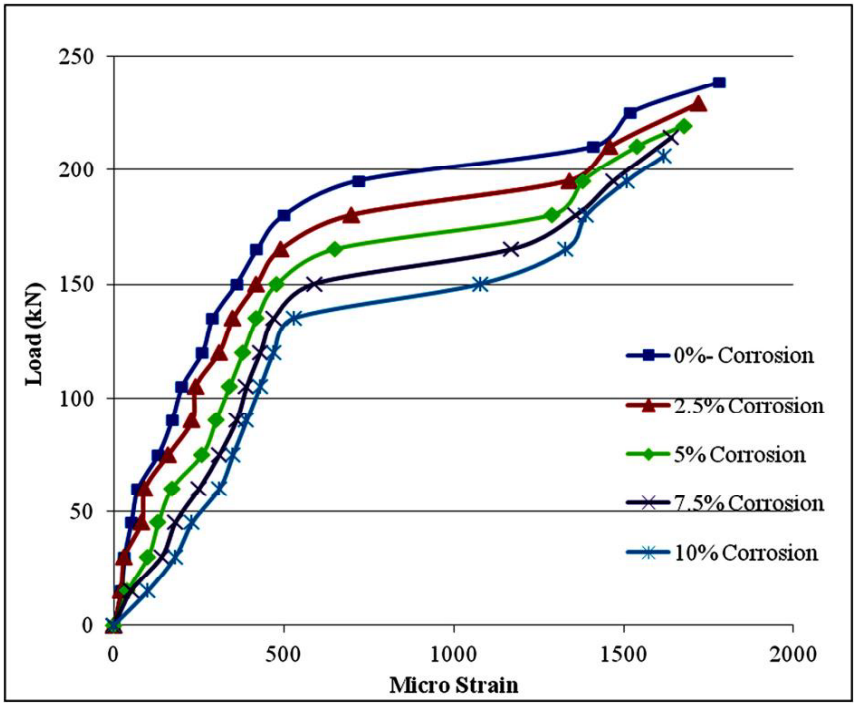

Fig. 5.13: Effect of corrosion on load strain behaviour of PPC concrete beam specimens at right side loading point

5.3.9 Bar Force and Bond Stress Performance of NBS Beam

Bond stress results for different levels of corrosions are obtained from Chapter 3, Eq. (3.8). From Table 5.9 and Table 5.10 it is observed that as the corrosion level increases bond stress decreases. Poisson's effect was not considered in reduction of bar diameter. Percentage reduction in bond stress for different levels of corrosion i.e. 2.5%, 5%, 7.5% and 10% with respect to control specimen were 6.59%, 13.17%, 21.56% and 29.34% respectively for OPC concrete and for PPC concrete 4.32%, 10.65%, 18.93% and 26.04% respectively.

From Fig. 5.14 it is observed that bond stress drops by about 2.6% and 2% respectively for OPC and PPC concrete beam specimen, considering initial slip point for every percentage increase in corrosion level. On the other hand, from Fig.5.15 it is seen that bond stress drops by about 2% and 2.1% respectively for OPC and PPC concrete beam specimens, considering end slip point, for every percentage increase in corrosion level.

Table 5.9: Bar force, reduced diameter and bond stress performance for different levels of corrosion in OPC concrete beam specimens

	Bar force and Bond Stress values at slip region								
	Initiation of slip point					End of slip point			
Corrosion Levels (%)	**Micro Strain**	**Stress in bar (N/mm^2)**	**Reduced Diameter (mm)**	**Bond Stress (N/mm^2)**		**Micro Strain**	**Stress in bar (N/mm^2)**	**Reduced Diameter (mm)**	**Bond Stress (N/mm^2)**
0	700	199.21	25	1.67		1330	367.96	25	3.08
2.5	660	188.85	24.69	1.56		1275	353.58	24.69	2.92
5	600	177.59	24.37	1.45		1210	337.08	24.37	2.75
7.5	560	163.25	24.04	1.31		1110	310	24.04	2.49
10	505	148.13	23.72	1.18		1050	293.93	23.72	2.33

Table 5.10: Bar force, reduced diameter and bond stress performance for different levels of corrosion in PPC concrete beam specimens

	Bar force and Bond stress values at slip region								
	Initiation of slip point					End of slip point			
Corrosion Levels (%)	**Micro Strain**	**Stress in bar (N/mm^2)**	**Reduced Diameter (mm)**	**Bond Stress (N/mm^2)**		**Micro Strain**	**Stress in bar (N/mm^2)**	**Reduced Diameter (mm)**	**Bond Stress (N/mm^2)**
0	710	201.75	25.00	1.69		1290	387.00	25.00	3.24
2.5	690	196.46	24.69	1.62		1240	371.88	24.69	3.07
5	645	185.04	24.37	1.51		1150	354.85	24.37	2.89
7.5	585	170.13	24.04	1.37		1070	325.13	24.04	2.62
10	530	154.94	23.72	1.23		1010	303.13	23.72	2.41

Bond stress values for different degree of corrosion can be calculated from following equations obtained from Figs.5.14 and 5.15,

At initial at slip region

(OPC concrete) $y = -0.049x + 1.678$ $R^2 = 0.996$ (5.9)

(PPC concrete) $y = -0.046x + 1.718$ $R^2 = 0.982$ (5.10)

At final slip Region

(OPC concrete) $y = -0.076x + 3.099$ $R^2 = 0.992$ (5.11)

(PPC concrete) $y = -0.084x + 3.269$ $R^2 = 0.990$ (5.12)

where x=corrosion levels (%) and y= bond stress (N/mm^2).

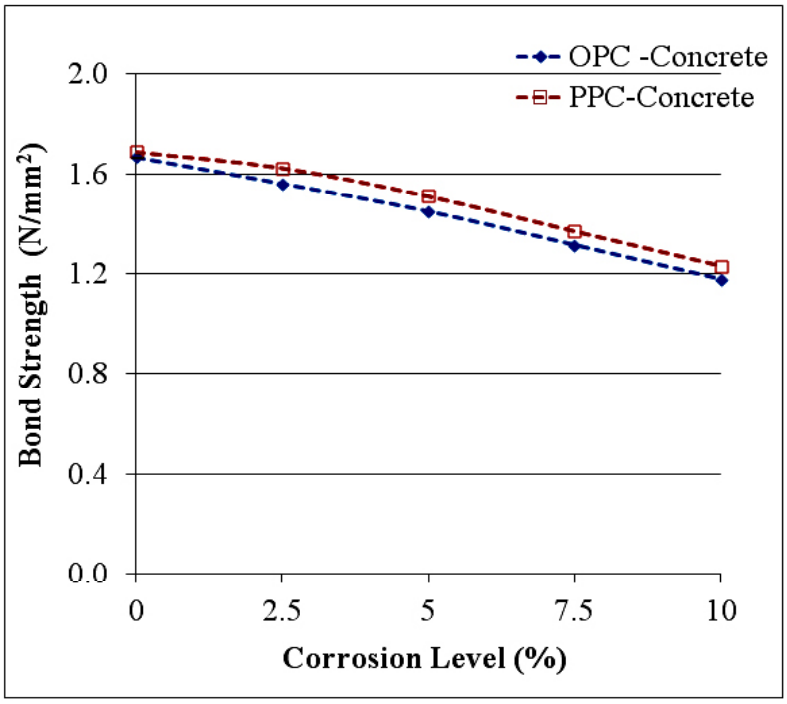

Fig.5.14: Effect of corrosion levels on bond stress at initial point

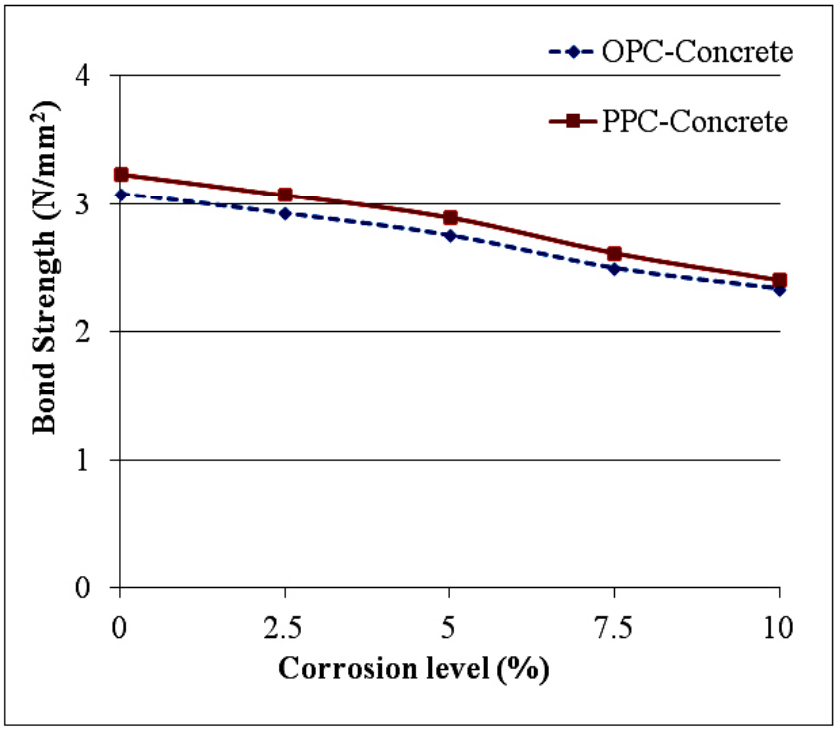

Fig.5.15: Effect of corrosion levels on bond stress at final slip point

5.4 NUMERICAL MODELLING

5.4.1 General

In the present section comparison of experimental results with numerical modelling results are discussed. Effect of corrosion on ultimate load carrying capacity, load deflection characteristics and bond behaviour of reinforced concrete members are presented.

5.4.2 Ultimate Load Carrying Capacity of NBS Beam Specimen

Load carrying capacity against corrosion level is shown in Fig.5.16. The values obtained by experiments as well as numerical modelling are presented here. It is observed that ultimate load carrying capacity decreases as the corrosion level increases. From the slope of the line, about 1.6% drop in load carrying capacity for every percentage increase in corrosion level is evident from experimental results. Corresponding results obtained from finite element analysis yield 1.8%, which is in close agreement with experimental results.

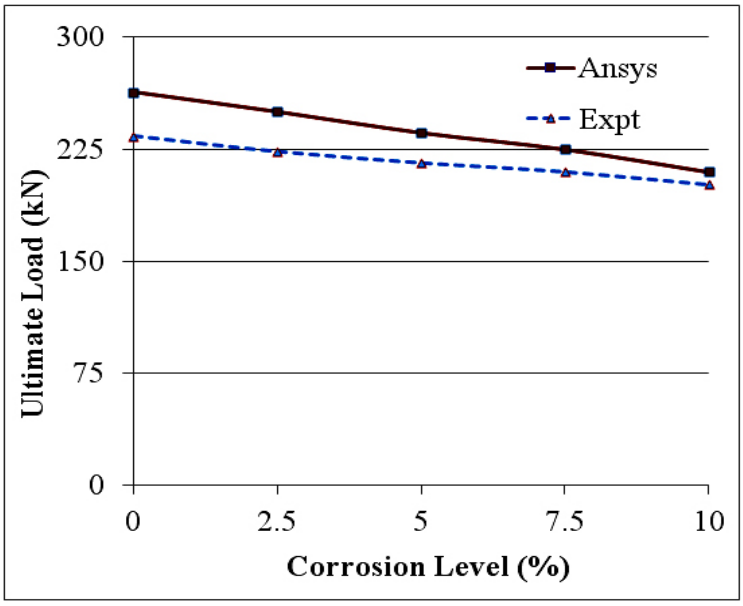

Fig.5.16: Effect of corrosion on ultimate load carrying capacity of beam specimens

5.4.3 Load Deflection Behaviour

A view of deflection for control beam specimen is shown in Fig.5.17. Effect of corrosion on comparison of load deflection behavior for experimental and numerical modeling results is represented in Fig.5.18.

From the experimental results it is seen that deflection values increase by 29% to 45% compared to control beam specimens for 2.5% to 10% corrosion levels Also, from the results of FE model, it is observed that deflection values increases by 27% to 53% compared to control beam specimens for similar corrosion levels.

It is also observed that higher deflection is observed in experiments than numerical modelling. At 195kN load level experimental result shows 10.8%, 6.8%, 4.65%, 3.3% and 2.1% larger deflection value compared to the numerical model for the corresponding corrosion levels of 0%, 2.5%, 5%, 7.5% and 10% respectively.

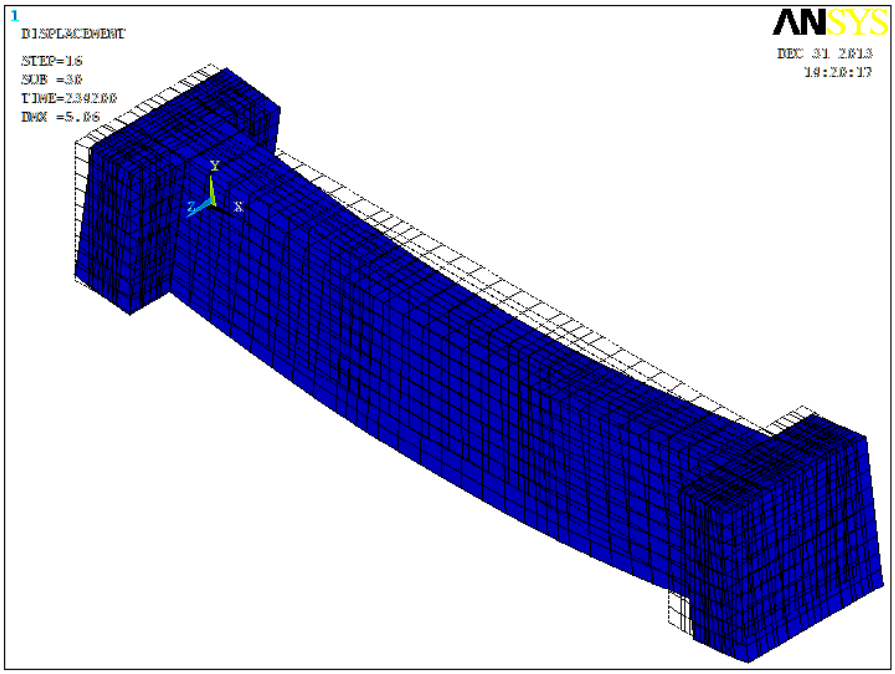

Fig.5.17: View of deflection for control beam specimen

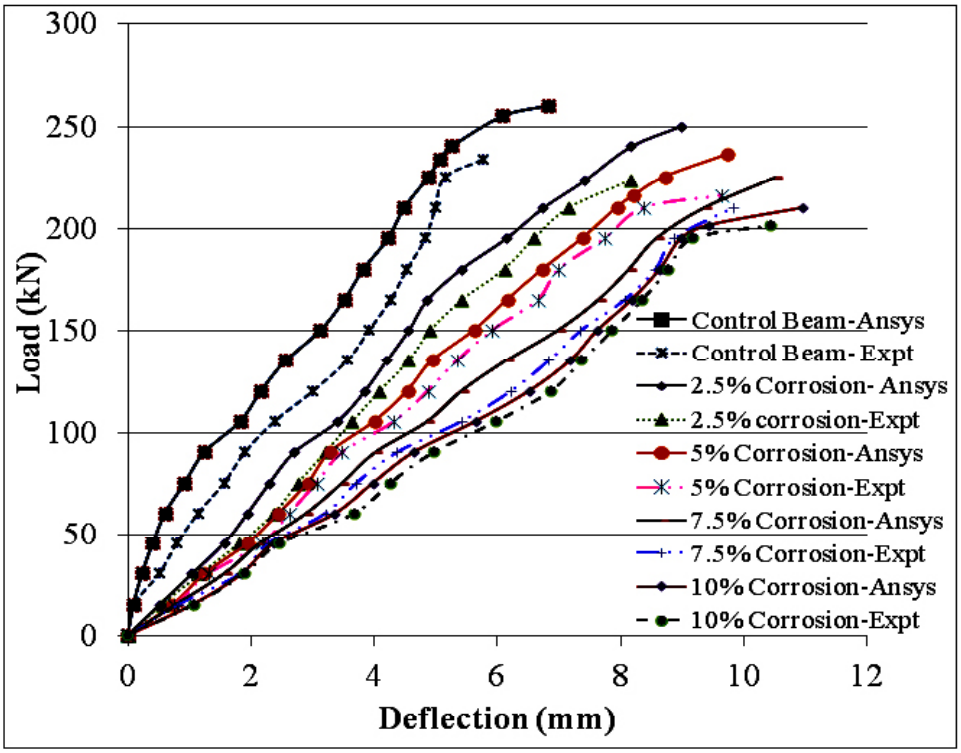

Fig.5.18: Effect of corrosion on central deflection of beam specimens

5.4.4 Load Strain Behaviour of NBS Beam

Effect of corrosion on comparison of load strain behavior for experimental and numerical modeling results is represented in Fig.5.19 for 0%, 2.5% and 5% corrosion and in Fig.5.20 for 0%, 7.5% and 10% corrosion level. It is observed that strain value for numerical model is less compared to the strain value for experimental specimens at the same load level. From Fig.5.19 and Fig.5.20 it is seen that strain value increases linearly with the increase in load level. Sudden increase in strain values are observed for both numerical model and for experimental specimens. The sudden increase in strain value was observed at loads at considerably lower than the yield strength of main bar used in the study. This indicates an increase in slip value without increase in the load level. Further view of strain contour for control beam specimen is shown in Fig.5.21.

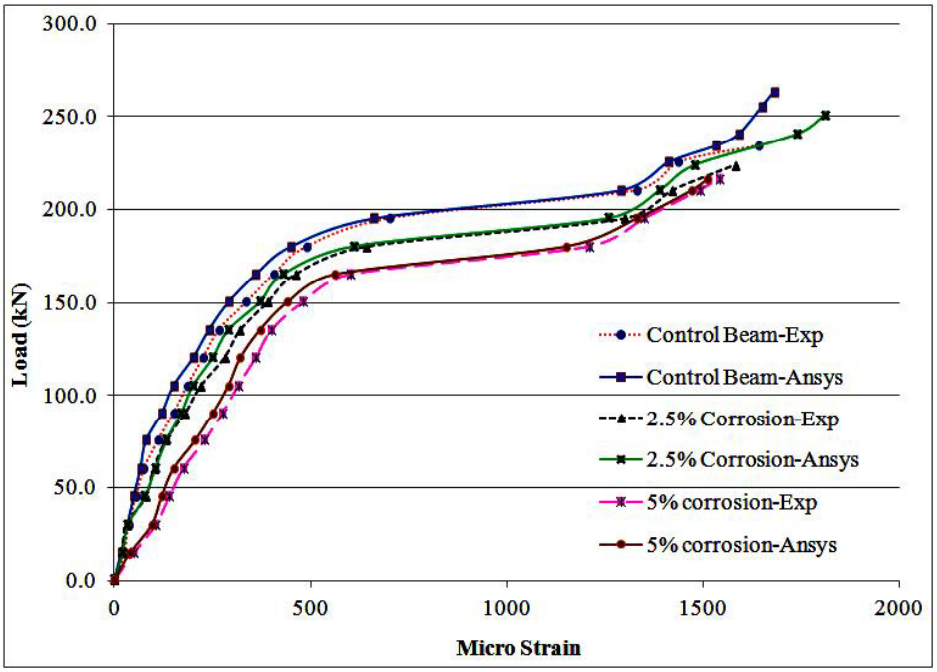

Fig.5.19: Effect of different levels of corrosion on load strain behavior of Beam specimen

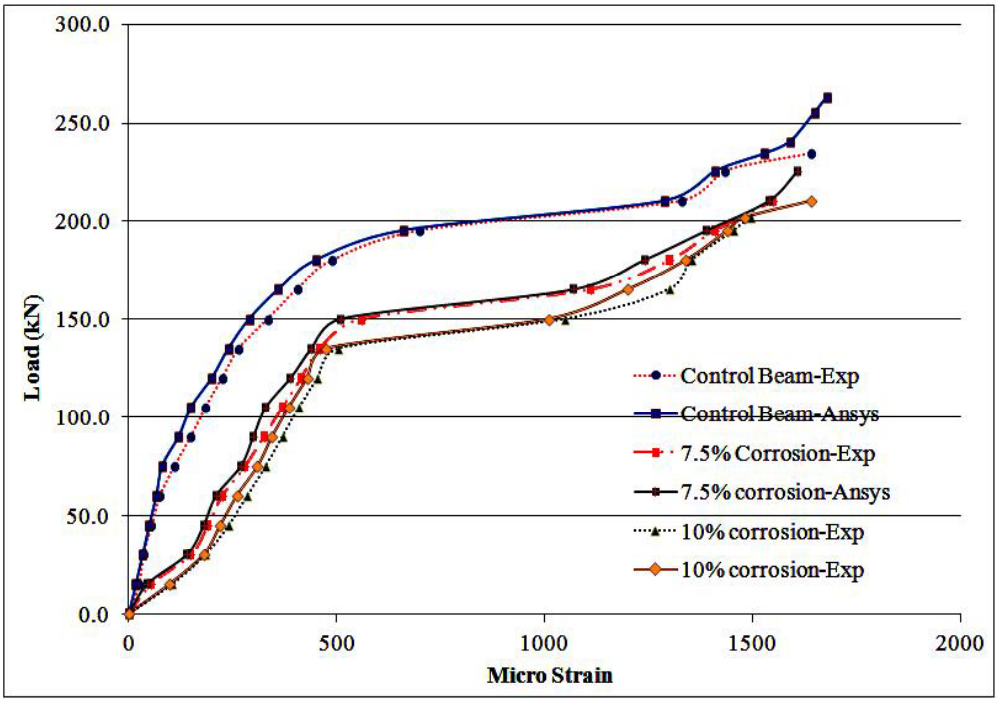

Fig.5.20: Effect of different levels of corrosion on load strain behaviour of beam Specimen

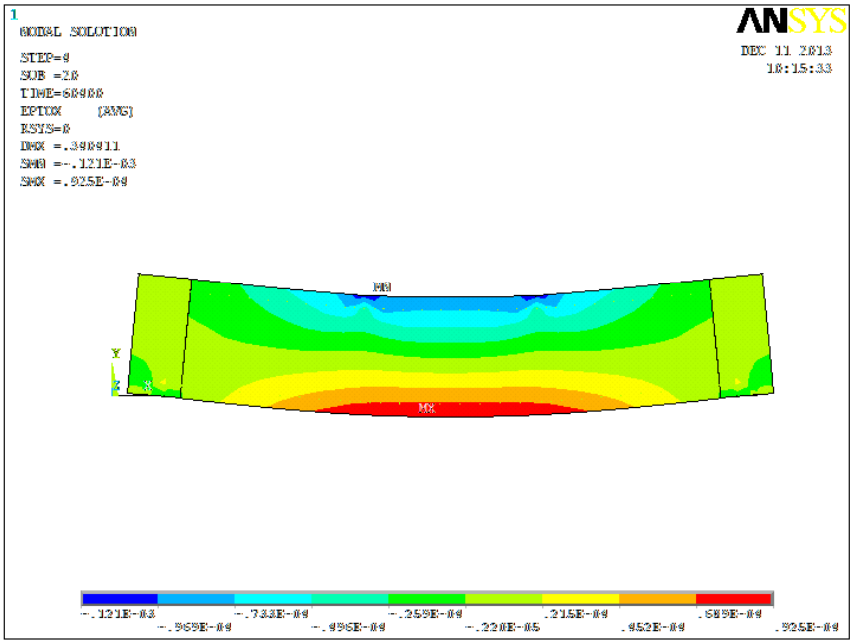

Fig.5.21: A view of strain contour at control beam specimen

5.4.5 Bar Force and Bond Stress Performance of NBS Beam

Bond stress results for different levels of corrosions were obtained from Chapter 3, (Eq. 3.8) and Tabulated in Tables 5.9 and 5.11. It is observed that as the corrosion level increases bond stress value decreases. Percentage reduction in bond stress for different levels of corrosion i.e. 2.5%, 5%, 7.5% and 10% with respect to control beam specimen are 6.59%, 13.17%, 21.56% and 29.34% respectively for experimental beam specimens and for numerical model it varies as 7.6%, 15.82%, 24% and 30.4% respectively.

From Fig.5.22 and Fig.5.23 it is exhibited that bond stress approximately drops for about 2.64% at initiation of slip point and 2.07% for end of slip point in experimental beam specimen and numerical model beam yields about 3.04% at initiation of slip point and 2.12% at end of slip point for every percentage increase in corrosion level. Experimental results shows closer agreements with the numerical modelling results this is because the input data's for the model are used from the experimental study.

Table 5.11: Bar force, reduced diameter and bond stress performance for different levels of corrosion in Numerical model beam specimens

	Bar force and Bond Stress values at slip regions								
	Initiation of slip point					End of slip point			
Corrosion Levels (%)	**Micro Strain**	**Stress in bar (N/mm^2)**	**Reduced Diameter (mm)**	**Bond Stress (N/mm^2)**		**Micro Strain**	**Stress in bar (N/mm^2)**	**Reduced Diameter (mm)**	**Bond Stress (N/mm^2)**
0	660	188.9	25	1.58		1290	360	25.0	3.01
2.5	610	176.2	24.69	1.46		1240	344.7	24.69	2.85
5	560	163.3	24.37	1.33		1150	321	24.37	2.62
7.5	510	149.5	24.04	1.20		1070	299	24.04	2.41
10	470	138.5	23.72	1.10		1010	283.8	23.72	2.25

Bond stress values for different degree of corrosion can be calculated from following equations obtained from Figs.5.22 and 5.23,

At initiation of slip point

(Experimental) $y = -0.049x + 1.678$ $R^2 = 0.996$ (5.13)

(Numerical) $y = -0.049x + 1.577$ $R^2 = 0.999$ (5.14)

At end of slip point

(Experimental) $y = -0.076x + 3.099$ $R^2 = 0.992$ (5.15)

(Numerical) $y = -0.078x + 3.019$ $R^2 = 0.996$ (5.16)

where x=corrosion levels (%) and y= bond stress (N/mm^2).

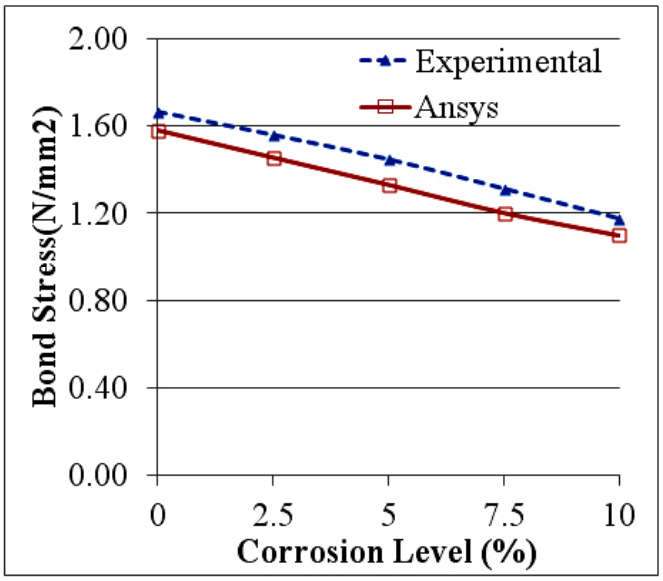

Fig.5.22: Effect of corrosion levels on bond stress at initial slip point

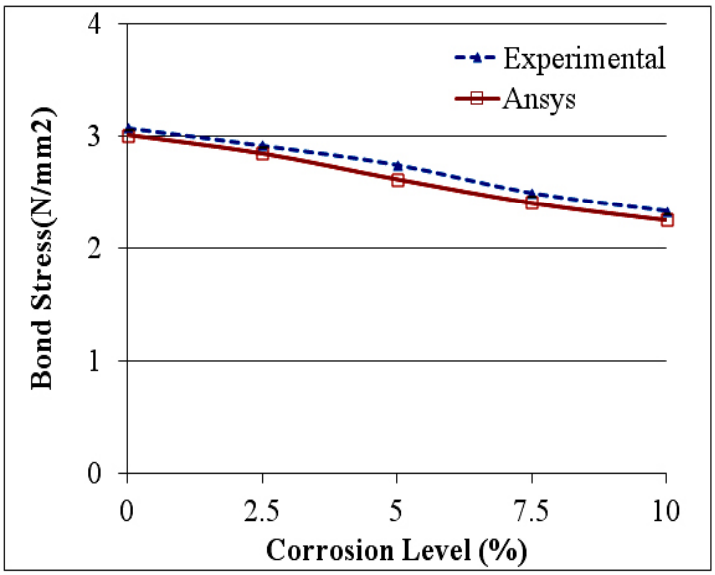

Fig.5.23: Effect of corrosion levels on bond stress at final slip point

5.5 SUMMARY

Details of experimental and analytical investigations carried out to study the performance of bond behaviour have been elaborated.

Results of corrosion current density for different levels of corrosion in pull out test specimens and flexural beam specimens are presented. For the beam specimens effects of corrosion on load carrying capacity, load deflection behaviour and crack width have been presented.

Results of anchorage bond values are compared with the empirical models proposed by the various researchers and the regression equation is suggested for the present study at different levels of corrosion.

It is observed that numerical modelling results show an error less than 10% in load carrying capacity as well as in bond strength compared to experimental results.

Assessment of load carrying capacity and bond strength behaviour in the real life structures subjected to different levels of corrosion can be made by using the proposed prediction equations.

CHAPTER 6

POTENTIAL APPLICATIONS OF PREDICTION EQUATIONS-ILLUSTRATIONS

6.1 GENERAL

Experimental and analytical investigations on effect of corrosion on bond strength and load carrying characteristics have been discussed in Chapter 3 and Chapter 4. The results have been discussed and the findings have been highlighted. Prediction equations for bond strength determination have been proposed. The potential application of the findings in real time health monitoring of structures is presented in the sections that follow.

6.2 ILLUSTRATIONS

Illustration I: Element Assessed-An RC beam in the swimming pool complex at NITK Surathkal.

Beam has a width of 230mm and depth of 300 mm. Main bar 3 No's-16mm have been provided at a clear cover of 25mm. Concrete grade used is M15. Corroded rebar inside beam element is shown in Fig.6.1.

Fig.6.1: Corroded rebar inside beam

Fig.6.2: View of working electrode connection to rebar

Fig.6.3: Monitoring of beam specimen with guard ring

Test set up of field data acquisition set up for corrosion current density ($i_{corr,}$ $\mu A/cm^2$) determination using ACM instrument as shown in Figs.6.2 and 6.3. Real time plot of Potential (mV) vs current (mA/cm^2) for corroded beam is shown in Fig.6.4. For the polarisation value obtained from the plot, corrosion current density value is determined using Stern-Geary formula (Chapter 3, Eq. (3.4)). Table 6.1 represents the values of corrosion current density.

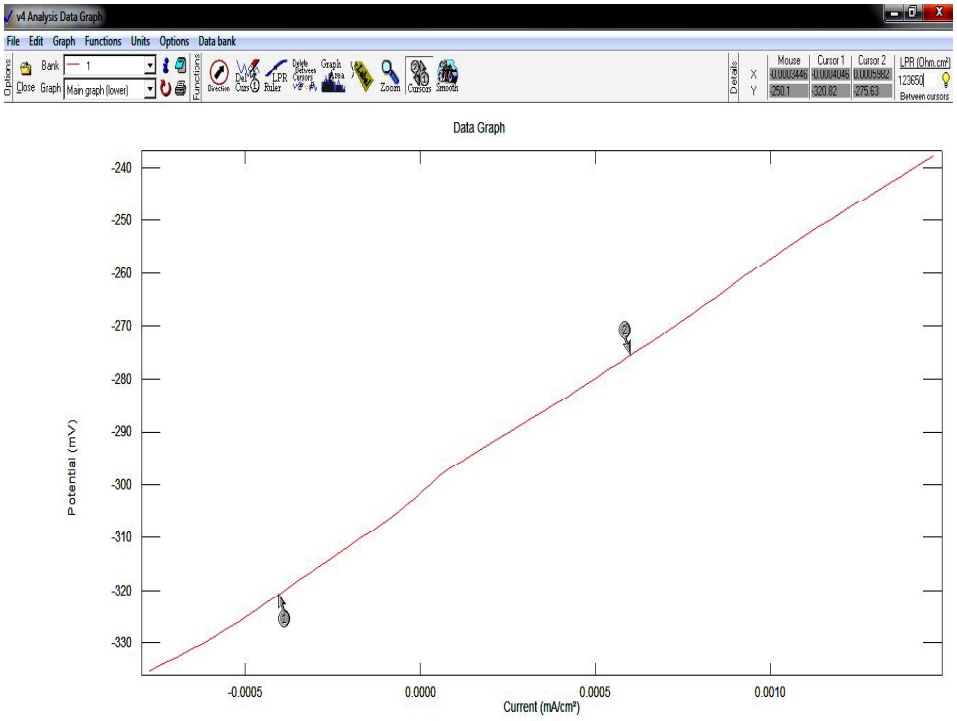

Fig.6.4: Real time plot of corroded beam using ACM instrument

Degree of corrosion percentage (ρ) can be determined using Faradays law as detailed in Eq. (3.1).

For the beam in question the required data for corrosion percentage determination are as under:

W_i= Initial weight of steel reinforcements (=93,469g)

F=Faradays Constant (=96487 Amp-sec)

w= equivalent weight of iron (=27.925 g)

Πdl=Surface area (=73,915cm^2)

t= Time in seconds, from field test (=19×365×24×3600)

Table 6.1: Corrosion current density ($\mu A/cm^2$) of corroded RC beam

Corrosion current density (i_{corr})($\mu A/cm^2$)			
Grid-1	**Grid-2**	**Grid-3**	**Average**
0.583	0.563	0.582	0.576

And substitution in Eq. (3.1) yield corrosion % as

$$(0.576\times10^{-6}) = \frac{\rho\times93469\times96487}{100\times73915.39\times27.925\times19\times365\times24\times3600}$$

$$\therefore \rho = 7.9\%$$

Based on proposed prediction equation for M30 grade concrete:

$$Bond\ \ Strength = -0.076(Corrosion\ Percentage) + 3.099 = 2.5N/mm^2$$

Corresponding bond strength for M15 grade concrete:

$$Bond\ \ strength = 2.5\times0.707 = 1.77N/mm^2$$

Illustration II: Element Assessed- An RC column of the swimming pool complex at NITK Surathkal.

Column has a cross section of (230mm×230mm). Main bar 4 No's-16mm have been provided at a clear cover of 40mm. Footing has a outeside dimension of 1200mm×1200mm and inside dimension of 900mm×900mm. Reinforcement of 6 No's-8mm have been provided at a clear cover of 50mm. Concrete grade used is M15. Corroded rebar inside beam element is shown in Fig.6.1.

A view of corroded rebar inside the RC column is shown in Fig.6.5. Monitoring of column specimen for the determination of corrosion current density using ACM instrument is shown in Fig.6.6.

Fig.6.5: View of corroded rebar

Fig.6.6: Monitoring of RC column

To get the corrosion percentage, the required details given below are substituted in Eq. (3.1).

W_i= Initial weight of steel reinforcements (=25,553g)

F=96487 Amp-sec

w= equivalent weight of iron (=27.925 g)

Πdl=Surface area (=9,042.7cm^2)

t= Time in seconds from field test (=19×365×24×3600)

Similar procedure was followed as per Illustration-I to measure and to get the corrosion current density values. Corrosion current density values obtained for the corroded column is represented in Table 6.2.

Table 6.2: Corrosion current density $(\mu A/cm^2)$ of RC column

Corrosion current density i_{corr} $(\mu A/cm^2)$			
Grid-1	**Grid-2**	**Grid-3**	**Average**
1.246	1.412	1.401	1.353

From the above data, degree of corrosion percentage is,

$$(1.353\times10^{-6}) = \frac{\rho\times25553\times96487}{100\times9042.7\times27.925\times19\times365\times24\times3600}$$

$$\therefore \rho = 8.3\%$$

Bond strength values, considering the prediction equation for M30 grade concrete,

$$Bond\ \ Strength = -0.076(Corrosion\ Percentage) + 3.099 = 2.4N/mm^2$$

For M15 grade bond strength value is,

$$Bond\ \ Strength = 1.69N/mm^2$$

Illustration III: Beam specimens exposed to natural corrosion near the beach of NITK were studied.

Beam has a width of 300mm and depth of 400 mm. Main bars of 2No's-20mm and 1No-16mm have been provided at a clear cover of 30mm. Concrete grade used is M20. View of monitoring of naturally exposed beam specimens near beach side determination is shown in Fig.6.7.

Fig.6.7: View of monitoring of naturally exposed beam near NITK beach

The required data for corrosion percentage determination are given below:

W_i= Initial weight of steel reinforcements (=52346g)

F=96487 Amp-sec

w= equivalent weight of iron (=27.925 g)

Πdl=Surface area (=17,688.5cm^2)

t= Time in seconds from field test (=3×365×24×3600)

Corrosion current density values and the degree of corrosion percentage are given in Table 6.3.

Table 6.3: Corrosion current density and corrosion percentage of naturally exposed RC beam

Corrosion current density($\mu A/cm^2$)				**Corrosion (%)**
Grid-1	**Grid-2**	**Grid-3**	**Average**	
1.100	1.057	1.036	1.064	0.98≈1

Based on the prediction equations, bond strength value for M20 grade concrete is 2.5N/mm^2.

Illustration IV: Measurement of corrosion levels on beam elements have been considered for the study in Civil Engineering Department at NITK Surathkal.

Two floors with different ages have been considered for the study. Beam has a width of 230mm and depth of 530mm. Main bar 2No's-20mm diameter have been provided at a clear cover of 25mm. Concrete grade used is M15. Required Data for the determination of corrosion percentage are given as follows:

W_i= Initial weight of steel reinforcements (=60,267g)

F=Faradays constant, 96487 Amp-sec

w= equivalent weight of iron (=27.925 g)

Πdl=Surface area (=32,997cm^2)

Corrosion current density values obtained from the field study and Corrosion percentage values determined based on the Faradays law are given in Table 6.4.

Table 6.4: Corrosion current density and corrosion percentage of RC beams

Storey	**Age (T) (years)**	**Corrosion current density** ($\mu A/cm^2$)				**Corrosion (%)**
		Grid-1	**Grid-2**	**Grid-3**	**Average**	
Ground	14	0.747	0.721	0.742	0.737	5.16
1st Floor	8	0.745	0.667	0.712	0.708	2.83

For M15 grade of present illustration:

Bond strength values for corrosion levels of 5.16% and 2.83% are 1.9N/mm^2 and 2N/mm^2 respectively.

6.3 CORROSION LEVEL AS A FUNCTION OF TIME

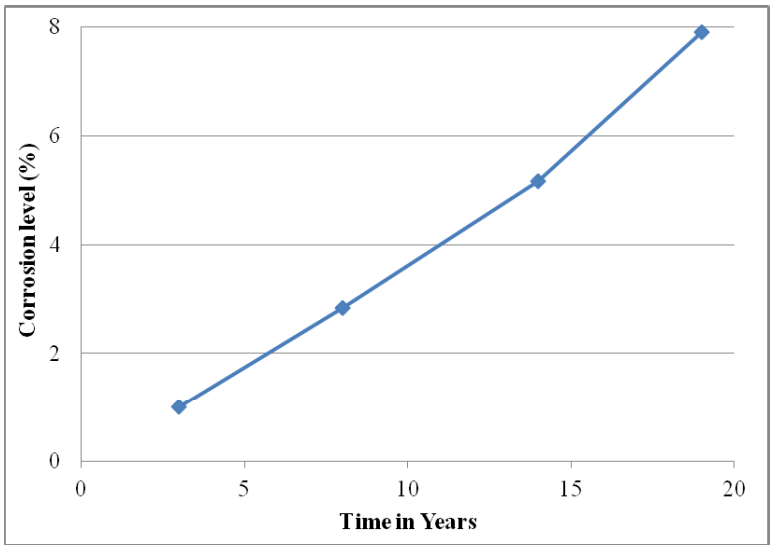

Fig.6.8: Progress of corrosion level with time

Different corrosion levels obtained in field study for different ages (years) are represented in Fig.6.8. It is observed that the corrosion level increases with passage of time as expected.

Considering the Faradays Eq.(3.1) i.e.

$$i_{corr} = \frac{W_i \times F \times \rho}{(\pi d l) \times w \times t}$$

for any given structural element, $\frac{W_i \times F}{(\pi d l) \times w}$ values will be known. Corrosion current density (i_{corr}) value can be determined from the field study using the ACM instrument. ρ is the degree of corrosion can be determined either by extracting the samples per meter length and by measuring the mass loss. Then corrosion initiation time can be determined. This helps in the assessment of service life of structures. In other hand, if the exact corrosion initiation time is monitored in the field, we can calculate the corrosion percentage.

6.4 COMPARATIVE EVALUATION PERFORMANCE FOR THE NBS CORRODED BEAM SPECIMENS

Results on Load deflection behaviour of NBS beam specimens have been discussed in Chapter 5. In this section the performance evaluation of corroded beam specimens for OPC concrete are elaborated. Table 6.5 represents the results on load deflection behaviour of beam specimens for different levels of corrosion.

Table 6.5: Load deflection behaviour on the corrosion of beams

ρ	P_u (kN)	du_1 (mm)	P_y(kN)	dy (mm)	du_2 (mm)
0	234.2	5.78	225.4	5.15	5.94
2.5	223.9	8.16	210.4	7.16	8.41
5	216.4	9.64	201.4	7.99	10.04
7.5	209.4	9.82	195.4	8.87	10.06
10	201.4	10.44	180.4	9.10	10.78

du_1= Deflection at ultimate load (mm); P_y= Yield load (kN); dy= Deflection at yield load); du_2= Deflection at 0.75 P_u in the post ultimate region; P_u= ultimate load; ρ = Corrosion Level (% weight loss).

Following method is suggested for evaluating the performance reduction factor in reinforced concrete structures. Using the equivalence of energy approach, the equivalent linear elastic load is calculated from the following equation (Ramesh et al. 2010)

$$P_{e1} = \left[2 A_e (P_y / dy)\right]^{1/2} \quad (6.1)$$

Where P_{e1} is the equivalent elastic load, d*y* is the yield deformation, P_y is the yield load and A_e is the area of the load deflection curve upto a deflection corresponding to a load of 75% of the peak load in the post peak region

Similarly, the equivalent elastic load P_{e2} using the equivalent of failure deformation is obtained as

$$P_{e2} = P_y (du_1 / dy) \quad (6.2)$$

where, du_1 is the ultimate deformation, The values of P_{e1} and P_{e2} derived from energy and deformation approaches are given in Table 6.6.

Table 6.6: Performance factors of the corrosion beams for OPC concerte

Corrosion (%)	P_{e1} (kN)	P_{e2} (kN)	f_1	f_2
0	251.6	252.97	1	1
2.5	224.83	239.78	0.89	0.95
5	221.58	226.99	0.88	0.90
7.5	205.8	216.33	0.82	0.85
10	193.6	206.96	0.77	0.82

Definition of the performance factors f_1 and f_2 is given below:

$f_1 = P_{e1}$ (Corroded beam) / P_{e1}(Control beam)

$f_2 = P_{e2}$ (Corroded beam) / P_{e2}(Control beam)

Two performance factors have been evaluated, the equivalent linear load is derived from equivalence of energy approach and also from equivalent of failure deformation. Performance factors have also been derived from them. Performance factor is the ratio of the equivalent linear load of the beam to that of the control beam. As expected the performance of the beams have reduced with the increase in the corrosion level. It is seen from the Table 6.6 that the performance level drops to a level of 0.77 to 0.95 times that of control beam specimen. Hence these values are of great concern from the serviceability point of view.

6.5 SUMMARY

In this chapter, corroded RC beam structural elements are considered for the potential applications of prediction equations. Determination of reduction in bond strength for the corroded structural elements is elaborated. Performance evaluation factors have been evaluated for different levels of corrosion. Assessment of structure gives the condition of structure required for repairs and rehabilitation.

CHAPTER 7

CONCLUSIONS

The effect of reinforcement corrosion on bond strength of RC members has been studied in this thesis.

Investigations have been carried out using detailed experiments followed by numerical modelling. Equations for predicting corrosion levels have been proposed and some case studies have been performed to show the applicability of prediction equations to field situations.

Major findings of this investigation are listed below:

- With regard to anchorage bond strength, at low level corrosion (0 to 2.5%), the bond strength is unaffected because of the increased roughness at the bar surface. When the corrosion level increases beyond 2.5%, there is a decrease in the load carrying capacity as well as in the bond strength.

- With regard to flexural bond strength, reinforcement corrosion leads to the decrease of load carrying capacity. Decrease in strength is linearly proportional to the amount of corrosion. The drop in strength, obtained experimentally is about 1.6%, per percentage increase in corrosion level, while the corresponding value for numerical modelling is about 1.8%.
- Effect of reinforcement corrosion on crack width variation is small at lower levels of corrosion. However above 5% corrosion level, crack width increases rapidly.
- Reinforcement corrosion causes degradation of the bond behavior. The strain value becomes large due to corrosion. Also the larger the corrosion, the lesser is the bond stress value.

- PPC concrete beam specimen performs better than OPC concrete beam specimen with respect to Load carrying capacity, load deflection behavior, crack width and bond strength characteristics. This is because the later strength gains due to the hydration process and also due to the low permeability property.

- In experimental investigation, bond strength degradation of 2.6% at slip initiation and 2.1% at end of slip have been observed for every percentage increases in corrosion level. The corresponding values in numerical modelling are 3% and 2.4%.

- Numerical results are in close agreement with the experimental values and hence it is concluded that the numerical modelling can address satisfactorily corrosion effects on load deflection behaviour and bond strength issues for the levels considered in the present study.

- Proposed regression equation is very much useful for quick assessment to predict the bond strength values for different corrosion levels in structures. Structures can be monitored for different corrosion levels by using the applied corrosion monitoring instrument. Based on measured corrosion current density values, corrosion percentage can be determined. With the help of empirical prediction equation for different corrosion percentage, drop in bond strength values can be determined

- Versatility of the results is applicable to the RC beam structures for the different levels of corrosion within the experimental data.

- Assessment of structures and performance evaluation factors gives the condition of structure required for repairs and rehabilitation.

SCOPE FOR FUTURE WORK

- Study may be carried out in different exposure conditions such as, natural corrosion and sea corrosion, to study the effect of corrosion on strength and durability aspects of structures.
- Experimental results can be compared with the high performance concrete for the specified corrosion rates.
- Studies on beam column joints in coastal environment can be carried out to study the residual strength of RC member.

APPENDIX - A

CONCRETE MIX DESIGN

Design of M30 Grade OPC and PPC Concrete Mix

DESIGN STIPULATIONS

The design procedure followed is as per IS: 10262-2009

Desired characteristic strength of the concrete f_{ck} - 30N/mm^2

Maximum size of aggregates (angular) - 20mm &12.5mm

DATA

1) Cement used – Ultra Tech 43-grade conforming to IS 1489 (Part-I):1991.

2) Specific gravity of:

(a) Cement : 3.10

(b) Fine Aggregate : 2.6

(c) Coarse Aggregate : 2.8

3) Sieve analysis– Fine Aggregate confirming to zone III gradation requirements as per IS: 383-1970.

PROCEDURE

Step 1. Target mean strength: $f_t = f_{ck} + 1.65\ S$

(Using tolerance factor =1.65)

Standard deviation S=6, Table - 8 of IS: 456 –2000

Target Strength $f_t = 30 + 1.65 \times 5$

$f_t = 39.90$ N/mm^2

Step 2. Selection of water to cement ratio:

Maximum water cement ratio has to be used for Coastal environment

Adopt w/c ratio – 0.45

Step 3. Selection of water and sand content and cement content:

For 20mm and 12mm Nominal size aggregate and sand confirming to zone III

Sand content = 40% of volume of sand to volume of F.A

Cement = 400 kg/m^3

Step 4. Determination of Fine Aggregate content:

$$V = [W + \frac{C}{Sc} + \frac{1}{P}\frac{Fa}{S_{Fa}}]\frac{1}{1000}$$

$$1 = [180 + \frac{400}{3.10} + \frac{1}{0.4} \times \frac{Fa}{2.6}]\frac{1}{1000}$$

F.A = 718.61 kg/m^3

Step 5. Determination of Coarse Aggregate content :

$$V = [W + \frac{C}{Sc} + \frac{1}{(1-p)} \times \frac{Ca}{Sca}]\frac{1}{1000}$$

$$1 = [180 + \frac{400}{3.10} + \frac{1}{(1-0.4)} \times \frac{Ca}{2.8}]\frac{1}{1000}$$

C A = 1160.83 kg/m^3

MIX PROPORTION

C	**:**	**FA**	**:**	**CA**	**:**	**W**
400	:	718.61	:	1160.83	:	180
1	:	1.8	:	2.9	:	0.45

Cement = 400.00 kg/m^3

Fine Aggregate = 718.61 kg/m^3

Coarse Aggregate = 1160.83 kg/m^3

Water = 180.00 kg/m^3

Super plasticizer SP 430 (Conplast) = 2ml/kg of cement

APPENDIX - B

DESIGN CALCULATION TO FIX THE REINFORCEMENT DETAILS

From Chapter 3; Fig.3.10,

L= 2440mm, l=2240mm, B=203mm, d=394.5mm, diameter of bar 25mm

Assumed Parameters f_{ck}=30N/mm^2, f_y= 415 N/mm^2

$$0.36\times f_{ck}\times b\times X_u = 0.87\times Ast\times f_y$$

$$0.36\times 30\times 0.203\times X_u = 0.87\times \frac{\pi}{4}\times (25)^2\times 415$$

$$X_u = 80.44mm \prec 0.48\times d$$

$$M_u = 0.87\times \frac{\pi}{4}\times (25)^2\times 415\times (394.5-0.416\times 80.44)$$

$$M_u = 63.986\ kN-m$$

Two Point Loading

$$\frac{6\times M_U}{L}\geq P$$

$$\underline{P = 177.44kN}$$

$$\frac{P}{2} = V_u$$

$$\frac{177.44}{2} = V_u$$

$$\underline{V_u = 88.72kN}$$

<u>One legged 8mm diameter stirrups</u>

$$Vus = \frac{\left(\frac{\pi}{4}\right)\times 8^2\times 0.87\times 415\times 394.5}{S_v} \quad \underline{\Rightarrow S_V = 8mm\ @\ 75mm\ c/c}$$

APPENDIX - C

1. Theoretical Load and deflection Calculation for OPC Concrete beam

Load Calculation

L= 2440mm, B=203mm, d=394.5mm, diameter of bar 25mm

Experimentally obtained values

f_{ck}= 34.44N/mm^2, f_y=485 N/mm^2

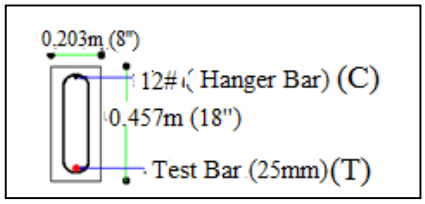

C=T

$$0.543\times f_{ck}\times b\times X_u = f_y\times Ast$$

$$0.543\times 34.44\times 203\times X_u = 485\times\left(\frac{\pi\times 25^2}{4}\right)$$

$$X_u = 62.71mm$$

$$\left(\frac{X_{u\max}}{d}\right)=\frac{0.0035}{0.0055+\frac{f_y}{E_S}}$$

$$\left(X_{u\max}\right)=174.21mm$$

$$X_u \prec \left(X_{u\max}\right)$$

Hence Section is under reinforced.

$$M_u = C(d-0.416X_u)$$

$$M_u = 0.543\times 34.44\times 203\times 62.71(394.5-0.416\times 62.71)$$

$$M_u = 87.70kN-m$$

$$\frac{6\times M_U}{L}\geq P$$

$$\frac{6\times 87.70}{2.24}=P$$

$$P = 234.91kN$$

Deflection Calculation (As per IS 456-2000 (Annex 'C')

$$A_{SC} = \left(\frac{\pi \times 12^2}{4}\right) = 113.097\,mm^2, \qquad A_{st} = \frac{\pi \times 25^2}{4} = 490.87mm^2,\ d = 394.5mm,\ d_c = 62.5mm$$

$$m = \frac{280}{35.23} = 8$$

$$\frac{bn^2}{2} + (1.5m - 1) \times A_{sc}(n - d_c) = mA_{st}(d - n)$$

$$\frac{203 \times n^2}{2} + (1.5 \times 8 - 1) \times 113.097(n - 62.5) = 8 \times 490.87(394.5 - n)$$

$$101.5n^2 + 5170.46n - 1.6269 \times 10^6 = 0$$

$$\Rightarrow n = 103.67mm$$

$$I_{cr} = \frac{bn^3}{3} + (m \times A_{st}) \times (d - n)^2 + (1.5m - 1)A_{sc}(n - d_c)^2$$

$$I_{cr} = \frac{203 \times (103.67)^3}{3} + (8 \times 490.87) \times (394.5 - 103.67)^2 + (1.5 \times 8 - 1) \times 113.097(103.67 - 62.5)^2$$

$$I_{cr} = 0.40977 \times 10^9\ mm^4$$

$$I_{eff} = \frac{I_{cr}}{1.2 - \left(\frac{M_r}{M_{\max}} \times \frac{Z}{d}\right)\left[1 - \left(\frac{x}{d}\right)\right]\left(\frac{b_w}{b}\right)}$$

$$M_r = 0.7\sqrt{34.44} \times \left(\frac{203 \times 457^2}{6}\right)$$

$$M_r = 29.03kN - m$$

$$Z = 394.5 - \left(\frac{103.67}{3}\right) = 359.94mm$$

$$x = 103.67\,mm$$

$To\ \det er\min e\ M_{\max}$

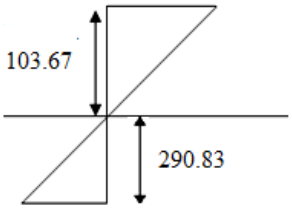

$$f_{st} = 0.58 \times f_y$$
$$= 0.58 \times 485$$
$$= 281.3 N/mm^2$$

$\frac{b_w}{b} = 1$; *for beams*

$$\frac{f_{st}}{m} = \frac{281.3}{8} = 35.16 N/mm^2$$

$$f_c = \frac{35.16}{290.83} \times 103.67 = 12.53 N/mm^2$$

$$M_{\max} = \frac{bnf_c}{2} \times \left(d - n/3\right) + (1.5m - 1) \times A_{sc} \times f_{sc} \times (d - d_c)$$

$$M_{\max} = \frac{230 \times 103.67 \times 12.53}{2} \times \left(394.5 - 103.67/3\right) + (1.5 \times 8 - 1) \times 113.097 \times 12.53 \times (394.5 - 62.5)$$

$M_{\max} = 58.95 kN - m$

$$I_{eff} = \frac{I_{cr}}{1.2 - \left(\frac{M_r}{M_{\max}} \times \frac{Z}{d}\right)\left[1 - \left(\frac{x}{d}\right)\right]\left(\frac{b_w}{b}\right)}$$

$$I_{eff} = \frac{0.40977 \times 10^9}{1.2 - \left(\frac{29.03}{58.95} \times \frac{359.94}{394.5}\right)\left[1 - \left(\frac{103.67}{394.5}\right)\right](1)}$$

$$\underline{I_{eff} = 0.4717 \times 10^{9} \qquad mm^4}$$

Deflection at centre,

$$\delta_{theoretical} = \frac{Pa(3l^2 - 4a^2)}{24EI}$$

$$\delta_{theoretical} = \frac{P \times 747[3(2240)^2 - 4(747)^2]}{24 \times 5000\sqrt{34.44} \times 0.4717 \times 10^{9}}$$

$$\delta_{theoretical} = P \times 2.845 \times 10^{-5}$$

$$\delta_{theoretical} = 235.36 \times 10^{3} \times 2.845 \times 10^{-5}$$

$$\underline{\delta_{theoretical} = 6.68mm}$$

APPENDIX – C2

2. Theoretical Load and deflection Calculation for PPC Concrete beam

Load Calculation

L= 2440mm, B=203mm, d=394.5mm, diameter of bar 25mm

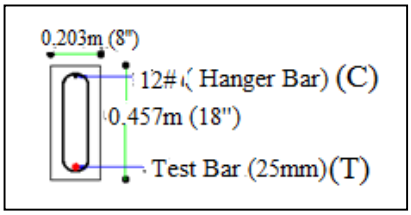

Experimentally obtained values

f_{ck}= 32.57N/mm^2, f_y=485 N/mm^2

C=T

$$0.543\times f_{ck}\times b\times X_u = f_y\times Ast$$

$$0.543\times 32.57\times 203\times X_u = 485\times\left(\frac{\pi\times 25^2}{4}\right)$$

$$X_u = 66.68mm$$

$$\left(\frac{X_{u\max}}{d}\right)=\frac{0.0035}{0.0055+\frac{f_y}{E_S}}$$

$$\left(X_{u\max}\right)=174.21mm$$

$$X_u \prec \left(X_{u\max}\right)$$

Hence Section is under reinforced.

$$M_u = C(d-0.416X_u)$$

$$M_u = 0.543\times 32.57\times 203\times 66.68(394.5-0.416\times 66.68)$$

$$M_u = 87.315\,kN-m$$

$$\frac{6\times M_U}{L}\geq P$$

$$\frac{6\times 87.315}{2.24}=P$$

$$P = 233.88\,kN$$

Deflection Calculation (As per IS 456-2000 (Annex 'C')

$$A_{SC} = \left(\frac{\pi \times 12^2}{4}\right) = 113.097\,mm^2, \qquad A_{st} = \frac{\pi \times 25^2}{4} = 490.87mm^2,\ d = 394.5mm,\ d_c = 62.5mm$$

$$m = \frac{280}{32.57} = 8 = 9$$

$$\frac{bn^2}{2} + (1.5m - 1) \times A_{sc}(n - d_c) = mA_{st}(d - n)$$

$$\frac{203 \times n^2}{2} + (1.5 \times 9 - 1) \times 113.097(n - 62.5) = 9 \times 490.87(394.5 - n)$$

$$101.5n^2 + 5831.5425n - 1.83119 \times 10^6 = 0$$

$$\Rightarrow n = 108.629mm$$

$$I_{cr} = \frac{bn^3}{3} + (m \times A_{st}) \times (d - n)^2 + (1.5m - 1)A_{sc}(n - d_c)^2$$

$$I_{cr} = \frac{203 \times (108.63)^3}{3} + (9 \times 490.87) \times (394.5 - 108.63)^2 + (1.5 \times 9 - 1) \times 113.097(108.63 - 62.5)^2$$

$$I_{cr} = 0.45078 \times 10^9\ mm^4$$

$$I_{eff} = \frac{I_{cr}}{1.2 - \left(\frac{M_r}{M_{\max}} \times \frac{Z}{d}\right)\left[1 - \left(\frac{x}{d}\right)\right]\left(\frac{b_w}{b}\right)}$$

$$M_r = 0.7\sqrt{32.57} \times \left(\frac{203 \times 457^2}{6}\right)$$

$$M_r = 28.23kN - m$$

$$Z = 394.5 - \left(\frac{108.63}{3}\right) = 358.29mm$$

$$x = 108.673mm$$

$To\ \det er\min e\ M_{\max}$

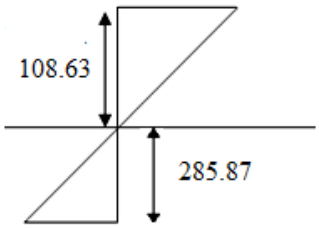

$$f_{st} = 0.58 \times f_y$$
$$= 0.58 \times 485$$
$$= 281.3 N/mm^2$$

$\frac{b_w}{b} = 1;\ for\ beams$

$$\frac{f_{st}}{m} = \frac{281.3}{9} = 31.26\ N/mm^2$$

$$f_c = \frac{31.26}{285.87} \times 108.63 = 11.88 N/mm^2$$

$$M_{\max} = \frac{bnf_c}{2} \times \left(d - n/3\right) + (1.5m - 1) \times A_{sc} \times f_{sc} \times (d - d_c)$$

$$M_{\max} = \frac{230 \times 108.63 \times 11.88}{2} \times \left(394.5 - 108.63/3\right) + (1.5 \times 9 - 1) \times 113.097 \times 11.88 \times (394.5 - 62.5)$$

$M_{\max} = 52.508\ kN - m$

$$I_{eff} = \frac{I_{cr}}{1.2 - \left(\frac{M_r}{M_{\max}} \times \frac{Z}{d}\right)\left[1 - \left(\frac{x}{d}\right)\right]\left(\frac{b_w}{b}\right)}$$

$$I_{eff} = \frac{0.45078 \times 10^9}{1.2 - \left(\frac{28.23}{52.508} \times \frac{358.29}{394.5}\right)\left[1 - \left(\frac{108.63}{394.5}\right)\right](1)}$$

$$I_{eff} = 0.5327 \times 10^9 \ \ mm^4$$

$$\underline{I_{cr} \le I_{eff} \le I_{gr} \qquad I_{gr} = 1.04 \times 10^9}$$

Deflection at centre,

$$\delta_{theoretical} = \frac{Pa(3l^2 - 4a^2)}{24EI}$$

$$\delta_{theoretical} = \frac{P \times 747[3(2240)^2 - 4(747)^2]}{24 \times 5000\sqrt{32.57} \times 0.5327 \times 10^9}$$

$$\delta_{theoretical} = P \times 2.625195 \times 10^{-5}$$

$$\delta_{theoretical} = 233.88 \times 10^3 \times 2.625195 \times 10^{-5}$$

$$\underline{\delta_{theoretical} = 6.13mm}$$

APPENDIX – D

A view of Crack propagation in NBS beam Specimen

Fig.D1(a)

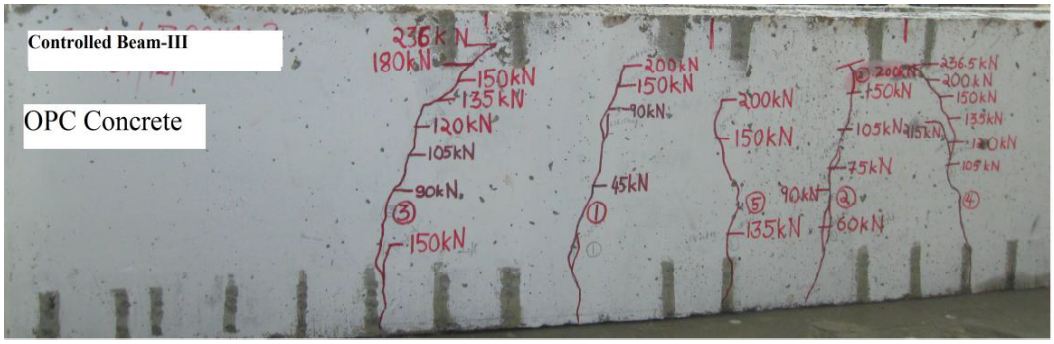

Fig.D1(b)

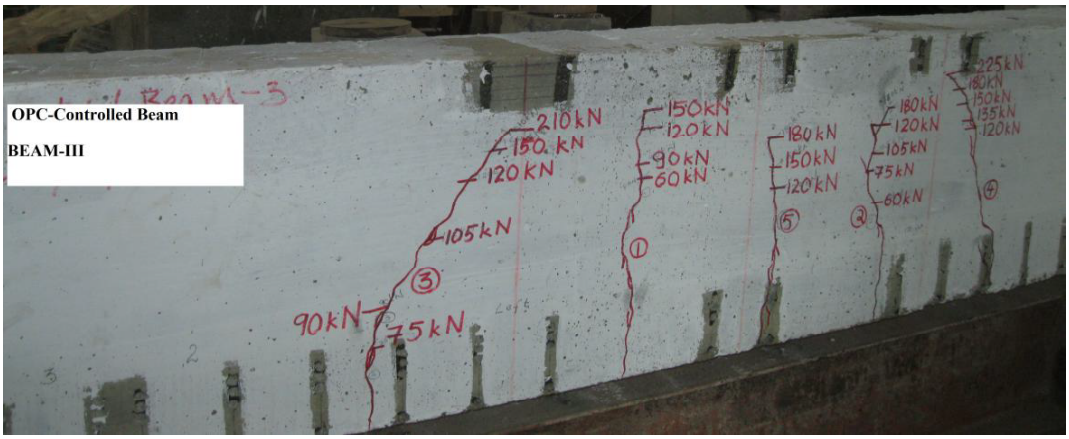

Fig.D1(c)

Fig.D1: Crack propagation in controlled beam specimens (OPC concrete)

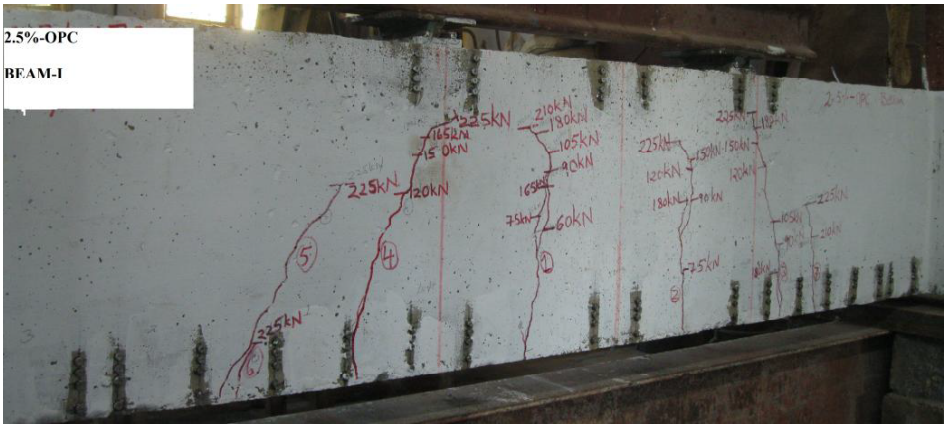

Fig.D1(d)

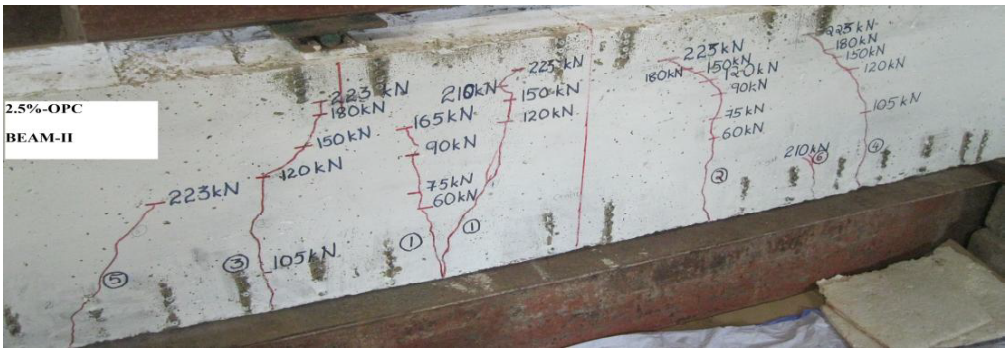

Fig.D2(a)

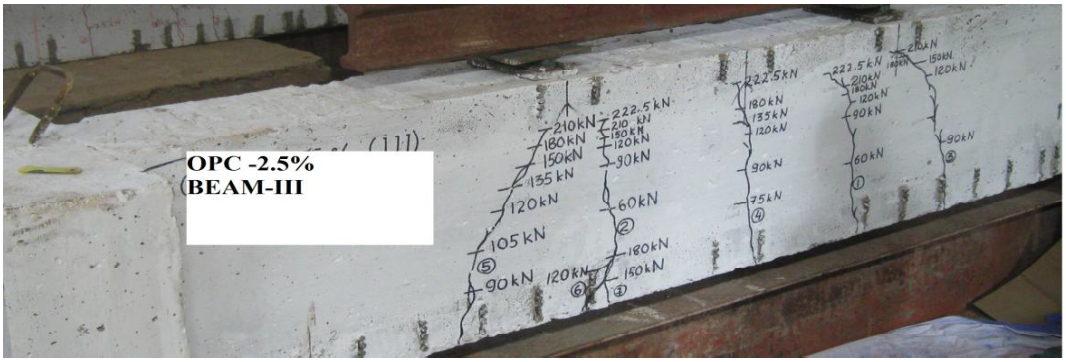

Fig.D2 (b)

Fig.D2: Crack propagation in beams with 2.5% corrosion (OPC concrete)

Fig.D3 (a)

Fig.D3(b)

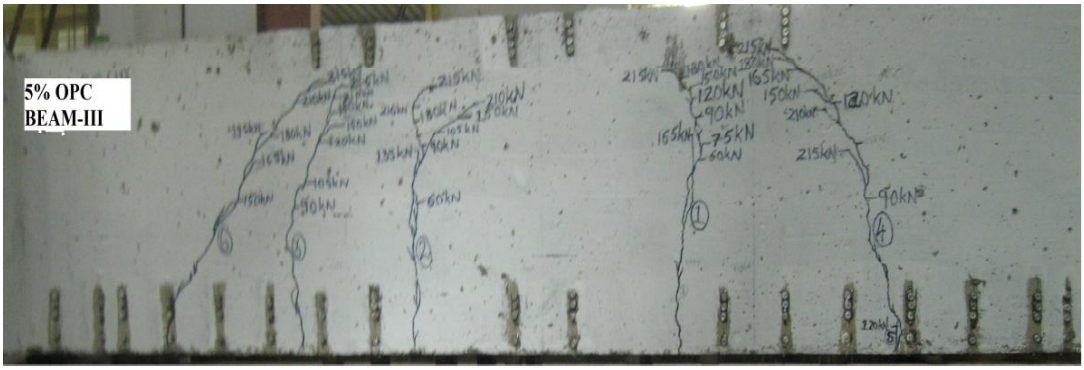

Fig.D3(c)

Fig.D3: Crack propagation in beams with 5% corrosion (OPC concrete)

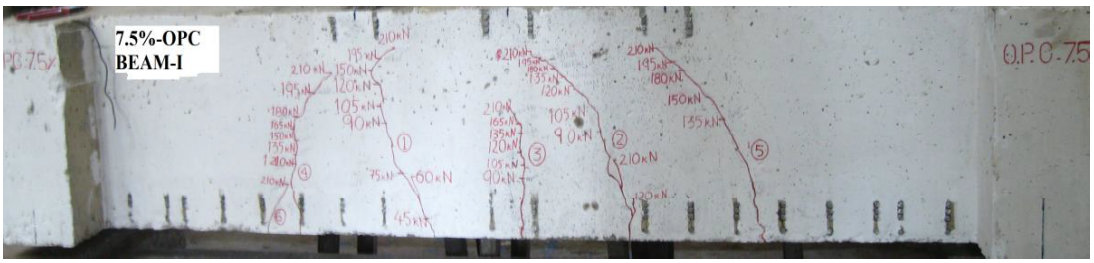

Fig.D4 (a)

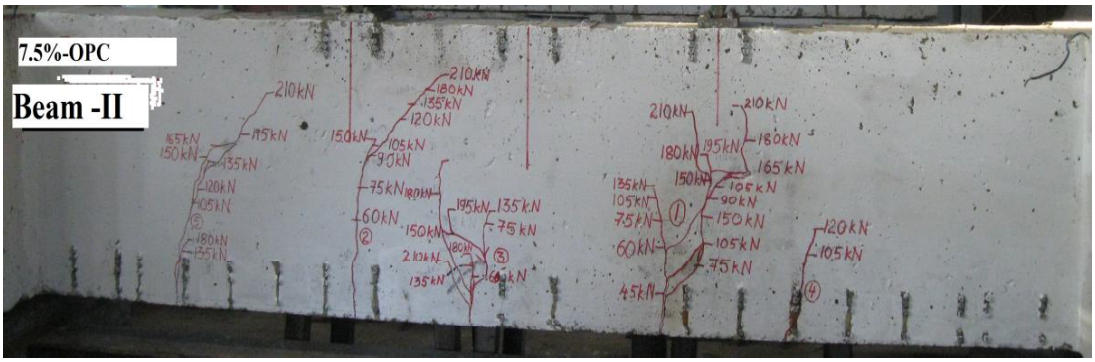

Fig.D4 (b)

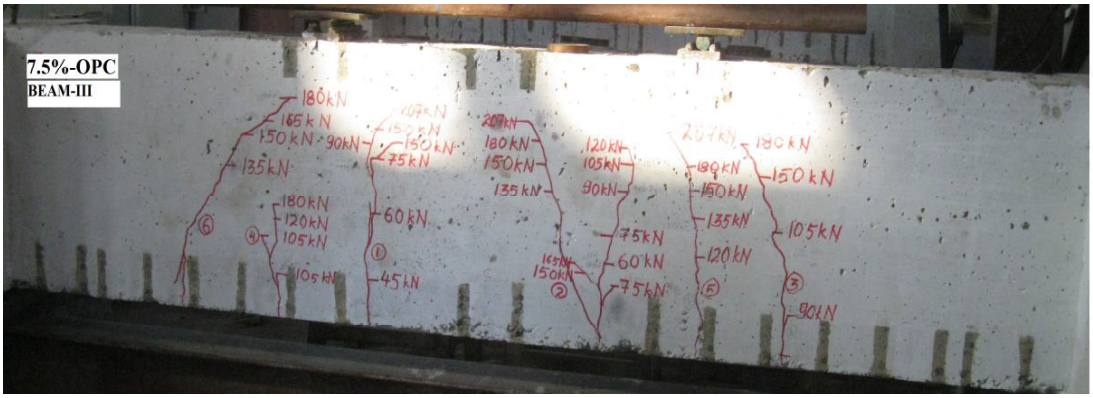

Fig.D4 (c)

Fig.D4: Crack propagation in beams with 7.5% corrosion (OPC concrete)

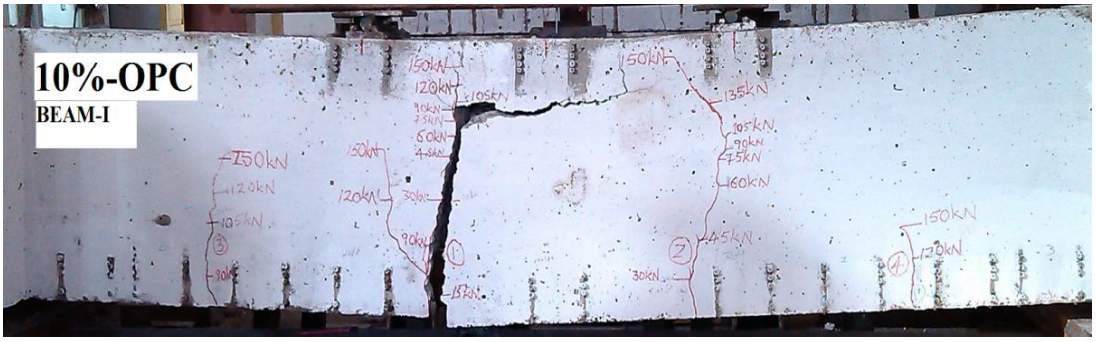

Fig.D5 (a)

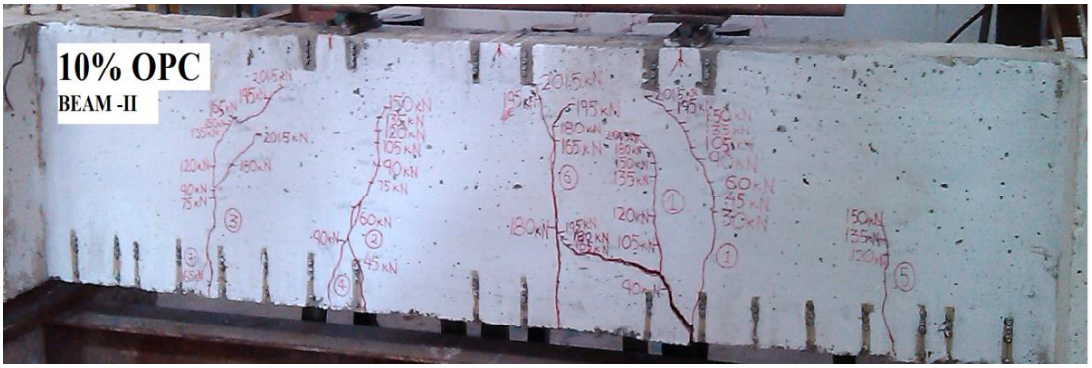

Fig.D5 (b)

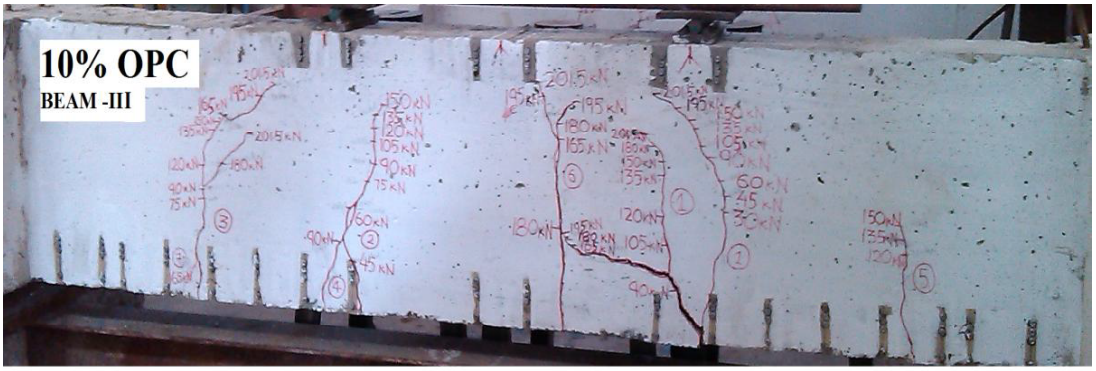

Fig.D5 (c)

Fig.D5: Crack propagation in beams with 10% corrosion (OPC concrete)

PPC Concrete

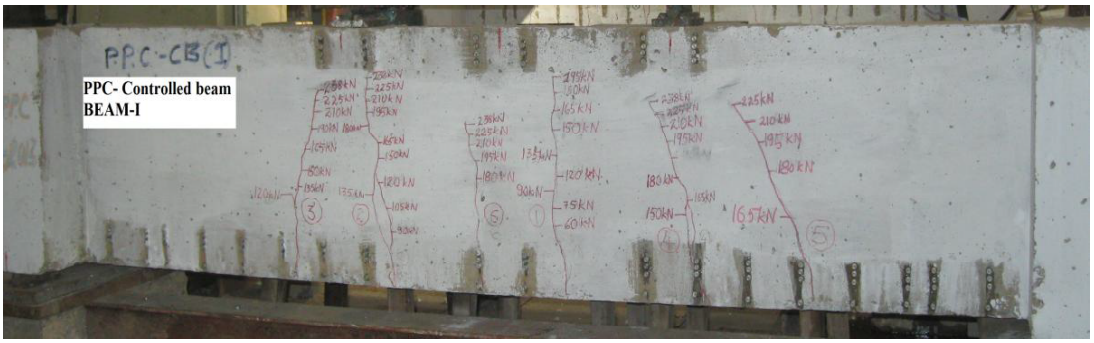

Fig.D6 (a)

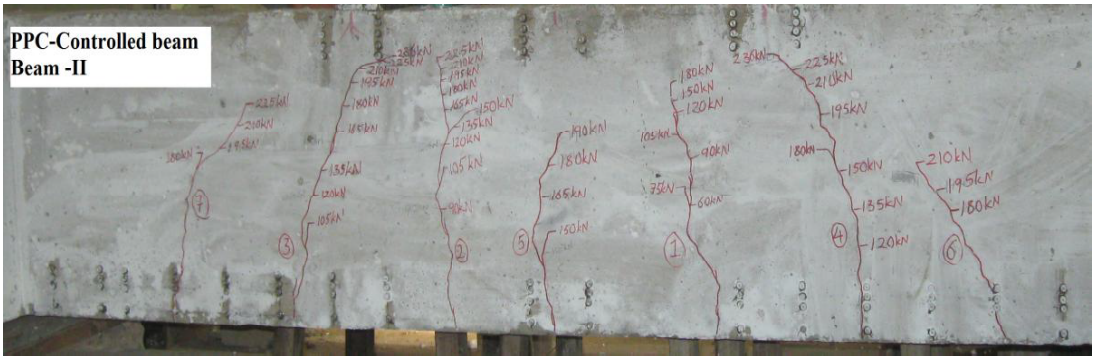

Fig.D6 (b)

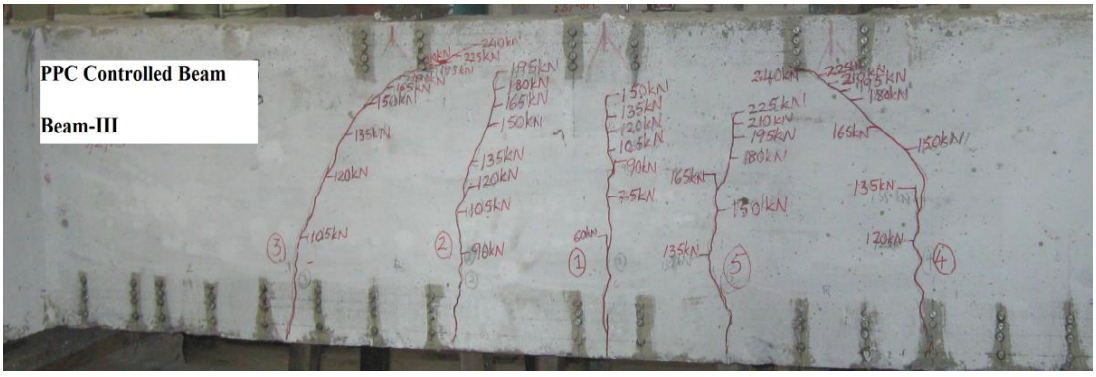

Fig. D6 (c)

Fig.D6: Crack propagation in Controlled beam specimens (PPC concrete)

Fig.D7 (a)

Fig. D7 (b)

Fig.D7: Crack propagation in beams with 2.5% corrosion (PPC concrete)

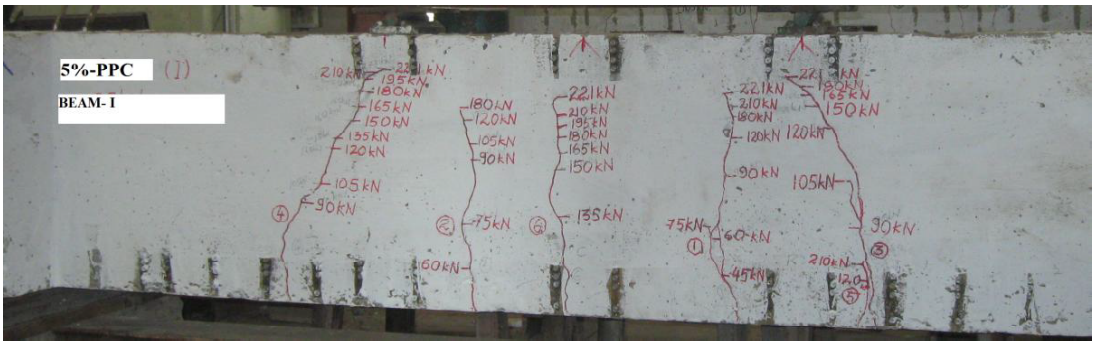

Fig.D8 (a)

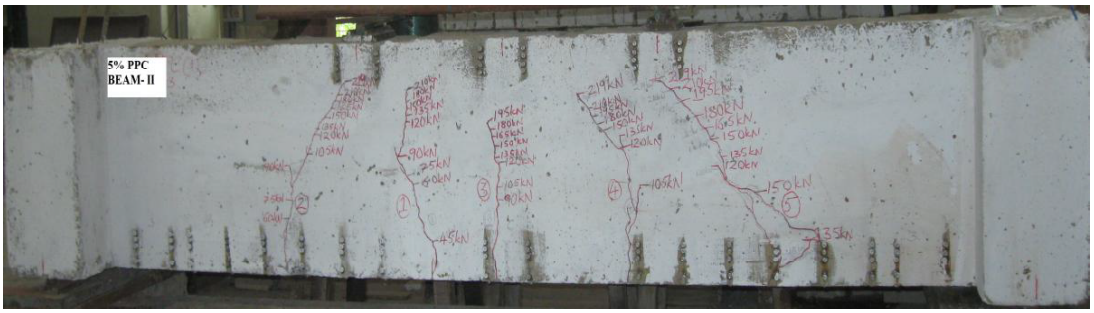

Fig.D 8 (b)

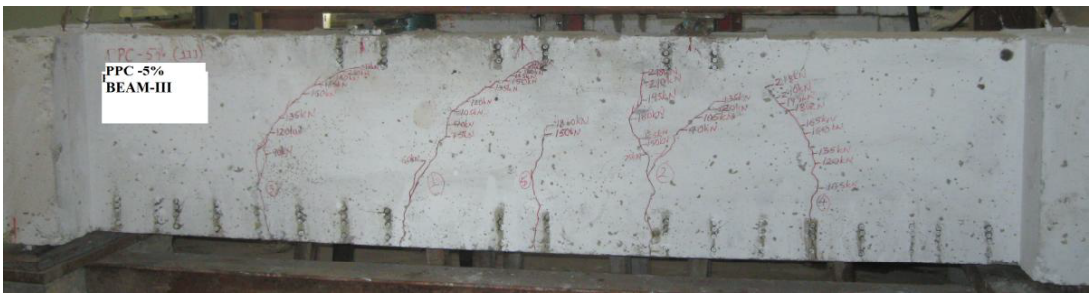

Fig.D8 (c)

Fig.D8: Crack propagation in beams with 5% corrosion (PPC concrete)

Fig.D9 (a)

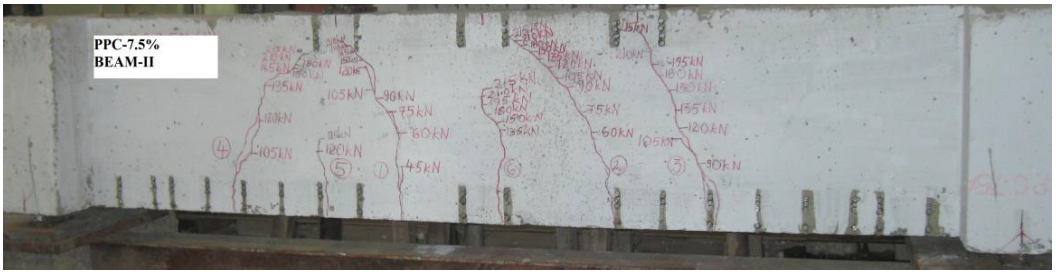

Fig.D9 (b)

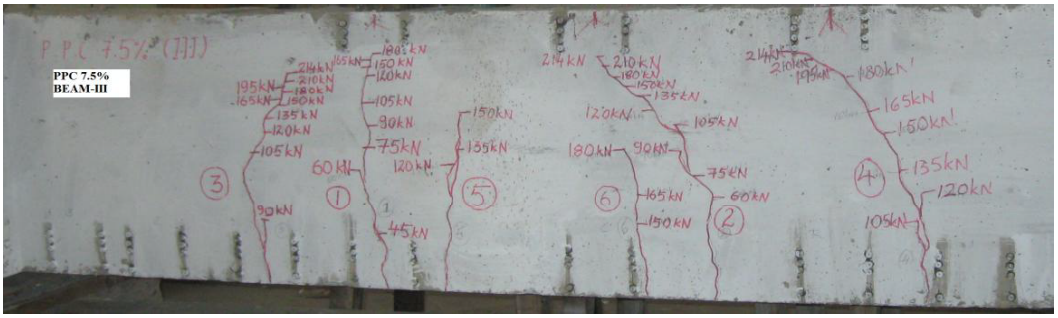

Fig. D9 (c)

Fig.D9: Crack propagation in beams with 7.5% corrosion (PPC concrete)

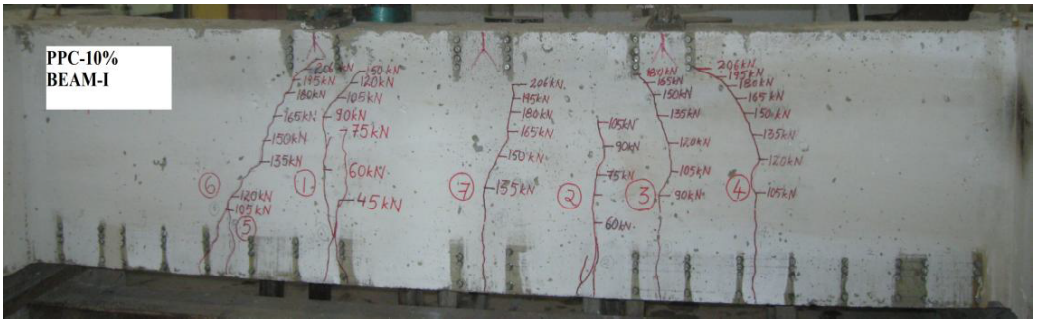

Fig.D10 (a)

Fig.D10 (b)

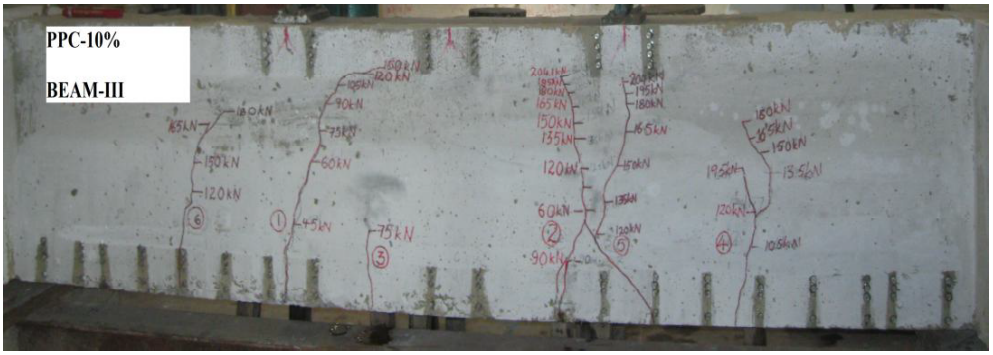

Fig.D10 (c)

Fig.D10: Crack propagation in beams with 10% corrosion (PPC concrete)

REFERENCES

- ACI Committee Report 408 (1991). "Bond and development of straight reinforcing bars in tension." 408R1-408R49.
- ACI-318 (1999). Standard building code requirement for reinforced concrete, American concrete institute, Detroit.
- Ahamad, S. (2009). "Techniques for inducing accelerated corrosion of steel in concrete." *The Arabian Journal of science and Engineering*,(34),Number 2C.
- Ahmad, S. (2003). "Reinforcement corrosion in concrete structures, its monitoring and service life prediction—A Review". *Cement & Concrete Composites,* 25, 459–471.
- Almusallam, A. A., (2001). "Effect of degree of corrosion on the properties of reinforcing steel bars." *Journal of Construction Building Materials,* 21(15), 361-8.
- Almusallam, A.A., Al-Gahtani, A. S., Aziz, A.R., and Rasheeduzzafar.(1996) "Effect of reinforcement corrosion on bond strength," *Construction and Building Materials,* 10(2), 123-129.
- Al-Sulaimani, G. J., Kaleemullah, M., Basunbul, I. A., and Rasheeduzzafar. (1990). "Influence of corrosion and cracking on bond behaviour and strength of reinforced concrete members". *ACI Structural Journal,* 87(2), 220-231.
- Amleh, L. (2000). "Bond Deterioration of concrete." PhD Thesis, Mc Gill University, Canada.
- Amleh, L. and Mirza, S. (2000).Corrosion influence on bond between Steel and Concrete. *Structural Journal,* 96(3), 415-423.
- ANSYS Commands Reference, (2012), ANSYS Inc., http:/www.ansys.com.
- Auyeung, Y., Balaguru, P., and Chung, L. (2000). "Bond behavior of corroded reinforcement bars." *ACI Materials Journal,* 97(2), 214-220.

- Azher, S. A. (2005). "A prediction model for the residual flexural strength of corroded reinforced concrete beams." MS thesis submitted to King Fahd University of Petroleum & Minerals, Saudi Arabia.
- Bazanth Z. P. (1979). "Physical model for steel corrosion in concrete sea structures – theory". Journal of Structural Division, ASCE, 105 (ST6) (1979) 1137 - 1153.
- Bhaskar S., Ravindra Gettu., and Bharatkumar B. H. (2011). "Corrosion of rebars in reinforced concrete-A review of the corrosion mechanisms, assessment techniques and control measures." *ICI Journal,* 35-54.
- Bhaskar, S., Bharatkumar, B.H., Ravindra, G. and Neelamegam. M. (2010). "Effect of corrosion on the bond behavior of OPC and PPC concrete". *Journal of Structural Engineering,* 37(1), 37-42.
- Browne, R. D. and Domone P. L. J (1975). "The long term performance of the concrete in the marine environment". Off shore structures, ICE, London, 49-59.
- BS 8110, (1985). Structural use of concrete, Part I, British Standards Institution London.
- Cabrera, J.G. and Ghoddousi, P. (1992). "The effect of reinforcement corrosion on the strength of the steel concrete interface." *Proceedings International Conference on Bond in Concrete from Research to Practise,* 11-24.
- Chung, L., Kim J.H.J., YI, ST., (2008). "Bond strength prediction for reinforced concrete members with highly corroded reinforcing bars". *Cement and Concrete Composites,* 30, 603-611.
- Clark A.P. (1949). "Bond of concrete reinforcing bars". Part of the journal research of the National Bureau of Standards (RP-2050), 43, U.S. Department of commerce.
- Cleary D.B. and Ramirez J.A. (1989). "Bond of epoxy coated reinforced steel in concrete bridge decks: Informational reports". School of civil engineering Indiana, department of highways, Joint Highway Research Project, JHRP 89-7, Purdue University.
- Cook R.D., (2001). "Concept and Application of Finite Element Analysis." 4th edition, University of Madison John Willey and Sons, Inc.

- Craig B. C, Soudki K. A. (2005). "Post-repair performance of corroded bond critical RC beams repaired with CFRP." *ACI Special Publication* SP-230-33, 563–78.
- Crisfield, M. A., and Wills, J. (1993). "The analysis of reinforced-concrete panels using different concrete models," *Journal of Engineering Mechanics*, ASCE, 15 (3), 578-597.
- Du, Y., Cullen M., and Li. C. (2013). "Structural effects of simultaneous loading and reinforcement corrosion on performance of concrete beams." *Construction and building materials*, 39,148-152.
- Fang, C., Lundgren, K., Chen, L., and Zhu, C. (2004). "Corrosion influence on bond in reinforced concrete." *Cement Concrete Resear*ch. 34 (11), 2159–2167.
- Fang, C., Lundgren, K., Chen, Plos, M., and Gylltott,K. (2006). "Corrosion influence on bond in reinforced concrete." *Journal of Cement and Concrete Resear*ch. 36, 1931-1938.
- Fib (International Federation of Structural Concrete) Bulletin 34, (2006). "Model Code for Service Life Design". ISBN 978-2-88394-074-1.
- Fontana, M.G., (2005). Corrosion Engineering. Tata McGraw-Hill Education Private Limited, New Delhi.
- Foster, S. J., Budino, and Gilbert, R. I., (1996). "Rotated crack finite element model for reinforced concrete structures," *Computers and Structures*, 58(1), 43-50.
- Frank, R. H., Pecknold, D. A. and Schnobrich, W. C. (1973). "Nonlinear Layered Analysis of RC Plates and Shells," *Journal of the Structural Division*, 99(7), 1491-1505.
- Goto, Y. (1971). "Cracks formed in concrete around deformed tension bars", *ACI Journal Proceedings*, 68(4), 244-251.
- Griffin, D. and Henry, R. (1963). Proceedings, *American Society for Testing and Materials*, (63) 1046-1079.
- Hammoud, R.A., Khaled Soudki, Timothy H.T. (2010). "Bond analysis of corroded reinforced concrete beams under monotonic and fatigue loads." *Cement & Concrete Composites*, 32, 194–203.

- Ha-Won song and saraswathy, V. (2007). "Corrosion Monitoring of Reinforced Concrete Structures – A Review". *International journal of Electrochemical Science*, 2(2007), 1-28.
- Hussain R. R., Ishida T., and Wasim M. (2012). "Oxygen Transport and Corrosion of Steel in concrete under varying concrete cover, *w/c* and moisture." *ACI Materials Journal*, 109(1), 3-10.
- Ichinose, T., Kanayama, Y., Inoue, Y., and Bolander Jr. J.E., (2004). "Size effect on bond strength of deformed bars." *Construction and building materials,* DTD 4.3.1, 1-10.
- *IS 1489* (*Part* 1)- *1991,* Portland Pozzolana Cement – specification (fly ash based)
- IS 2386 (Part III):1968, Methods of test for aggregates for concrete: Part III Specific gravity, density, voids, absorption and bulking, Bureau of Indian standards, New Delhi.
- IS 383:1970, Coarse and Fine aggregates from natural sources for concrete Bureau of Indian Standards, New Delhi.
- IS 4031:1988, "Methods of physical tests for hydraulic cement", Bureau of Indian Standards, New Delhi.
- IS 456:2000, plain and reinforced concrete – Code of practice, Bureau of Indian Standards, New Delhi.
- IS 8112 (1989), 43 Grade Ordinary Portland cement – Specification
- IS: 10262 (2009), Recommended guidelines for concrete mix design, Bureau of Indian standards, New Delhi.
- IS: 2770 (Part I) - (1967). "Methods of testing bond in reinforced concrete". Bureau of Indian Standards, New Delhi.
- Jhy Chang,J., Weichung Yeih., and Ran Huang (1999). "Degradation of the bond strength between rebar and concrete due to the impressed cathodic current." *Journal of Marine Science and Technology*, 7(2), 89-93.
- JIN Wei-liang and ZHAO Yu-xi. (2001). "Effect of corrosion on bond behavior and bending strength of reinforced concrete beams." *Journal of science*, Zhejiang *University*, 2(3), 298-308.

- Kachlakev Damian, Miller Thomas, and Yim Solomon (2001). "Finite Element Modeling of Reinforced Concrete Structures Strengthened with FRP Laminates," Report for Oregon Department of Transportation, Salem.
- Karve, S.R. and Shah, V.L. (1994). Limit State Theory and Design of Reinforced Concrete Structures Publishers, Jal Tarang, 36 parvati, Pune.
- Kayyali, O.A., and Yeomans S.R. (1995), "Bond and slip of coated reinforcement in concrete." *Construction and building materials*, 9(4), 219-226.
- Kazim T. and Yildirim M.S., (2003). "Bond Strength of reinforcement in splices in beams." *Structural engineering and Mechanics*, 16(4), 1-10.
- Kazim, T., Ahmet B., and Yusuf C. (2009). "Bond strength of tension lap slices in Full-Scale Self compacting concrete beams." *Turkish J. Eng. Env. Sci.*, 32(2008), 377-386.
- Law, D. W., Millard, S. G., & Bungey, J. H. (2000). "Linear polarisation resistance measurements using a potentiostatically controlled guard ring". *NDT and E International, 33*, 15–21.
- Lee, H.S., Noguchi, T., Tomosawa, F., (2002). "Evaluation of the bond properties between concrete and reinforcement as a function of the degree of reinforcement corrosion". *Journal of Cement Concrete Research*. 32 (8), 1313–1318.
- Lin C. S., Scordelis A. C. (1975). "Nonlinear analysis of RC shells of general form." *Journal of Structural Division* ASCE, 101, 523-538.
- Lutz L.A. (1978). "Bond with reinforcing steel- Significance of tests and properties of con concrete and concrete making materials." *ASTM special technical publication169B*, American society for testing and materials, 320-321.
- Lutz, L.A. and Gergely, P. (1966). "Mechanics of bond and slip of deformed bars in concrete." Structural Engineering Report No. 324, Cornell University.
- Lutz, L.A. and Gergely, P. (1967). "Mechanics of bond and slip of deformed bars in concrete." *ACI Materials Journal*, 711-721.

- MacGregor, J. G. (1992). "*Reinforced Concrete Mechanics and Design*," Prentice-Hall, Inc.,Englewood Cliffs, NJ.
- Mangat P.S., and Elgarf M.S. (1999). "Bond characteristics of corroding reinforcement in concrete beams." *Materials and Structures/Materiaux et Constructions*, 32, 89-97.
- McGinley, T.J. and Choo B. S. (1990). Reinforced Concrete – Design Theory and Examples, E. & F.N. Spon, London.
- Mehmet, K., Kazim T., and Zulfu C. U. (2010). "Investigation on bond between lap-spliced steel bar and self compacting concrete: The role of silica fume." *Published by NRC research press Can. J. Eng. Sci*, 37, 420-428.
- Mehta, P. Kumar, (1993), "Concrete Structure, Properties, and MateriaIs," PrenticeHall, Inc., Englewood Cliffs, N.J. 07632.
- Oh, H., Sim, J., Ju, M., and Kang, T. (2008). "Flexural bonding characteristics of deformed GFRP rebar under variable amplitude loading." *Fourth International Conference on FRP composites in civil Engineering (CICE2008)*, Zurich, Switzerland.
- Orangun, C. O., Jirsa, J.O. and Breen, J.E. (1977). "A re-evaluation of test data on development length and splices." *ACI Materials Journal*, 114-122.
- Parande, A., Dhayalan, P., Karthikeyan, M. S., Kumar, K. and Palaniswamy, N. (2008). "Assessment of Structural Behavior of Non-corroded and Corroded RCC Beams Using Finite Element Method," *Sensors & Transducers Journal*, 96(9), 121-136.
- Park, R., and Paulay, T. (1975). Reinforced Concrete Structures. John Wiley & Sons, Inc. New York.
- Paul R.J. (1978), "Top-bar and embedment length effects in reinforced concrete beams." Master Thesis, Department of Civil Engineering and Applied Mechanics, Mc Gill University Canada.
- Phuvoravan, K. (2010). "Effect of steel corrosion level on flexural behaviour of reinforced concrete beam." Report from Kasestart University, Bangkok, Thailand.

- Pillai, S.U. and Menon, D. (1999). Reinforced Concrete Design, Tata McGraw-Hill Publishing Company Limited.
- Pradhan, B. and Bhattacharjee, B. (2009). "Performance evaluation of rebar in chloride contaminated concrete by corrosion rate." *Construction and Building Materials,* 23, 2346-2356.
- Purushothaman P. (1984). **"**Reinforced Concrete Structural Elements Behaviour, Analysis and Design." Ta Ta Mc-Graw Hill Publication Co. Ltd. New Delhi, 141-166.
- Ramesh G., Sundar K.S., Bharatkumar B.H. and Krishnamoorthy T.S. (2010). "*Proceedings Advances in Materials mechanics and management*." 1, 134-141.
- Rehm, G. (1957). "The fundamental law of bond." *Proc. Symposium on Bond and Crack Formation in Reinforced Concrete*, Stockholm, Paris Publication.
- RILEM/CEB/FIP Recommendation, (1973). "Bond test for reinforcing steel." Matter. Struct. 6(32).
- Rodriguez, J., Ortega, L. and Garcia, A. (1994). "Corrosion of reinforcing bars and service life of RC Structures: corrosion and bond deterioration". *Concrete across Borders, Proceedings, Odense,* Denmark, vol. II, 315–326.
- Rteil, A. A., Khaled, A. S. and Topper, T. H. (2008). "CFRP Repair of corrosion damaged bond region." *Fourth international conference on FRP composites in civil engineering,* Zurich Switzerland.
- Saether, I. and Sand, B (2009). "FEM simulations of reinforced concrete beams attacked by corrosion," Northern Research Institute Report Narvik (Norut Narvik), Norway.
- Saifullah, I., Hossain, M. A., Uddin, S. M. K., Khan, M. R. A. and Amin, M. A. (2011). "Nonlinear Analysis of RC Beam for Different Shear Reinforcement Patterns by Finite Element Analysis," *International Journal of Civil & Environmental Engineering,* 11(01), 86-98.
- Sakamoto, N., and Iwasaki, N. (1982). "Influence of sodium chloride on the concrete/ steel and galvanised steel bond," *Bond in Concrete*, Applied Science Publishers, London England.

- Schicheng Tao, (1994). "Bond of glass fiber-reinforced –plastic reinforcing bars to concrete." PhD Thesis, University of Arizona.
- Scordelis A. C. and Chan, E.C. (1989). "Nonlinear analysis of reinforced concrete shells," *Computer applications in Concrete technology*, ACI SP-98, American concrete institute, 25-57.
- Sen T., Mishra, U. And Shubhalakshmi B.S. (2010). "Nonlinear finite element analysis of retrofitting of RCC beam column joint using CFRP," *International journal of Engineering and Technology*, 2(5) 459-467.
- Seshu, P. (2006). "Finte Element Analysis", Prentice Hall of India, New Delhi.
- Shaahiq Khan, M., Reddy, A.R., Shariq, M., and Prasad, J. (2007), "Studies in bond strength in RC flexural members." *Asian journal of civil engineering (Building and Housing)*, 8(1), 89-96.
- Shalon, R. and Raphael, M. (1959). "Influence of sea water on corrosion of reinforcement." *ACI Materials Journal*, 1251-1268.
- Simioni, P., (2009). "Seismic response of reinforced concrete structures affected by reinforcement corrosion". Thesis of Civil engineering and environmental Sciences university of Braunschweig and Florence.
- Stanish, K. (1997). "Corrosion effects on bond strength in reinforced concrete." Master's Thesis, Graduate department of civil engineering, University of Toronto.
- Tepfers, R. (1973). "A theory of bond applied to overlapped tensile reinforcement splices for deformed bars." Division of Concrete Structures. Chalmers University of Technology, Goteborg, Sweden, Publication 73 (2), 328.
- Treece R.A. and Jirsa J.O. (1987). "Bond strength of epoxy-coated reinforcing bars." Report on a Research Project Department of Civil Engineering / Bureau of Engineering Research. The University of Texas at Austin.
- Tuutti K. (1982). "Corrosion of steel in concrete." Report submitted to Swedish Cement and Concrete Research Institute, Stockholm.

- Val, D. V. (2007). "Deterioration of strength of RC beams due to corrosion and its influence on beam reliability". *Journal of Structural Engineering*, 133(9), 1297–1306.
- Vecchio, F. J. and Tata, M. (1999). "Approximate analysis of reinforced concrete slabs," *structural Engineering and Mechanics*, 8(1), 1-18.
- Vidal, T., Castel, a., and Francois, R. (2006). "Corrosion process and structural performance of a 17 year old reinforced concrete beam stored in chloride environment". *Cement and Concrete Research*, 37(11), 1551–1561.
- Weathersby J. H. (2003). "Investigation of bond slip between concrete and steel reinforcement under dynamic loading conditions." PhD Thesis, Graduate Faculty of the Louisiana State University and Agricultural and Mechanical College.
- Webster M. P. (2000). "The assessment of corrosion-damaged concrete structures." PhD Thesis, School of Civil Engineering, Birmingham.
- Wolanski, A. J. (2004). "Flexural behavior of reinforced and pre-stressed concrete beams using finite element analysis," Ph.D Thesis, Marquette University, Wisconsin, USA.
- Wolanski, A. J. (2004). "Flexural Behavior of Reinforced and Prestressed Concrete Beams Using Finite Element Analysis," Ph.D Thesis, Marquette University, Wisconsin, USA.
- Xiaoming Yang and Hongqiang Zhu (2012). "Finite element investigation on load carrying capacity of corroded RC beam based on bond-Slip," *Jordan Journal of Civil Engineering*, 6(1), 134-146.
- Xiaoming Yang and Hongqiang Zhu (2012). "Finite Element Investigation on load carrying capacity of corroded RC beam based on Bond-Slip," *Jordan Journal of Civil Engineering*, 6(1), 134-146.
- Xu, S. 2003. "The models of deterioration and durability evaluation of reinforced structure [D]. Report, XI'an University of Architecture and Technology.
- Yuan, Y. and Yongsheng, J. (2009). "Modeling corroded section configuration of steel bar in concrete structures". *Construction and Building Materials*, 23(6), 2461-2466.

- Zhang, W., and Ba, H. (2011). "Accelerated life test of concrete in chloride environment." *Journal of Materials in Civil Engineering*, 23(3), 330-334.
- Zienkiewicz, O.C., Taylor and Zhu, J.Z. (2007). "The Finite Element Method Its Basis and Fundamental". 6th edition, Burlington, USA.

LIST OF PUBLICATIONS BASED ON THE PRESENT RESEARCH WORK

JOURNALS

1. Akshatha Shetty, Katta Venkataramana and K.S. Babunarayan (2013). "Effect of corrosion on degradation of RC members". *International Review of Applied Engineering Research*. 3(1), 55-66.

2. Akshatha Shetty, Katta Venkataramana and K. S Babunarayan (2013). "Effect of corrosion on Load deflection behavior of OPC concrete in NBS Beam". *International Journal of Scientific Engineering Research*. 4(5), 111-114.

3. Akshatha Shetty, Katta Venkataramana and K.S. Babunarayan (2013). "Bond strength behaviour in reinforced concrete members exposed to corrosive environment-An Overview". *International Journal of Earth Sciences and Engineering*, 6(3), 530-535.

4. Akshatha Shetty, Katta Venkataramana and K.S. Babunarayan (2013). "Experimental Investigation on effect of corrosion in reinforced concrete beams," *Built Expressions. 2(10), 52-57.*

5. Akshatha Shetty, Katta Venkataramana and and Babu Narayan K.S. (2014). "Flexural bond strength behaviour in OPC concrete Of NBS beam for various corrosion levels," *International Journal of structural Engineering and Mechanics, Techno Press.* 49(1), 81-93.

6. Akshatha Shetty, Katta Venkataramana and and Babu Narayan K.S. (2014). "Investigation on Load Carrying Capacity of Corroded NBS RC Beam Using Finite Element method," *IOSR- Journal of Mechanical and Civil Engineering,* 1, 60-65.

7. Akshatha Shetty, Katta Venkataramana and and Babu Narayan K.S. (2014). "Effect of corrosion on flexural bond strength," *Journal of Electrochemical Science and Engineering*, 4(3), 123-134.

8. Akshatha Shetty, Katta Venkataramana and K.S. Babunarayan (2014). "Experimental investigation on corroded NBS RC beams". *International journal of Civil Engineering Research and Technology*, 2(1), 1-6.

CONFERENCES

1. Akshatha Shetty, Katta Venkataramana and K.S. Babunarayan. "Effect of Corrosion on loss of composite action between steel and concrete", *Proc. of Innovations in concrete construction (International UKIERI-13 concrete congress)*, presented at NITJ, Punjab, March 5th to 8th 2013.

2. Akshatha Shetty, Katta Venkataramana and K.S. Babunarayan. "Effect of corrosion on Load deflection behavior of OPC concrete in NBS Beam". *Proc. of International Conference on Innovations in Civil Engineering (ICICE-2013),* presented at S.C.M. School of Engineering, Ernakulam 9th and 10th May, 2013.

3. Akshatha Shetty, Katta Venkataramana and K.S. Babunarayan. "Experimental investigation on corroded PPC RC beams". *Proc. of National Conference on Advancement in Materials, Construction & Sustainable Environment (AMCSE-14),* presented at Kalasalingam University, Tamilnadu, and 29th March 2014.

4. Akshatha Shetty, Katta Venkataramana and K.S. Babunarayan. "Investigation on Load Carrying Capacity of Corroded NBS RC Beam Using Finite Element method". *Proc. of International Conference on Innovations in Civil Engineering (ICICE-2014),* presented at S.C.M. School of Engineering, Ernakulam 8th and 9th May, 2014.

5. Akshatha Shetty, Katta Venkataramana and K.S. Babunarayan. "Corrosion effects on flexural bond strength of RC members". *Proc. of International Conference on Emerging Trends in Engineering (ICETE-2014)*, presented at NMAMIT Nitte, 15th to 17th May, 2014.

6. Akshatha Shetty, Katta Venkataramana and K.S. Babunarayan. "Studies on flexural bond strength of corroded NBS RC beams". *Proc. of 1st Annual Conference on Innovations and Developments in Civil Engineering (ACIDIC-2014)*, presented at NITK Surathkal, 19th and 20th May, 2014.

7. Akshatha Shetty, Katta Venkataramana and K.S. Babunarayan. "Experimental investigation on corroded NBS RC beams". *International Conferences on recent advances in Engineering Sciences (ICRAES-2014)*, presented at MSRIT Bangalore, 4 and 5th September, 2014.

8. Akshatha Shetty, Katta Venkataramana and K.S. Babunarayan. "Potential application of experimental prediction equation in estimating the corrosion of RC structures". *International Engineering Symposium (IES-2015)*, held at Kumamoto University Japan, 4th to 6th March (accepted for presentation).

CURRICULUM VITAE

Name : AKSHATHA SHETTY

Contact No. : +91-9880898436

E-Mail : akshathashetty16@gmail.com, akshathashetty12@rediffmail.com.

Date of Birth : 16-03-1988

Educational Qualifications

Degree	University	Year of Passing
B. E. (Civil)	VTU	2009
M. Tech (Research) Structural Engineering	NITK	2012

Teaching Experience

Name of Institute	Post held	Period
NITK	Lecturer	July 2009-May 2010

Industrial Experience / Interaction

Organization	Nature of work	Period
NITK (BRNS, Sponsored Project)	Junior Research Fellow	July 2010-July 2012
	Senior Research Fellow	July 2012-March 2013

Research Publications

	International	National
Journal Papers	13	02
Conference Publications	12	04
Workshops	-	04

Honours and Awards

- 2 Best Paper award in the year of 2012 and 2014, in ICETE held at Nitte.
- Appreciation Certificate on Teachers day celebration during 2003-2004 for obtaining medal in State level Hockey Tournament.
- Secured third Place in VTU Inter collage athletic meet during November 2006-07, held at S.J.B.I.T Bangalore.
- Secured third Place in amateur athletic meet during 28th to 30th October 2003.
- Represented in National Level 'Hockey' Tournament held on January 3rd to 6th 2004 at Ranchi.